Regulation of gene expression in specific mouse brain cells during neurodegenerative prion disease

Dissertation

zur

Erlangung des Doktorgrades (Dr. rer. nat.)

der

Mathematisch-Naturwissenschaftlichen Fakultät

der

Rheinischen Friedrich-Wilhelms-Universität Bonn

vorgelegt von

Melvin Schleif

aus

Dormagen

Bonn, September 2017

Angefertigt mit Genehmigung

der Mathematisch-Naturwissenschaftlichen Fakultät

der Rheinischen Friedrich-Wilhelms-Universität Bonn

1. Gutachter
Prof. Dr. Ina Vorberg
Gruppenleiterin
Deutsches Zentrum für Neurodegenerative Erkrankungen, Bonn

2. Gutachter
Prof. Dr. Walter Witke
Institutsdirektor und Gruppenleiter
Institut für Genetik, Universität Bonn

Tag der Promotion: 24.04.2018

Erscheinungsjahr: 2018

I. Table of contents

II. List of abbreviations

II.A Used abbreviations

°C	Degree Celsius
µ	Micro
2logFC	Log2 FoldChange
3’	Three prime end of nucleic acid
5’	Five prime end of nucleic acid
A	Ampere
ADP	Adenosine diphosphate
AG	Research group
AP	Anterior – posterior
Astro	Astrocytes
ATP	Adenosine triphosphate
B6	C57Bl/6N inbred mouse strain
bp	Base pair
BP	Biological process
BSE	Bovine spongiform encephalopathy, “mad cow” disease
CC	Cellular compartment
cDNA	Complementary DNA
CHO	Carbohydrate (N-linked glycosylation site)
CJD	Creutzfeldt-Jakob disease
Cnx43	Connexin 43, gap junction alpha-1 protein (GJA1)
CoQ	Coenzyme Q_{10}, ubiquinone
Cre	Cre recombinase
CT	Cycle threshold
d	Day
Da	Dalton
DEG	Differentially expressed gene
DNA	Deoxyribonucleic acid
dNTP	Deoxynucleoside triphosphate
DZNE	German Center for Neurodegenerative Diseases
e^-	Electron
EEG	Electroencephalography
EMG	Electromyography

FAD	Flavin adenine dinucleotide (FAD / $FADH_2$)
FBS	Fetal bovine serum
FFI	Fatal familial insomnia
For	Forward
FRT	Flippase recognition target
g	Earth's gravitational acceleration
G	Gauge
g	Gram
GABA	GABAergic neurons
Gad2	Glutamate decarboxylase 2
Glut	Glutamatergic neurons
GO	Gene ontology
GPI	Glycophosphatidylinositol
GSS	Gerstmann-Sträussler-Scheinker syndrome
h	Hour
H^+	Proton
HA	Hemagglutinin
HRP	Horseradish peroxidase
Hz	Hertz
IEGs	Immediate early genes
IP	Immunoprecipitation
IPA	Ingenuity Pathway Analysis
IRES	Internal ribosomal entry site
k	Kilo
l	Liter
lfcSE	Log2 FoldChange Standard Error
loxP	Cre recombinase target sequence
m	Meter
m	Milli
M	Molar
MF	Molecular function
min	Minute
MIT	Massachusetts Institute of Technology
ML	Medial – lateral
mRNA	Messenger ribonucleic acid
n	Nano
n	number, sample size

NAD	Nicotinamide adenine dinucleotide (NAD^+ / $NADH+H^+$)
NBH	Normal brain homogenate
NCBI	National Center for Biotechnology Information
ND	Neurodegenerative disease
NREM	Non rapid eye movement sleep, deep slow wave sleep
ORF	Open reading frame
padj	Adjusted p-value, false discovery rate (FDR)
PAGE	Polyacrylamide gel electrophoresis
PBS	Phosphate-buffered saline
PCR	Polymerase chain reaction
pH	Negative of logarithm to base 10 of hydrogen ion activity
PK	Proteinase K
PMCA	Protein misfolding cyclic amplification
POL	Polymerase
Prnp	Prion protein gene
PrP 27-30	N-terminally truncated PrP^{Sc} by proteinase K
PrP	Prion protein
PrP^{C}	Endogenous, cellular isoform of prion protein
PrP^{Sc}	Misfolded, pathogenic isoform of prion protein
PV	Parvalbumin neurons
pval	P-value, probability value
Pvalb	Parvalbumin
qPCR	Real-time quantitative PCR
REM	Rapid eye movement sleep, paradoxical sleep
Rev	Reverse
REV-ERBs	Orphan nuclear hormone receptors
RML	Mouse adapted Rocky Mountain Laboratory scrapie strain
RNA	Ribonucleic acid
RNase	Ribonuclease
RORs	Retinoid related orphan receptors
ROS	Reactive oxygen species
RPKM	Reads per kilobase per million mapped reads
Rpl22	Large subunit ribosomal protein 22
rpm	Revolutions per minute
RT	Reverse transcription, reverse transcriptase
RT	Room temperature
Rtag	RiboTag

s	Second
S2	Biosafety containment level 2
S4	129S4/SvJae inbred mouse strain
SCN	Suprachiasmatic nucleus
S-S	Disulfide bond
SST	Somatostatin, somatostatin neurons
TSEs	Transmissible spongiform encephalopathies
U	Unit
UER	Unique exon read
UPR	Unfolded protein response
UTR	Untranslated region
V	Volt
Vglut2	Vesicular glutamate transporter 2
vs.	Versus
wpi	Weeks post infection

II.B Primary nucleobases

Name	1 letter code
Adenine	A
Cytosine	C
Guanine	G
Thymine	T
Uracil	U

II.C Proteinogenic amino acids

Name	1 letter code	3 letter code
Alanine	A	Ala
Arginine	R	Arg
Asparagine	N	Asn
Aspartic acid	D	Asp
Cysteine	C	Cys
Glutamic acid	E	Glu
Glutamine	Q	Gln
Glycine	G	Gly
Histidine	H	His
Isoleucine	I	Ile
Leucine	L	Leu
Lysine	K	Lys
Methionine	M	Met
Phenylalanine	F	Phe
Proline	P	Pro
Pyrrolysine	O	Pyl
Selenocysteine	U	Sec
Serine	S	Ser
Threonine	T	Thr
Tryptophan	W	Trp
Tyrosine	Y	Tyr
Valine	V	Val

1. Introduction

1.1 Neurodegenerative diseases

Neurodegenerative diseases (ND) are a heterogeneous group of disorders of the nervous system caused by redundant aggregation of misfolded, toxic proteins and dysfunctional trafficking of proteins. Examples of NDs are Alzheimer's disease, Parkinson's disease, Huntington's disease, amyotrophic lateral sclerosis and transmissible spongiform encephalopathies (TSEs) (Taylor et al. 2002, Dobson 2003, Rubinsztein 2006, Ramanan and Saykin 2013, Sheikh et al. 2013).

NDs are associated with the accumulation and aggregation of abnormal or misfolded proteins. Neuronal cell death is common, leading to degeneration of the structure and function of the nervous system. Depending on the affected brain region the neurodegeneration causes movement problems or impairment of mental functioning. There are several NDs and they all differ in etiology and their morphological and pathophysiological features (Nieoullon 2011, Ramanan and Saykin 2013, Sheikh et al. 2013).

In addition to protein misfolding and aggregation, factors leading to and associated with NDs are mitochondrial dysfunction, altered protein modifications, oxidative stress, free radical formation, metal dyshomeostasis and aging (Figure 1.1) (Dobson 2003, Sheikh et al. 2013). Nervous system cell pathways altered in NDs can be functionally grouped into intracellular mechanisms (apoptosis, autophagy, mitochondrial functions, oxidative stress response, proteasome), local tissue environment (cell adhesion, endocytosis, neurotransmission), systemic environment (inflammation, immune system) and development and aging (epigenetics, telomeres) (Ramanan and Saykin 2013).

In addition to genetic risk factors like familial mutations leading to NDs, the risk to suffer from any ND increases with age. Other risk factors depend on geography, hereditary, viral and toxicological exposure (Emard et al. 1995). Due to the demographic change in society, especially in the industrialized countries, NDs are becoming an ever-increasing problem (Brookmeyer et al. 2007).

The exact mechanism of how misfolded, aggregated proteins lead to toxicity and neurodegeneration is still unknown. For therapeutic approaches the mechanism of aggregation and toxicity of the disease related proteins have to be further investigated. Therapeutic approaches are needed because NDs currently take up a very large proportion of the massive amount of money spent on health care and the

ever-expanding aged population will amplify this problem in the future (Taylor et al. 2002, Andlin-Sobocki et al. 2005, Brookmeyer et al. 2007, Katsuno et al. 2012, Panegyres and Armari 2013).

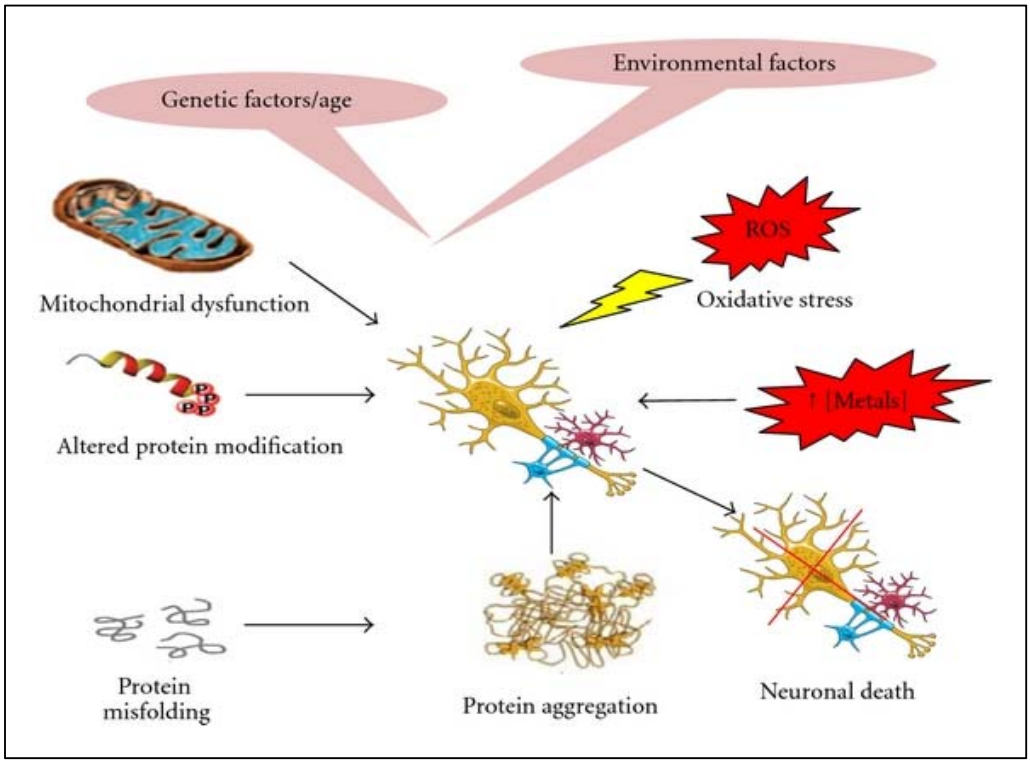

Figure 1.1: Factors causing and associated with neurodegenerative diseases leading to neuronal death. (Sheikh et al. 2013)

1.2 Selective vulnerability

NDs initially affect only specific regions of the brain, a phenomenon known as selective vulnerability (Figure 1.2). For example, brain regions important for motor control are severely damaged in Huntington's disease and Parkinson's disease, while brain regions important for memory are severely damaged in Alzheimer's disease (Table 1.2). The fact why other brain regions remain unaffected in these diseases is still unknown (Guentchev et al. 1999, Jackson 2014, Mattsson et al. 2016).

Since these and many other neurodegenerative diseases are thought to be caused by misfolding and aggregation of specific proteins, a reasonable explanation is that the most affected regions have the highest expression levels of the toxic proteins.

However, this is not the case and something else must be determining selective vulnerability (Jackson 2014).

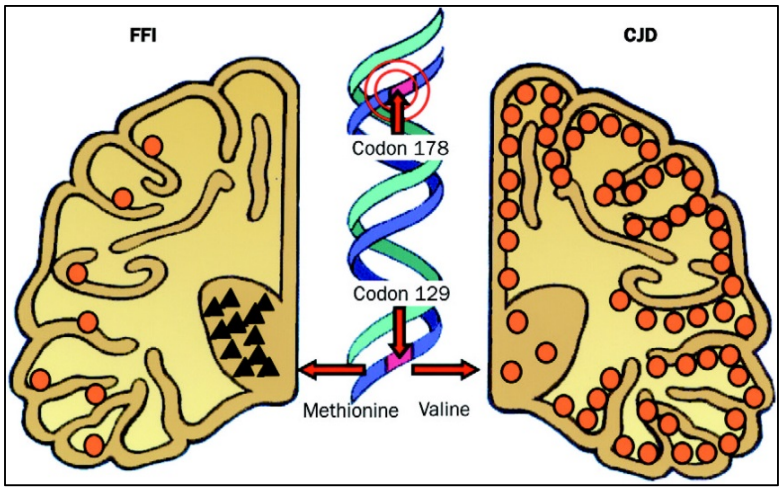

Figure 1.2: Selective vulnerability of neuropathological changes, namely neuronal loss (triangles) and spongiosis (circles), in fatal familial insomnia (FFI) and Creutzfeldt-Jakob disease (CJD). Both diseases are linked to a codon 178 mutation (D178N), but segregated by a codon 129 polymorphism. (Montagna et al. 2003)

Table 1.2: Examples of NDs, their major disease related genes or proteins and their most affected brain regions

Disease	Related gene / protein	Targeted region
Alzheimer's disease	Amyloid precursor protein, presinilin 1+2, tau protein	Hippocampus, cortex
Amyotrophic lateral sclerosis	Superoxide dismutase 1	Motor cortex
Creutzfeldt-Jakob disease (CJD)	Prion protein	Cortex
Fatal familial insomnia (FFI)	Prion protein	Thalamus
Frontotemporal dementia	Tau protein, granulin	Frontal lobe, temporal lobe
Gerstmann-Sträussler-Scheinker syndrome (GSS)	Prion protein	Cerebellum
Huntington's disease	Huntingtin	Striatum, cortex
Parkinson's disease	Alpha-synuclein	Substantia nigra

Specific brain regions possess specific brain cells and the phenomenon of selective vulnerability could be caused by these specific brain cells in these regions having unique strategies and capacities to cope with various disease related protein conformers. Furthermore, next to the complete proteasome the protein quality control machinery differs between different cell types due to different compilations of machinery components and clients and these differences strongly influence selective vulnerability (Jackson 2014). It is also discussed for some diseases, including TSEs, if a cofactor needed for misfolding of the disease related protein is

available only in these specific cell types (Prusiner 1998, Colby and Prusiner 2011). A better understanding of the phenomenon of selective vulnerability could support therapeutic approaches for many neurodegenerative diseases (Jackson 2014).

1.3 Transmissible spongiform encephalopathies

TSEs, also known as prion diseases, are a group of rare, transmissible, infectious and always fatal neurodegenerative disorders affecting the nervous system of humans and other mammals. TSEs are caused by prions, the misfolded, aggregated and infectious form of the endogenous prion protein (Prusiner 1982, Fields et al. 2001, Colby and Prusiner 2011, Whitechurch et al. 2017). Examples of TSEs are Creutzfeldt-Jakob disease, fatal familial insomnia, Gerstmann-Sträussler-Scheinker syndrome and kuru in humans, bovine spongiform encephalopathy (BSE, “mad cow” disease) in cattle and scrapie in sheep and goats (Table 1.3) (Colby and Prusiner 2011).

Table 1.3: Prion diseases in humans and animals and the mechanism of pathogenesis (Colby and Prusiner 2011).

Disease	Host	Mechanism of pathogenesis
BSE	Cattle	Infection or sporadic
Chronic wasting disease	Deer, elk, moose	Infection
Exotic ungulate encephalopathy	Greater kudu, nyala, oryx	Infection with prion-contaminated meat and bone meal
Familial CJD	Humans	Germline mutations in the *PRNP* gene
Feline spongiform encephalopathy	Felidae	Infection with prion-contaminated bovine tissues or meat and bone meal
FFI	Humans	Germline mutations in the *PRNP* gene
GSS	Humans	Germline mutations in the *PRNP* gene
Iatrogenic CJD	Humans	Infection from prion-contaminated human growth hormone, medical equipment
Kuru	Humans	Infection through ritualistic cannibalism
Scrapie	Sheep, goats	Infection
Sporadic CJD	Humans	Somatic mutation or spontaneous conversion of PrP^{C} to PrP^{Sc}
Sporadic fatal insomnia	Humans	Somatic mutation or spontaneous conversion of PrP^{C} to PrP^{Sc}
Transmissible mink encephalopathy	Mink	Infection with prions from sheep or cattle
Variant CJD	Humans	Infection from bovine prions

1.3.1 Prions

Prions (proteinacious infectious particles) are infectious proteins causing TSEs, the only known infectious protein misfolding disorders (Prusiner 1982, Ma and Wang 2014). They have been identified in both fungi and mammals. In mammals they are the misfolded, disease causing form of the prion protein (PrP), an endogenous glycoprotein which is located primarily on the surface of central nervous system cells (Prusiner 1998, Aguzzi and Calella 2009, Colby and Prusiner 2011, Whitechurch et al. 2017) .

The protein-only hypothesis proposes that prions consist only of protein and self-replicate without any nucleic acids (Safar et al. 2005b, Ma and Wang 2014). There is still some controversy about the protein-only hypothesis. Some researchers suppose that prion diseases are caused by slow viruses (Manuelidis 2007, Manuelidis et al. 2007), a self-replicating nucleic acid bound to PrP (Virino) (Dickinson and Outram 1988) or bacteria (Tiwana et al. 1999, Bastian and Foster 2001). Nonetheless, the protein-only hypothesis is widely accepted in the prion field (Aguzzi and Calella 2009, Soto 2011).

While in mammals prions are definitely fatal pathogens, in lower eukaryotes they can be either harmful or beneficial to the host organism (True and Lindquist 2000, True et al. 2004, Tyedmers et al. 2008). Indeed, this concept has been exploited to study the replication and transmission of amyloid proteins of these organisms (Halfmann et al. 2012, Hofmann and Vorberg 2013, Krauss and Vorberg 2013).

The natural function of PrP is still poorly understood. Prion diseases exist in genetic, sporadic and acquired forms. Prions replicate when normal cellular prion protein (PrP^{C}) (Figure 1.3.1) misfolds into the disease-causing form (PrP^{Sc}) (Figure 1.3.1). PrP^{Sc} accumulates to high levels in the nervous system leading to nervous system dysfunction, neurodegeneration and eventually to death. Monomeric PrP^{Sc} forms dimers, then oligomers and finally large aggregates and amyloids (Figure 1.3.1). The amyloids can fragment to build seeds for transmission (Prusiner 1998, Fields et al. 2001, Aguzzi and Calella 2009, Colby and Prusiner 2011, Biasini et al. 2012, Prusiner 2013, Whitechurch et al. 2017).

The singularity of prions compared to other pathogens like bacteria and viruses is that prions consist only of protein and are free from nucleic acids (Safar et al. 2005b). Furthermore, prions are nonimmunogenic. The misfolded, pathogenic isoform of the prion protein fails to activate an immune response in mammals, like that caused by bacteria and viruses (Prusiner et al. 1993). Prion disease infection from one species to another is restricted by the so called species barrier. Crossing

to another species is more likely if the evolutionary relationship between host and new recipient is close so that their PrP sequences are very similar (Scott et al. 1989). Astonishingly, this one protein, by misfolding, can lead to several different TSEs caused for example by mutations or polymorphism in the prion protein sequence or spontaneous misfolding. But even for the same prion disease like scrapie there are many different strains. Prion strains are phenotypic TSE variants causing disease with consistent characteristics, including specific incubation times and brain lesions. Importantly, different strains cannot be encoded by nucleic acid sequence or primary structure of the protein (Pattison and Millson 1961, Aguzzi et al. 2007). The strain difference has to be somehow encoded by higher structure conformations of PrP^{Sc} (Prusiner 1991, Telling et al. 1996, Whitechurch et al. 2017).

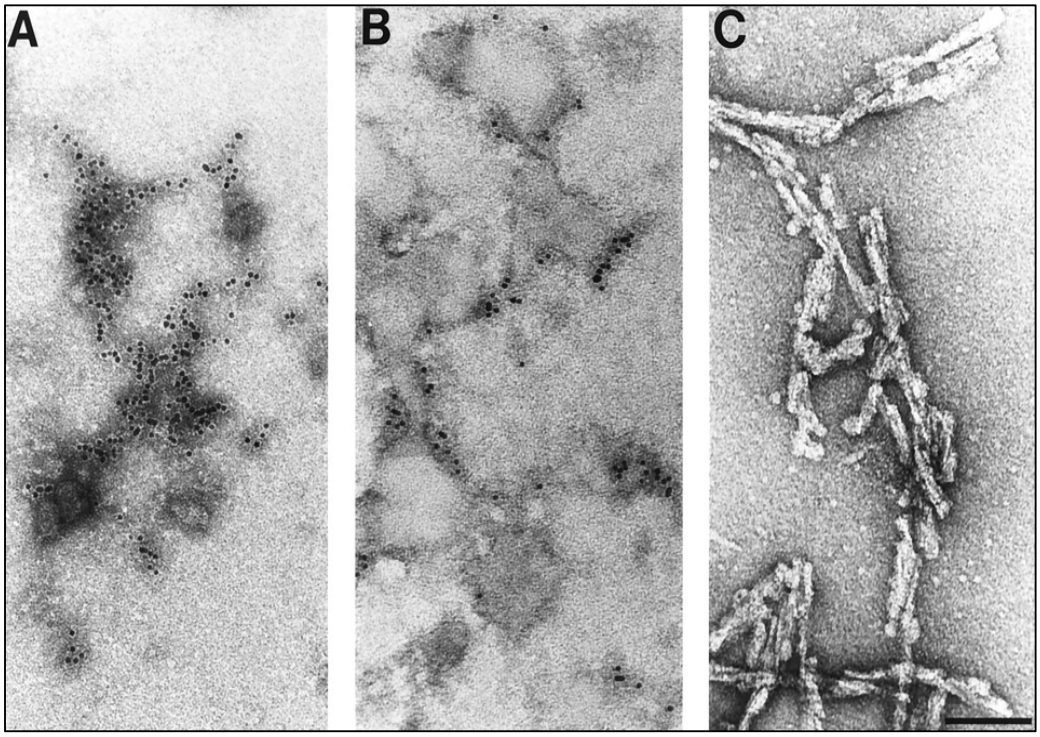

Figure 1.3.1: Electron microscopy of negatively stained and ImmunoGold labeled prion proteins. A. PrP^{C}, B. PrP^{Sc}, C. Prion aggregates consisting mainly of PrP 27–30; bar: 100nm (Prusiner 1998)

1.3.2 Prion protein gene

PrP is encoded by the nuclear gene *PRNP* (human: chromosome 20) / *Prnp* (mouse: chromosome 2) (Sparkes et al. 1986). *Prnp* is known in many species and its sequence is evolutionary highly conserved (Krakauer et al. 1996, van Rheede et

al. 2003). The complete open reading frame (ORF) of all mammalian PrP genes is located within one exon (Linden et al. 2008). Mouse, rat, bovine and sheep PrP genes consist of three exons, the last exon contains the ORF and the 3'untranslated region (UTR). Human *PRNP* and hamster *Prnp* have two exons and, again, the terminal exon contains the ORF. Gene expression is controlled by sequences in the 5'flanking region, within the first intron and sequences in the 3'UTR (Figure 1.3.2) (Linden et al. 2008, Damberger et al. 2011).

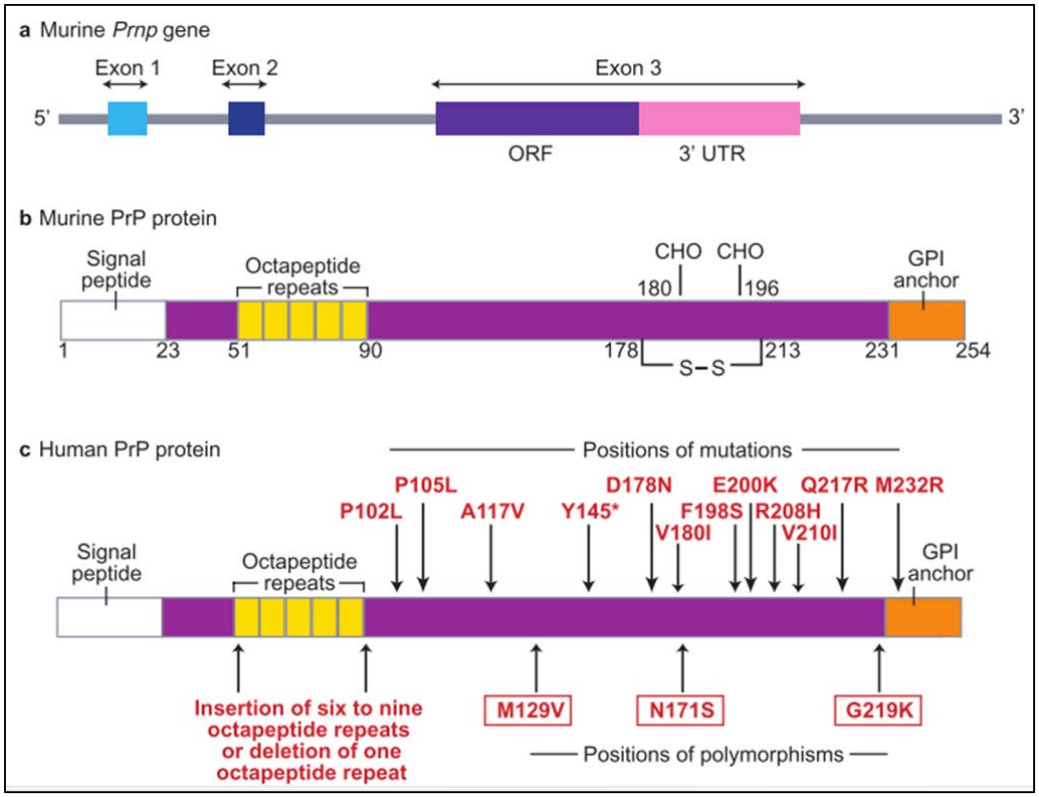

Figure 1.3.2: A. The murine *Prnp* gene consists of 3 exons. Exon 3 contains the complete ORF and a 3'UTR. B. Murine PrP consists of 254 amino acids including a 22 amino acid signal peptide, five octapeptide repeats, one disulfide bond (S-S) between cysteine residues 178 and 213 and two potential sites for glycosylation (CHO) at residues 180 and 196. A GPI anchor is attached to the C-terminus of PrP at residue 231, replacing residues 232 to 254. C. Human PrP is 253 amino acids long with the same features as the mouse PrP. This diagram shows polymorphisms (boxes under the gene) and insertions, deletions and point mutations in the human PrP linked to familial prion disease. The asterisk (*) indicates a mutation caused stop codon and therefore a truncated protein. (Modified figure) (Manson and Tuzi 2001)

PrP is expressed in many different tissues (skeletal muscle, kidney, heart, secondary lymphoid organs), but is most abundant in the adult central nervous system (Oesch et al. 1985, Ford et al. 2002, Peralta and Eyestone 2009). However, only a few cell types support aggregation of PrP^{Sc}, namely neurons, myocytes,

follicular dendritic cells, B-lymphocytes and perhaps astrocytes (Kitamoto et al. 1991, Raeber et al. 1999, Bosque et al. 2002, Ford et al. 2002, Heikenwalder et al. 2005, Jackson et al. 2014).

1.3.3 Prion protein

The human *PRNP* gene encodes a 253 amino acid long precursor protein. The mature human PrP^{C} is 208 amino acids long and has one disulfide bond and a sequence for addition of a glycophosphatidylinositol (GPI) anchor. The 22 amino acid long N-terminal signal peptide is cotranslalionally cleaved off during synthesis in the endoplasmic reticulum. Once inside the endoplasmic reticulum, a 23 amino acid GPI anchor signal sequence is cleaved off the C-terminus during the addition of the GPI anchor to PrP. Then, the GPI anchor facilitates the attachment to the cell membrane (Stahl et al. 1990, Linden et al. 2008). The N-terminal region of PrP contains an octapeptide repeat region (Figure 1.3.3.1). The structure of PrP is mainly alpha-helical (40% alpha helical, little beta-sheet structure). The molecular mass of PrP is 35-36 kDa. Due to two asparagine sites the protein can have zero, one or two glycans, resulting in PrP appearing on western blots with a three band pattern (Endo et al. 1989, Linden et al. 2008).

The pathogenic isoform, PrP^{Sc}, has the same primary sequence as PrP^{C}, but differs in the secondary and tertiary structure (Linden et al. 2008). The exact structure is not known, but PrP^{Sc} has more beta-sheet structure (45% beta-sheet, 30% alpha-helical structure) which somehow makes it partially resistant to proteolysis (Figure 1.3.3.1, Figure 1.3.3.2) (Pan et al. 1993).

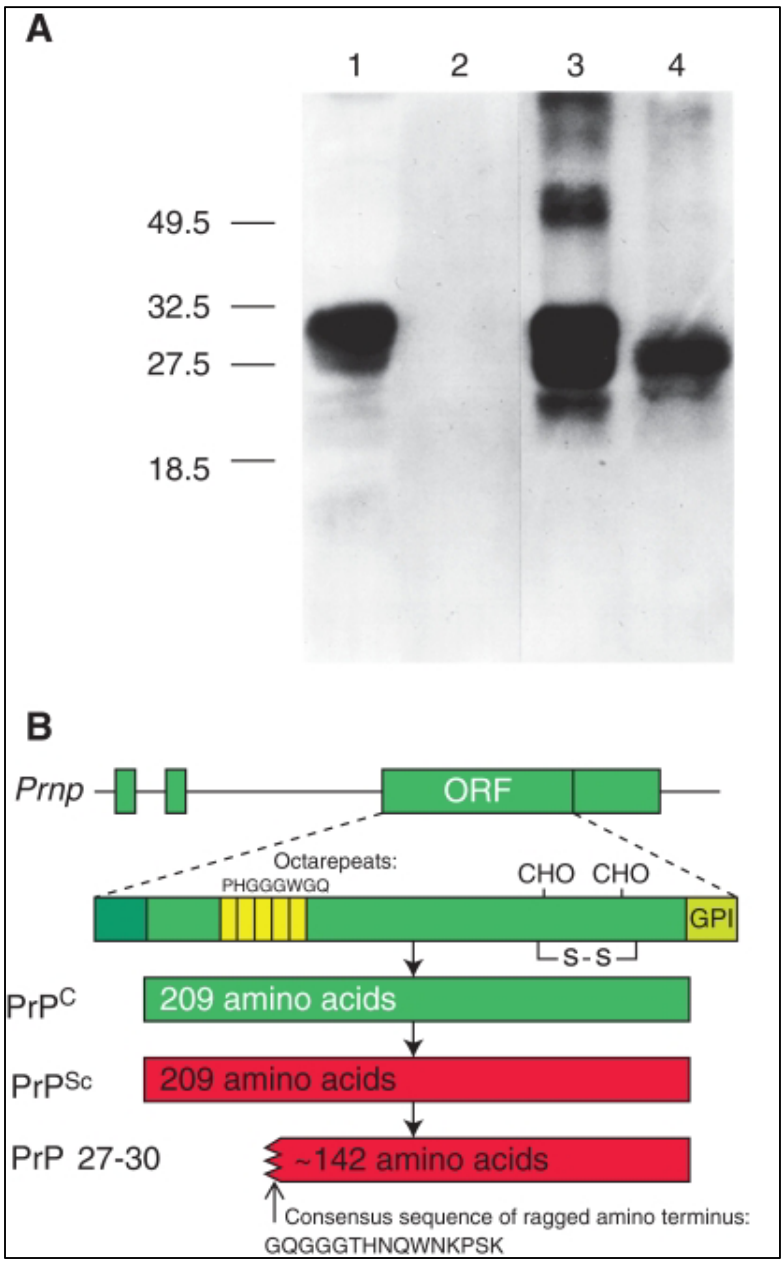

Figure 1.3.3.1: A. Western blot of brain homogenates of not infected (lane 1+2) and prion infected (lane 3+4) Syrian hamsters. Lanes 2+4 were proteinase K treated, completely hydrolyzing PrP^{C} (lane 2) and generating PrP 27-30 out of PrP^{Sc} (lane 4). B. Diagrams of hamster *Prnp* gene and isoforms. (Colby and Prusiner 2011)

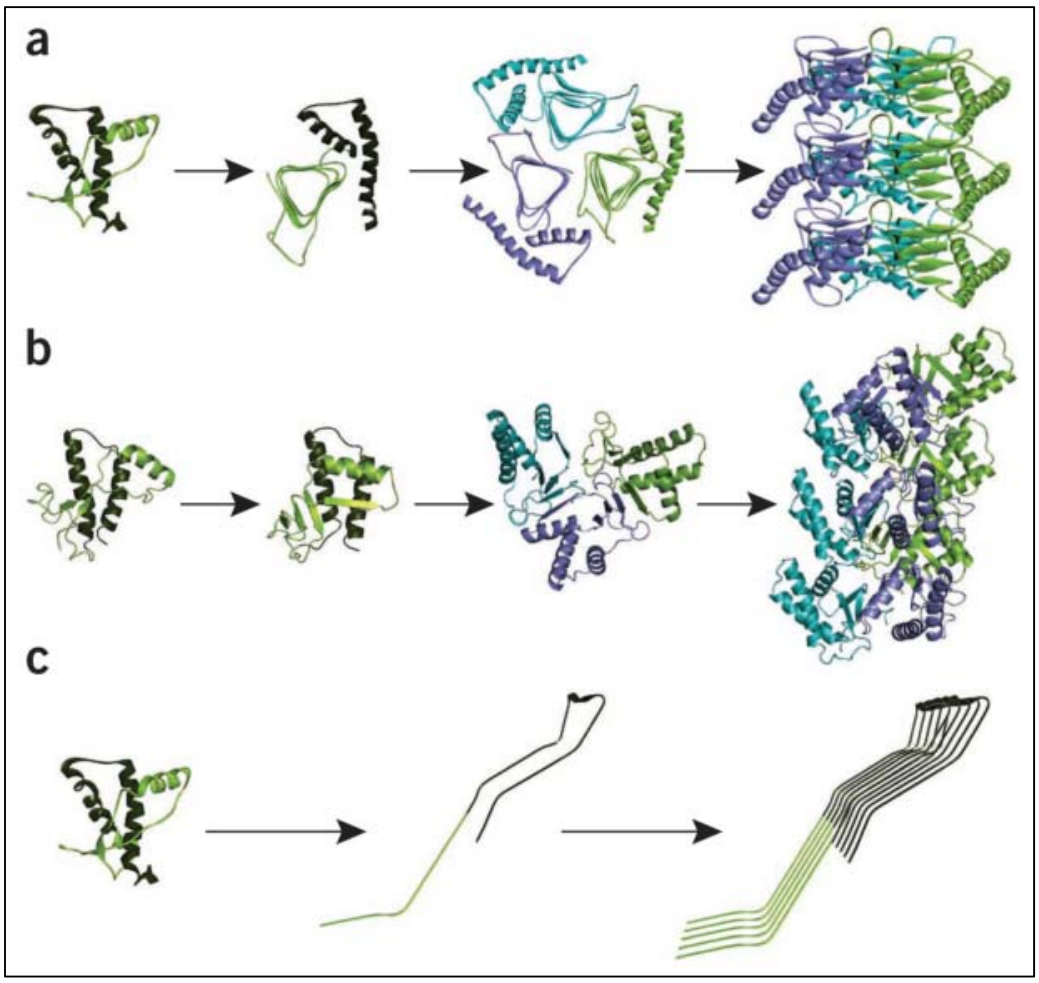

Figure 1.3.3.2: Predicted models for the PrP^{Sc} structure. A. Beta-helical model with proposed refolding of the N-terminus of PrP 27-30 (residues 9-177) into a beta-helical structure (light green). The C-terminus (residues 178-230) keeps its α-helical structure (dark green). B. The "beta-spiral model" predicted by molecular dynamics simulation contains a spiraling core of extended short beta-strand sheets. C. The "parallel in-register extended beta-sheet model" predicts a structure containing mainly beta-sheets. In all panels the corresponding motifs are indicated by the same color. (Diaz-Espinoza and Soto 2012)

1.3.4 Prion replication

Prions replicate by a poorly understood mechanism where PrP^{C} converts into the pathogenic PrP^{Sc}. Monomeric PrP^{Sc} forms dimers, then oligomers and finally large aggregates and amyloids. There are two models of prion replication; the refolding and the seeding model (Figure 1.3.4) (Weissmann et al. 2002, Aguzzi and Sigurdson 2004, Weissmann 2004, Aguzzi and Calella 2009).

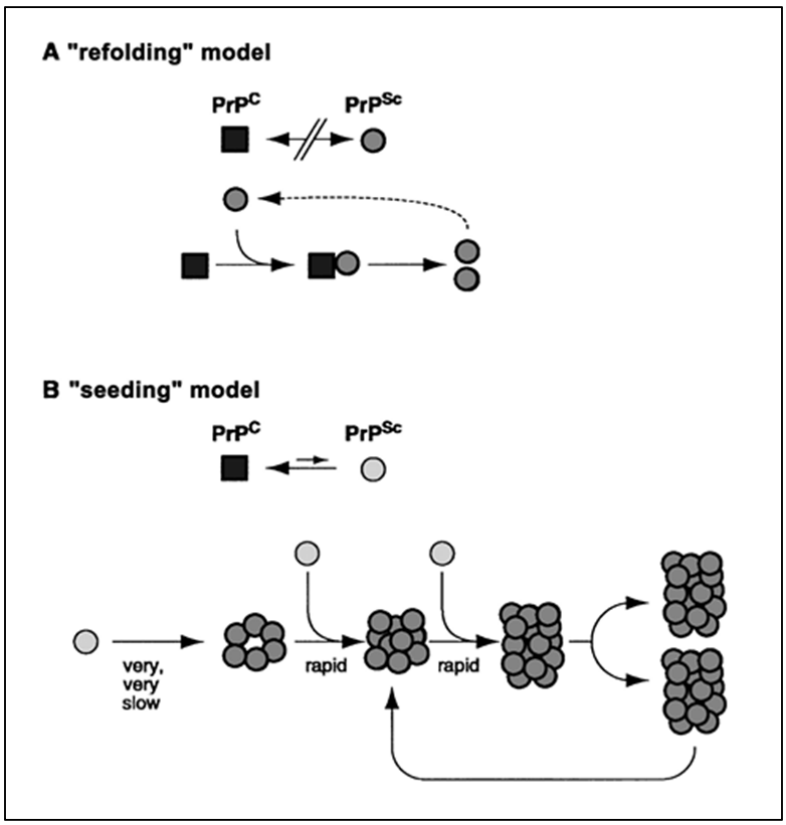

Figure 1.3.4: A. The refolding model of prion replication postulates an interaction between PrP^{Sc} and PrP^{C}, which is induced to transform into more PrP^{Sc}. B. The seeding model of prion replication proposes that PrP^{C} and PrP^{Sc} form an equilibrium, in which PrP^{C} is highly in favor. If monomeric PrP^{Sc} aggregate, more monomeric PrP^{Sc} can be recruited. (Weissmann et al. 2002)

The refolding or template-directed assistance model of prion replication postulates an interaction between PrP^{Sc} and PrP^{C}, in which PrP^{C} is induced by PrP^{Sc} to transform itself into more PrP^{Sc}. PrP^{C} and PrP^{Sc} form in the process a heterodimer and PrP^{Sc} acts as a folding template. The emerging PrP^{Sc} homodimer divides into more folding templates (Weissmann et al. 2002, Aguzzi and Sigurdson 2004, Weissmann 2004, Aguzzi and Calella 2009).

The seeding or nucleation–polymerization model of prion replication proposes that PrP^{C} and PrP^{Sc} form a reversible thermodynamic equilibrium. The equilibrium would be shifted towards PrP^{C} in a healthy state with low levels of PrP^{Sc}. Only if monomeric PrP^{Sc} aggregates, more monomeric PrP^{Sc} can be recruited for potential aggregation. In this case monomeric PrP^{Sc} would not be infectious, only the aggregated seeds would have infectivity (Weissmann et al. 2002, Aguzzi and Sigurdson 2004, Weissmann 2004, Aguzzi and Calella 2009).

There was also a method invented to replicate prions *in vitro*, called protein misfolding cyclic amplification (PMCA), which works in technical sense like

polymerase chain reaction (PCR) does for DNA. In PMCA a small amount of misfolded prion protein is incubated with an excess of PrP^{C}, so that transformation from PrP^{C} in PrP^{Sc} can take place. The growing PrP^{Sc} aggregates are treated with ultrasound to fragment them into smaller seeds to cause more transformation. By repeating the cycle PrP^{C} is rapidly transformed into misfolded prions (Saborio et al. 2001, Saa et al. 2006).

The rate of prion replication depends on many factors. Prion formation is inversely related to the incubation time length and correlates to the PrP expression level in the brain and the amount of PrP^{Sc} template. The PrP sequence itself is another factor, the more identical the sequences of PrP^{C} and PrP^{Sc}, the faster the prion replication. Prion replication also depends on the present prion strain. Prion strains differ in incubation time and therefore also in prion formation. Reasons for these strain differences could be the different conformations of PrP^{Sc}, stability of PrP^{Sc}, targeting of PrP^{Sc} to replication competent cells and the PrP^{Sc} clearance rate (Masel et al. 1999, Fields et al. 2001, Aguzzi and Sigurdson 2004, Aguzzi and Calella 2009).

It is also discussed in prion research if an auxiliary protein or cofactor is needed for prion replication. There are some arguments for this hypothesis (Prusiner 1998, Colby and Prusiner 2011). For example, prion formation is restricted to some cell types, even though PrP is widely expressed (Kitamoto et al. 1991, Bosque et al. 2002, Heikenwalder et al. 2005). Furthermore, only a few PrP expressing cell lines can be infected by prions (Beranger et al. 2001, Grassmann et al. 2013, Krauss and Vorberg 2013). Moreover, polyanions, lipids or lipid-like molecules are important cofactors for *in vitro* amplification of the infectious Prp^{Sc} (Ma 2012, Wang and Ma 2013). Therefore PrP expression is necessary but not sufficient for prion replication (Giri et al. 2006).

1.3.5 Prion strains, prion infectivity, neurotoxicity and species barrier

Prion strains are phenotypic TSE variants causing disease with consistent characteristics like incubation time, pattern of PrP^{Sc} and spongiosis distributions and severity of spongiosis in the brain. Prion strains carry a molecular thumbprint based on the size of the proteinase K resistant PrP^{Sc} fragments, as detectable by western blot, and these differ between strains (Aguzzi et al. 2007). The different strains cannot be encoded by nucleic acid sequence or primary structure of the protein. The strain difference has to be somehow encoded by PrP^{Sc}, probably as different

disease related conformations (Figure 1.3.5A) (Pattison and Millson 1961, Prusiner 1991, Aguzzi et al. 2007). These different conformations might be responsible for the various distinct characteristics of prion strains caused by stability of PrP^{Sc}, targeting of PrP^{Sc} to replication competent cells and the PrP^{Sc} clearance rate (Safar et al. 1998, Masel et al. 1999, Aguzzi et al. 2007, Aguzzi and Calella 2009). The glycosylation state of PrP could also be responsible for different prion strains, so that di-, mono- or unglycosylated PrP determine the structure of the emerging seeds and aggregates (Collinge 2005, Wiseman et al. 2005, Tuzi et al. 2008, Wiseman et al. 2015).

In the process of neurodegeneration, prions appear to spread from an infected neuron to uninfected neurons and to other brain regions via anterograde axonal transport to axon terminals (Bouzamondo-Bernstein et al. 2004). Thereby, prions accumulate in the nervous system, which leads to neurotoxicity and neurodegeneration. Neurodegenerative processes include presynaptic bouton degeneration, dendritic atrophy, vacuolation of neurons and hypertrophy of astrocytes, leading finally to cell death (Jendroska et al. 1991).

Although, prions consist of PrP^{Sc}, it is not necessarily the infectious unit that is neurotoxic. The infectious and / or toxic unit can contain primarily or exclusively PrP^{Sc}, it may be formations or intermediate products of PrP^{Sc} like oligomers or amyloid fibrils or even complexes with other cofactors (Prusiner 1998, Aguzzi et al. 2007, Colby and Prusiner 2011). Also the loss of function of the misfolded PrP could result in neurotoxicity (Aguzzi et al. 2007). Particles with masses of 14-28 PrP molecules, often called oligomers, appear to have the most infectivity (Silveira et al. 2005). However, even a monomeric, alpha-helical prion protein species can be toxic (Lasmezas and Zhou 2012). Therefore, the direct cause of neurotoxicity in TSEs remains unclear.

Prions isolated from one species are often less infectious to other species, demonstrated by longer incubation times and reduced attack rates (Aguzzi et al. 2007). This phenomenon is known as the species barrier and it depends on the different PrP sequences and structure of the host and the new recipient. The more different the PrP sequences are, the stronger the species barrier is (Aguzzi et al. 2007). With serial passages incubation times can decrease, a phenomenon called adaptation. With a very potent species barrier the new inoculated host shows no disease phenotype and stays healthy. However, brain isolates of these healthy, disease resistant animals can transmit disease to new susceptible animals. So they act as subclinical carriers (Figure 1.3.5B) (Aguzzi et al. 2007). The species barrier can be reduced by very high expression levels of heterologous PrP (Sigurdson et al.

2006). Interestingly, even hosts from the same species can show different incubation times and attack rates due to certain mutations or polymorphisms of their *Prnp* gene, known as transmission barrier (Figure 1.3.5B) (Aguzzi et al. 2007).

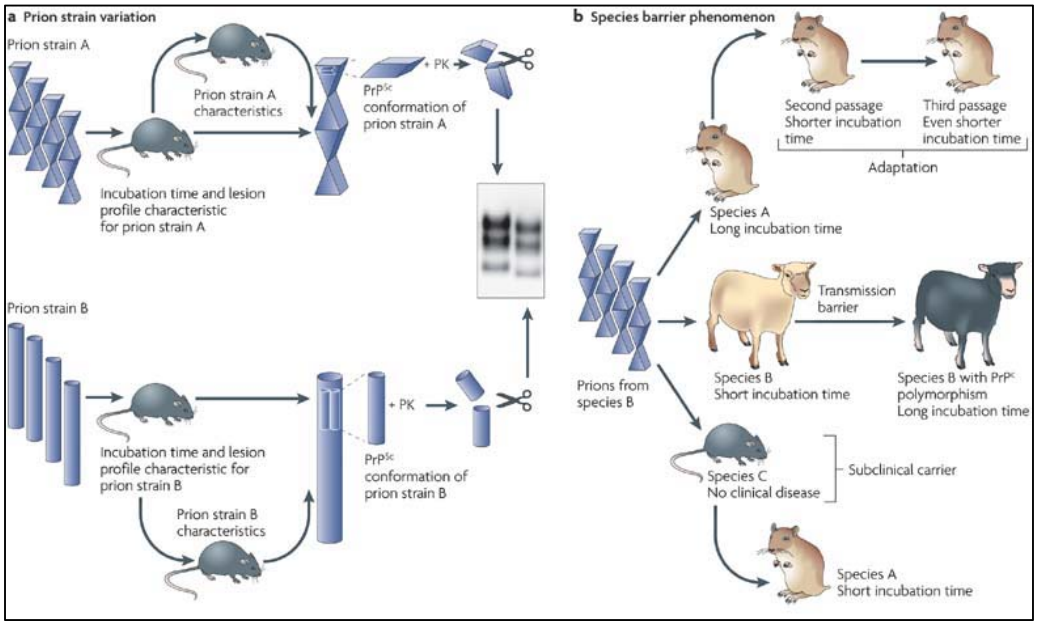

Figure 1.3.5: A. Different prion strains / isolates result in distinct disease phenotypes in identical hosts. These features persist in passages to new hosts. Strains can exhibit characteristic biochemical signatures because of different PrP^{Sc} conformations. B. Prions from one species are often less infectious to other species. This depends on different host PrP sequences. With serial passages incubation times decrease (adaption). With a potent species barrier the new inoculated host stays healthy. Brain isolates of these subclinical carriers can transmit disease to susceptible new hosts. Hosts from the same species can show different incubation times due to certain mutations or polymorphisms of the *Prnp* gene (transmission barrier). (Aguzzi et al. 2007)

One example well known in the general public of a bypass of the species barrier was the BSE crisis in the Eighties and Nineties in Europe, especially in the United Kingdom. Humans developed an unusual prion disease called variant CJD from consuming food contaminated with BSE from diseased cattle showing the zoonotic potential of prions. This prion disease features a relatively short incubation time and, surprisingly, the victims were much younger compared to those with other prion diseases. Humans infected with variant CJD had a specific *PRNP* genotype; they were homozygous for methionine at codon 129 (Hill et al. 1997, Heath et al. 2010, Takeuchi et al. 2013). Homozygosity for methionine at codon 129 of *PRNP* is thought to be a risk factor for human prion disease, approximately 40% of the Caucasian population has this *PRNP* genotype (Ward 2000, Bishop et al. 2009). However, if only this genotype is susceptible to variant CJD is uncertain. The

incubation time of CJD caused by BSE contaminated food for other *PRNP* genotypes might just be longer (Collinge 1999, Collinge 2005).

1.3.6 Prion protein function

The function of endogenous PrP is still poorly understood. Earliest studies reported that *Prnp* knock-out mice are healthy with normal development and lifespan and without any abnormalities (Bueler et al. 1992, Manson et al. 1994a). However, more recent studies have shown some abnormalities. One study showed abnormal sleep/wake cycles and altered circadian rhythm in mice lacking PrP (Tobler et al. 1996, Tobler et al. 1997). Another study reported deficits in long-term potentiation and learning (Criado et al. 2005). Also, different behavioral (decreased anxiety, increased locomotor and exploratory activity) and cellular abnormalities (reduced number of mitochondria, abnormal mitochondria, increased phagocytosis) could be shown (Steele et al. 2007b).

PrP seems to have a neuroprotective function because the absence of PrP contributes to an increased susceptibility to oxidative stress or apoptosis (Roucou et al. 2004, Biasini et al. 2012). Therefore, a putative function as a regulator of apoptosis and also immune system / immune response was proposed (Aguzzi and Polymenidou 2004). Furthermore, PrP could have a function in signal transduction and as growth factor for axons, neurites and dendrites to support neuronal polarity (Chen et al. 2003, Stuermer et al. 2004, Kanaani et al. 2005). PrP was also described to have functions in the self-renewal of long term repopulating haematopoietic stem cells and as a regulator of neural precursor proliferation during development and neurogenesis (Steele et al. 2006, Zhang et al. 2006). A function as a copper transporter has been discussed since the octapeptide repeat region of PrP can bind copper (Hornshaw et al. 1995, Requena et al. 2001).

1.3.7 Prion disease therapeutics

TSEs are always fatal and no therapies exist to stop or slow the disease. For inherited prion diseases molecular biology enables the indentification of people at risk because of mutations or polymorphisms in the *PRNP* even decades before symptoms occur (Chapman et al. 1994, Spudich et al. 1995, Prusiner 1998, Fields et al. 2001, Colby and Prusiner 2011). Therefore, carriers of *Prnp* mutations would be ideal candidates for the development of therapies.

There are several ways prion diseases may be altered by developing therapeutics. First, reduction of PrP^C levels prolongs incubation time (Bueler et al. 1993, Prusiner et al. 1993, Manson et al. 1994b, Safar et al. 2005a). Second, slowing down PrP^{Sc} formation also prolongs the incubation time (Kawasaki et al. 2007). Third, reducing the availability of PrP^C in prion infected cells allows for clearance of prions (Enari et al. 2001, Peretz et al. 2001, Safar et al. 2005a). Fourth, improvement of the PrP^{Sc} clearance would be useful as therapy (Supattapone et al. 1999, Supattapone et al. 2001).

Blocking the formation of PrP^{Sc} would be one approach promising for therapeutics. Thus, there are many potential therapeutic targets. Indeed, many compounds inhibiting conversion of PrP^C to PrP^{Sc} have been found (polysulfated anions, dextrans, Congo red dye, oligonucleotides and cyclic tetrapyrroles). But for an effective treatment an adequate access of the compounds to the nervous system is required (Fields et al. 2001, Trevitt and Collinge 2006, Sim and Caughey 2009, Colby and Prusiner 2011). Tricyclic derivatives of acridine, like quinacrine or chlorpromazine, inhibit prion formation. They can pass the blood brain barrier and therefore become candidates for prion disease treatment (Korth et al. 2001).

Also, recombinant antibodies and antibody fragments are tested for prion disease treatment. But here the passage through the blood brain barrier remains problematic (Peretz et al. 2001). Another therapeutic approach is the use of RNA interference, a method to silence posttranscriptionally gene expression in a sequence-specific manner. With help of this mechanism gene expression of PrP^C can be reduced and it could be shown that this reduction lead to neuronal rescue, prevention of symptoms and increased survival in prion diseased mice (Kong 2006, White and Mallucci 2009). However, for therapeutic approaches a better understanding of the mechanism of aggregation and toxicity of the disease related proteins is needed.

1.3.8 Scrapie

Scrapie, one of several TSEs in animals, was first reported in 1732 (Liberski 2012). It is a fatal and degenerative disease affecting the nervous system of sheep and goat. It is infectious and transmissible among conspecifics, but not infectious to humans even if humans eat infected meat of these animals (Detwiler 1992, Detwiler and Baylis 2003). Clinical signs of scrapie are the eponymous fleeces scraping off, itching sensation, lip smacking and an altered gait (Foster et al. 2001). Probable transmission routes are oral uptake of scrapie contaminated material, the admission

of scrapie material via skin lesions and the intrauterine transmission from the mother to the lamb (Detwiler and Baylis 2003). For scrapie, several prion stains are known with different incubation times and symptoms (Pattison and Millson 1961). The transmission of scrapie as a model disease into various animal models, especially rodents, has led to a better understanding of prion diseases and disease mechanism in the prion field (Foster et al. 2001).

The mouse adapted Rocky Mountain Laboratory scrapie strain (RML) is a well-known and commonly used model of prion disease. RML is highly precise and, although it is a slowly progressing disease, all mice become terminally ill within a very small time frame (Di Bari et al. 2012).

1.4 RiboTag

RiboTag is a method to isolate cell-type-specific, ribosome associated, actively translated mRNA from complex tissue. This is accomplished by expressing in specific cell types a modified ribosome protein that carries an antibody epitope and incorporates into translating ribosomes (Sanz et al. 2009). In the RiboTag mice the genetically engineered large subunit ribosomal protein 22 (Rpl22) has a floxed (flanked by loxP sites) wild type terminal exon (exon 4) followed by a copy of this exon with three copies of the hemagglutinin (HA) epitope before the stop codon (Figure 1.4.1). The HA epitope tag is derived from human influenza virus hemagglutinin protein, corresponding to amino acids 98-106 (nucleotide sequence: 5'-TACCCATACGATGTTCCAGATTACGCT-3'; amino acid sequence: YPYDVPDYA).
When the RiboTag mouse is crossed to a Cre recombinase expressing mouse, expression of the epitope-tagged ribosomal protein version is activated (Figure 1.4.1). By using a cell-type-specific Cre recombinase expressing mouse (Cre driver mouse, expression of Cre recombinase under control of a cell-type-specific promotor), expression of the epitope-tagged ribosomal protein version is activated in a cell-type-specific manner (Figure 1.4.2). The RiboTag bearing ribosomes and the mRNAs attached to them are affinity purified by immunoprecipitation (IP) from crude brain homogenates and the attached mRNAs are then isolated for following analyses (Sanz et al. 2009).

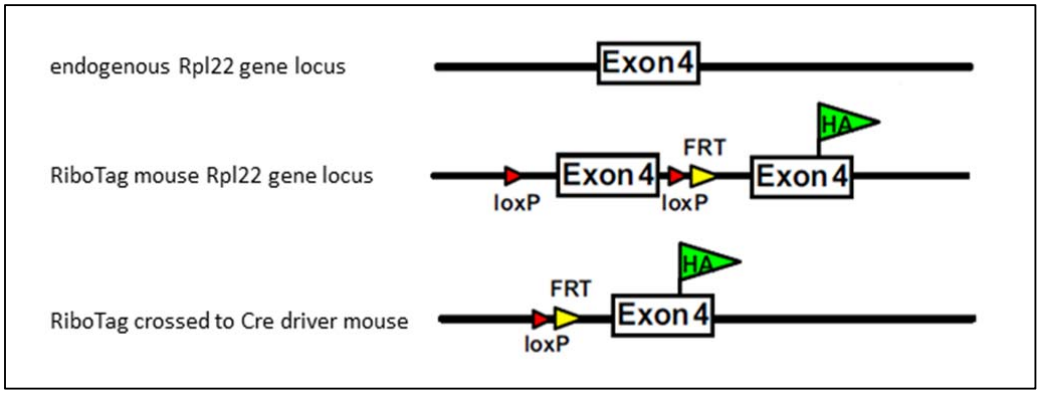

Figure 1.4.1: Endogenous Rpl22 gene locus (top), engineered RiboTag mouse Rpl22 gene locus with floxed wild type exon 4 followed by a copy of the wild type exon 4 with hemagglutinin epitope tag (middle) and the RiboTag mouse after crossing to a Cre driver mouse (bottom). (Modified figure) (Sanz et al. 2009)

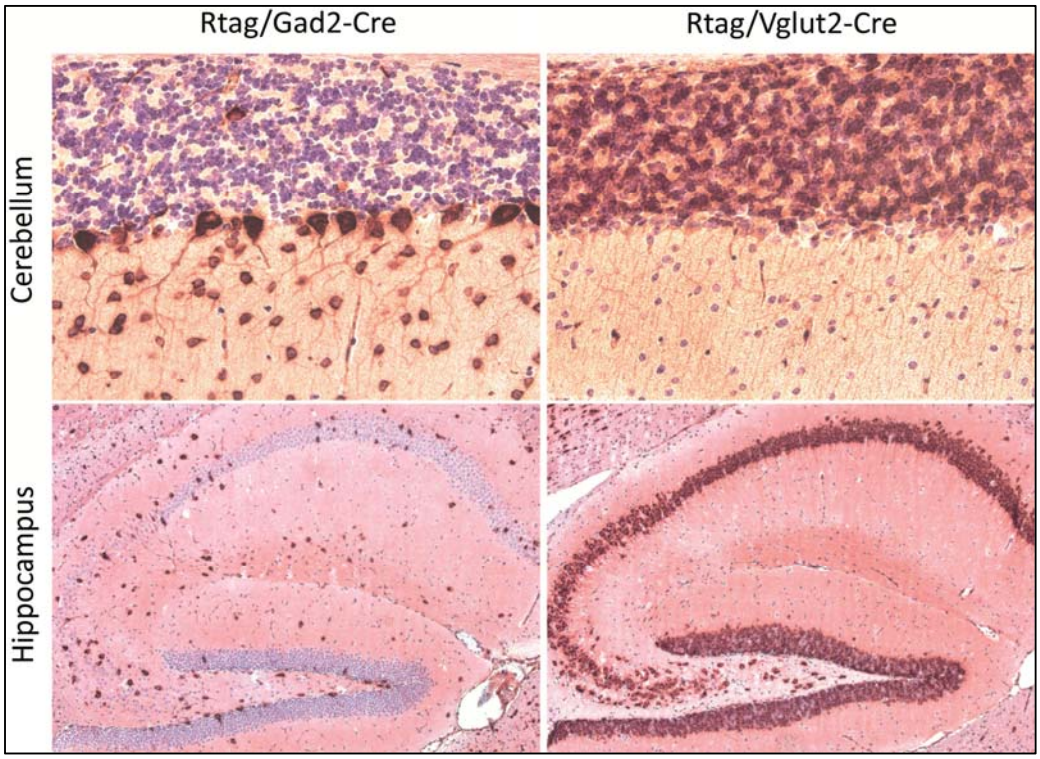

Figure 1.4.2: Immunohistochemistry staining of 4µm thick brain sections from RiboTag mice crossed to Gad2-Cre mice (left) or Vglut2-Cre mice (right). Staining with anti-HA antibody (red) to detect cells with expression of epitope-tagged ribosomes showing the cell-type-specific expression in GABAergic neurons (left) or glutamatergic neurons (right) in cerebellum and hippocampus (counterstain: hematoxylin). (Walker Scot Jackson, AG Jackson, DZNE Bonn)

This powerful tool accomplishes two special objectives at once. First it can capture mRNA from specific cell types, and second it specifically captures mRNAs that are being actively translated, which correlates with the proteome much better than total

mRNAs (Battle et al. 2015). Furthermore, since frozen tissues can be used, mRNA is well preserved, which can be difficult to achieve with methods that physically separate cells or cell bodies or other secluded cell compartments like axons or synapses. In addition, by engineering the mouse line the endogenous gene was modified and no random insertion of constructs into the mouse genome was done. Expression of the tagged ribosomal protein is still under control of the endogenous Rpl22 promotor. Therefore, the expression level and the expression locations are under native conditions (Sanz et al. 2009).

1.5 Next generation sequencing

DNA-sequencing is a biomolecular method to determine the exact order of nucleotides in a DNA molecule. After using the classical applications from Maxam and Gilbert or Sanger (Maxam and Gilbert 1977, Sanger et al. 1977), DNA-sequencing methods were further developed to become faster, cheaper, more accurate and also easier to operate as a high-throughput application. These new methods were called next generation sequencing and are employed for genome sequencing, transcriptome analysis, DNA-protein interactions and epigenome analysis (Mardis 2008, Pettersson et al. 2009, Liu et al. 2012).

For our study RNA-sequencing with Illumina sequencing method was used. Illumina sequencing consists of three basic steps: sample preparation, DNA cluster generation and sequencing (Figure 1.5).

In this method the isolated RNA is reverse transcribed into cDNA. The cDNA is fragmented into smaller molecules and ligated with different DNA adapter sequences at their ends. The adapters allow a reduced cycle amplification to add motifs to the cDNA fragments (sequencing primer binding sites, indices, complementary sequences to the flow cell oligonucleotides). The modified cDNA is loaded on a flow-cell where the DNA molecules can bind to the oligonucleotides on the plate. cDNA fragments are isothermally amplified by bridge amplification. Bridge amplification is repeated over and over again to build a DNA cluster on the flow cell. In the sequencing step the sequencing primer is extended step by step with four different fluorophor-coupled nucleotides. The process is called sequencing by synthesis. In each step the flow-cell is excited with a light source and emitted signal from every cluster on the flow cell is detected (Mardis 2008, Pettersson et al. 2009, Voelkerding et al. 2009, Liu et al. 2012).

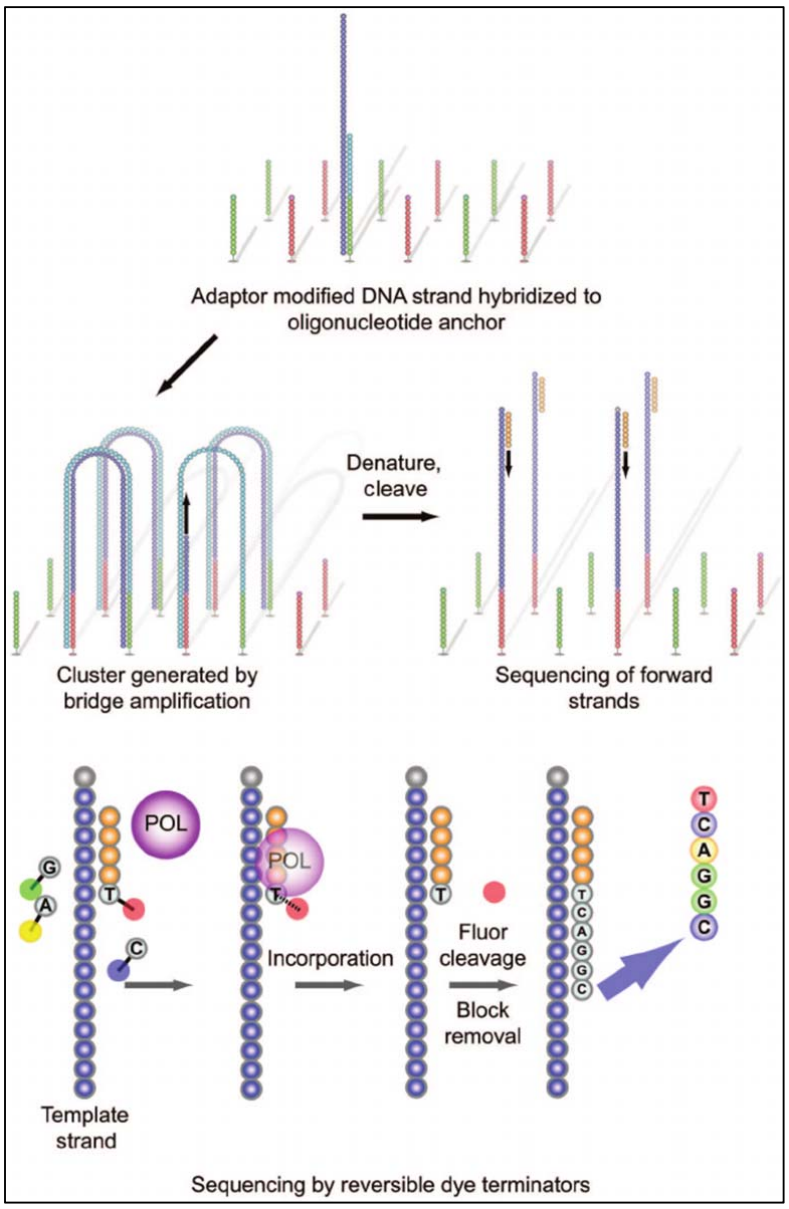

Figure 1.5: Adapter-modified DNA fragments are bound on a flow-cell for Illumina sequencing. cDNA fragments are isothermally amplified by repeated bridge amplification to build DNA clusters. Sequencing by synthesis is done with extension of the sequencing primer step by step with four different fluorophor-coupled nucleotides and emitted signal from each cluster is detected in every extension step. (Voelkerding et al. 2009)

2. Aim of study

Specific brain regions possess specific brain cells and we hypothesize that the phenomenon of selective vulnerability is caused by these specific brain cells in these regions having unique strategies and capacities to cope with various disease related conformers. We also hypothesize that next to the complete proteasome the protein quality control machinery differs between different cell types due to different compilations of machinery components and clients and these differences strongly influence selective vulnerability.

In this study infection with the RML scrapie strain was used as a model of neurodegenerative disease to investigate how gene expression in specific cell types in the mouse brain respond to an ensuing neurodegenerative disease. RML was chosen as our disease model because it is a well-known and commonly used disease model, highly precise and, although it is a slowly progressing disease, all mice become terminally ill within a very small time frame (Di Bari et al. 2012, Prusiner 2012). In addition, the hallmarks of RML infection in mice like prion aggregates, gliosis and spongiosis are similar to those ones occurring in human TSEs (Jackson et al. 2009).

To analyze the response to RML infection in a cell-type-specific manner the advantage of the RiboTag method was used. Mice expressing the epitope-tagged ribosomes in astrocytes (Astro) or subsets of neurons, including glutamatergic (Glut), GABAergic (GABA), parvalbumin (PV) or somatostatin neurons (SST) were used for this study. These cell types were chosen because GABAergic neurons were reported to be most vulnerable in different genetic NDs (Ferrer et al. 1993, Guentchev et al. 1997, Guentchev et al. 1998, Guentchev et al. 1999), because SST and PV neurons are abundant but mostly non overlapping GABAergic neuron subtypes and because the glutamatergic neurons provide an informative contrast. Astrocytes are studied because they undergo remarkable transformations during NDs and identifying the molecular underpinnings of these changes will also be important for a fuller understanding of disease mechanisms.
After selection of disease time points changes to gene expression were analyzed by next generation sequencing at a stage when clinical signs first become apparent and at a much earlier stage in the disease process. Neuropathological changes were investigated by specific IHC stainings.

This work gives clues into which brain cells are affected earliest and most severely and how they respond to the emerging disease. Investigating cell-type-specific mechanisms of selective vulnerability are needed for understanding NDs and developing therapies. A better understanding of ND mechanisms and development of therapies are absolutely essential because NDs currently take up a massive amount of money spent on health care and the ever-expanding aged population will amplify this problem in the future (Taylor et al. 2002, Andlin-Sobocki et al. 2005, Brookmeyer et al. 2007, Katsuno et al. 2012, Panegyres and Armari 2013).

3. Material and methods

3.1 Biosafety and animal experimentation

The major work was performed at German Center for Neurodegenerative Diseases (Deutsches Zentrum für Neurodegenerative Erkrankungen, DZNE, Bonn). All work was done under biosafety containment level 2 (S2) according to the German law (Gentechnikgesetz / Gentechnik-Sicherheitsverordnung). All potential contaminated and used equipment, reagents and material were collected, decontaminated and disposed following the official S2 regulations.
The experimental procedures were approved by the North Rhine-Westphalia State Environment Agency for Nature, Environment and Consumer Protection (Landesamt für Natur, Umwelt und Verbraucherschutz Nordrhein-Westfalen, Recklinghausen)

Reference numbers:
84-02.04.2013.A128
84-02.04.2013.A169

3.2 Mouse lines, holding and breeding

For electroencephalography (EEG) recordings and gene expression studies with the RiboTag method mice were bred and held at Federal Institute for Drugs and Medical Devices (Bundesinstitut für Arzneimittel und Medizinprodukte, Bonn). Throughout the study, mice were housed in individual ventilated cages (22°C; 60% humidity) on a standard 12h light (06:00-18:00) / 12h dark (18:00-06:00) cycle. All mice received rodent laboratory pellets and drinking water ad libitum.
For the behavioral comparison of wild type C57Bl/6N (n=24) and 129S4/SvJae (n=16) mice, animals were bred and held at the animal facility of Massachusetts Institute of Technology (MIT; Cambridge, Massachusetts, United States of America).
For EEG recordings and collateral body weight measurements ten male wild type 129S4/SvJaeJ mice were used and injected with 20µl 0.1% brain homogenate from either normal (NBH, n=5) or prion infected (RML; n=5) mice.
For gene expression analysis RiboTag mice were crossed to cell-type-specific Cre driver lines to express HA-tagged ribosomes in specific cell types. Rtag/Vglut2-Cre

mice were used for glutamatergic neurons (Glut, Cre driver: Vglut2), Rtag/Gad2-Cre for GABAergic neurons (GABA, Cre driver: Gad2), Rtag/SST-Cre for somatostatin neurons (SST, Cre driver: SST), Rtag/PV-Cre for parvalbumin neurons (PV, Cre driver: Pvalb) and Rtag/Cnx43-CreER for astrocytes (Astro, Cre driver: Cnx43). Used mice were bred heterozygous for both, RiboTag and Cre recombinase (Rtag: floxed/wild type; Cre recombinase: +/-). Heterozygosity of RiboTag and Cre recombinase was checked by genotyping. Rtag/Cre mice were in a 129S4/SvJaeJ genetic background (>99%). For each condition (5 Rtag/Cre lines, injected with 20µl 0.1% RML or NBH, sacrificed at 10 or 18 wpi) four mice were used (total n=80).

Wild type mouse lines:
129S4/SvJae for behavior, Rudolf Jaenisch (MIT)
129S4/SvJaeJ for EEG (009104), Jackson Laboratory
C57Bl/6N (B6NTac), Taconic Bioscience

Genetically engineered mouse lines:
RiboTag (B6N.129-Rpl22$^{tm1.1Psam}$/J; 011029), Jackson Laboratory
(Sanz et al. 2009)
Vglut2-IRES-Cre (Slc17a6$^{tm2(cre)Lowl}$/J ; 016963), Jackson Laboratory
(Vong et al. 2011)
Gad2-IRES-Cre (Gad2$^{tm2(cre)Zjh}$/J; 010802), Jackson Laboratory
(Taniguchi et al. 2011)
SST-IRES-Cre (Sst$^{tm2.1(cre)Zjh}$/J; 013044), Jackson Laboratory
(Taniguchi et al. 2011)
PV-Cre (B6;129P2-Pvalb$^{tm1(cre)Arbr}$/J; 008069), Jackson Laboratory
(Hippenmeyer et al. 2005)
Cnx43-CreER, Martin Theis / Klaus Willecke (Institute of Genetics, University Bonn)
(Eckardt et al. 2004)

3.3 Genotyping

The extraction of genomic DNA from mouse tail or ear tissue was done as described by Peter Laird and colleagues (Laird et al. 1991). To genotype the RiboTag and Rtag/Cre mice the PCR protocol of the original publication from Elisenda Sanz and colleagues was used (Sanz et al. 2009). Mice were genotyped for the presence of the Cre recombinase and the RiboTag allele.

For RiboTag genotyping the wild type PCR product is 260 bp long, the mutant PCR product from the floxed allele is 290 bp long. The Cre recombinase PCR product is 324 bp long.
The following PCR reaction was set up: 1µl genomic DNA (~ 50-100ng DNA), 2.5µl 10x PCR buffer, 0.2µl dNTPs, 0.2µl Primer mix; 0.2µl Taq-Polymerase, add water to a total volume of 25µl. The following reaction conditions were used: 95°C for 2min followed by 30 cycles of 95°C for 30s, 65°C for 30s and 72°C for 30s. For detection and separation of PCR products an agarose gel electrophoresis was done.

PCR primer:
Cre For: 5'-GCATTACCGGTCGATGCAACGAGTG-3'
Cre Rev: 5'-GAACGCTAGAGCCTGTTTTGCACGTTC-3'
RiboTag For: 5'-GGGAGGCTTGCTGGATATG-3'
RiboTag Rev: 5'-TTTCCAGACACAGGCTAAGTACAC-3'

Buffer:
Mouse tissue lysis buffer (100mM Tris pH = 8.5, 5mM EDTA, 0.2% SDS, 200mM NaCl, 0.25mg/ml proteinase K; proteinase K is added fresh before use)

Equipment:
Analog Heat Block, VWR
BioDoc-IT Imaging System, UVP
DNA Engine Tetrad2 Peltier Thermal Cycler, Bio-Rad
Heraeus Pico 17 Centrifuge, Thermo Fisher Scientific
Minicentrifuge Spectrafuge 3-1810, NeoLab
NanoPhotometer, Implen
PowerPac HC, Bio-Rad
Thermomixer Compact, Eppendorf
Vortex Genie I Touch Mixer, Scientific Industries

Reagents and materials:
100bp DNA Ladder (N3231), New England BioLabs
10x Standard Taq Reaction Buffer (B9014), New England BioLabs
1kb DNA Ladder (N3232), New England BioLabs
Agarose Low EEO (A2114), AppliChem
dNTP Set (M3015), Genaxxon Bioscience
Gel Loading Dye Purple 6x (B7025), New England BioLabs

GelRed Nucleic Acid Gel Stain (41003), Biotium
Proteinase K (P8044), Sigma-Aldrich
TAE buffer 50x (A1691), AppliChem
Taq DNA Polymerase (M0273), New England BioLabs

3.4 Video-based behavior-recognition

The video-based behavior-recognition is an automated, high resolution technology to analyze animal home cage behavior and detect behavior features and abnormalities in these animals. Six month old C57Bl/6N (n=24) and 129S4/SvJae (n=16) mice were used to compare these two wild type inbred mouse strains. The work was done by Walker Scot Jackson (AG Jackson, DZNE Bonn) at MIT. The method is described in the publication of Andrew Steele and colleagues (Steele et al. 2007a).

3.5 Intracranial injections and tissue dissection

Brain homogenate for intracranial injections was prepared as follows. First, 10% brain homogenate was made in 0.32M sucrose with a tissue grinder. Homogenate was sonicated twice for one minute at full power. Sonicated homogenate is centrifuged (1000g, 5min) and afterwards aliquoted and stored at -80C°. At the day of injection 10% brain homogenate aliquot was thawed and then diluted to 1% homogenate in phosphate-buffered saline (PBS) with 2% fetal bovine serum (FBS). It was treated in an ultrasound bath twice for one minute, centrifuged (1000g, 3min) and the supernatant transferred into a fresh reaction tube and diluted to the needed final concentration in PBS with 2% FBS.
20µl 0.1% brain homogenate of normal or RML infected mice was injected into the right brain hemisphere at the bregmatic suture (circa 2mm away from the sagittal suture) of 2-4 month old RiboTag mice for gene expression studies and twelve month old 129S4/SvJaeJ wild type mice for EEG recordings. Mice were shortly anesthetized with isofluran while injected. Injection depth was 3mm starting at the outer mouse head skin. All injections for the same experiment (EEG or RiboTag) were done on the same day. An analgesic (Rimadyl) was administered within the next 72h according to the manufacturer's instructions.
RiboTag mice were sacrificed after 10 or 18 wpi by CO_2 inhalation. Brains were removed, the two hemispheres separated, and one snap frozen for mRNA isolation

and the other formalin fixed for immunohistochemistry. Infectious prions in formalin fixed hemispheres were inactivated with formic acid prior to embedding in paraffin cassettes.
In the Rtag/Cnx43-CreER mouse line Tamoxifen is needed to activate the Cre recombinase. Daily freshly prepared Tamoxifen (10mg/ml; 10µl/g body weight; at 3d every 24h; in 90% sterile sunflower oil / 10% ethanol) was intraperitoneal injected in this mouse line starting at one week before killing.

Equipment:
Elmasonic S10H, Elma
Sonifier 102C, Branson

Reagents and materials:
Gibco Fetal Bovine Serum, Thermo Fisher Scientific
Isoflurane FORENE 100%, AbbVie
Omnifix-F Duo 25G (9161465V), B. Braun
Rimadyl Cattle 50 mg/ml Solution, Pfizer
Tamoxifen (T5648), Sigma-Aldrich
Tissue Grinder (5ml), Wheaton

3.6 Electroencephalogram

For electroencephalogram (EEG) five RML injected mice and five NBH injected mice were used. The experiments and data analysis were performed by Lars Dittrich (AG Jackson, DZNE Bonn).
Surgical procedure: After at least twelve and a maximum of 22 days incubation time, mice were implanted intraperitoneally with F20-EET transmitters (Channel bandwidth 1-50Hz) under isoflurane anesthesia. EEG leads were routed subcutaneously to the skull, placed epidurally above the left frontal cortex (AP: 1.5, ML: 1.5 mm from bregma, negative lead) and the right parietal cortex (AP: -2.5, ML: 2.0, positive lead) and fixed in place with dental acrylic. Electromyography (EMG) leads were anchored in the neck muscles. Mice were allowed at least two weeks of recovery before recordings.
Data acquisition and analysis: Undisturbed 24h baseline recordings were performed in the home cages. Mice were kept in individual cages but could hear, smell and see at least one other mouse of the same experiment. The cages were placed in

ventilated cabinets with a 12h light / 12h dark cycle. Sleep scoring and analysis was done as reported before (Morairty et al. 2013, Dittrich et al. 2015, Parks et al. 2016). EEG and EMG were recorded via telemetry using DQ ART software. Sampling frequencies were 500Hz. EEG low-pass filter cut off was 100Hz (in addition to the 1Hz high pass and 50Hz low pass antialiasing filtering built in the transmitter). EEG and EMG recordings were scored in 10s epochs as wake, rapid eye movement sleep or non-rapid eye movement sleep by an expert scorer who examined the recordings visually using NeuroScore 3.0 software. EEG spectra were analyzed with a fast Fourier transform algorithm using a Hanning Window without overlap (NeuroScore) on all epochs without stage transition or artifact. For direct comparisons of EEG power spectra, power was expressed as relative power, each frequency bin (0.122Hz) was divided by the sum of the values between 0 and 50Hz. Relative theta power was calculated as the power between 5 and 10Hz (summed values of the respective frequency bins) divided by the sum of the values between 0 and 50Hz.

Equipment:
AXIS 241Q Videoserver, Axis Communications
Data Exchange Matrix, DSI
Hair trimmer MT4640, Grundig
Induction Chamber 1 Liter, VetEquip
Isoflurane Vaporizer, VetEquip
Receiver Boards PhysioTel RPC-1, DSI
Small Animal Stereotaxic Instrument Model 900, David Kopf Instruments
Stereomicroscope Leica M80, Leica Biosystems
Transmitter F20-EET, DSI
Ventilated Cabinet, Techniplast
Video camera with Power Supply TVCCD-190COL, Monacor

Reagents and materials:
Cyanoacrylate, Loctite
Isoflurane FORENE 100%, AbbVie
Jet Dental Acrylic, Lang Dental
Omnifix-F Duo 25G (9161465V), B. Braun
PremiCron, B. Braun
Rimadyl Cattle 50 mg/ml Solution, Pfizer
Sugi absorbent swabs, Kettenbach

Supramid, B. Braun
Surgical instruments, Fine Science Tools
VaporGuard Activated Charcoal Filter, VetEquip

3.7 Immunoprecipitation

Cell-type-specific isolation of ribosome associated mRNA from Rtag/Cre mice is based on the publication of Elisenda Sanz and colleagues (Sanz et al. 2009). The original IP protocol was improved and done as follows. A frozen brain hemisphere was weighed and put into a tissue grinder with the corresponding volume of polysome buffer to prepare a 10% brain homogenate. Homogenate was prepared with help of a mechanical tissue grinding device (600rpm, ~30s) on ice and centrifuged (10000g, 10min, 4°C). Supernatant was transferred to a new reaction tube and used as IP input and for isolation of total RNA. For IP with magnetic beads pre-cleared supernatant (25µl beads and 200µl supernatant, 30min, 4°C) was first incubated with antibody anti-HA 12CA5 (200µl pre-cleared supernatant, 10µl antibody, 45min, 4°C) and this mixture then added to the magnetic beads (50µl beads, 1-2h, 4°C). Magnetic beads were washed three times with PBS (~500µl) before use and incubation steps of IP were done on a rotator. IP samples were put on a magnetic rack and the magnetic bead pellets were washed three times with high salt buffer (~500µl). Cell-type-specific mRNA was eluted from the magnetic beads by RLT buffer with supplemented 2-mercaptoethanol from the RNeasy Mini Kit (200µl, Thermomixer: 700rpm, 5-10min, RT) and afterwards isolated with this kit. For each supernatant two technical replicates of IP were done. Also total RNA from the input supernatant (200µl) was isolated in parallel. Quality and quantity of immunoprecipitated mRNA and total RNA isolated from the input supernatant were verified by Qubit Fluorometer and Agilent 2100 Bioanalyzer.

Buffer:
High salt buffer (50mM Tris pH = 7.5, 300mM KCl, 12mM $MgCl_2$, 1% Nonidet P-40, 1mM DTT, 100µg/ml cycloheximide; DTT and cycloheximide were added fresh before use)
Polysome buffer (50mM Tris pH = 7.5, 100mM KCl, 12mM $MgCl_2$, 1% Nonidet P-40, 1mM DTT, 1x Protease inhibitor, 100U/ml RNAse inhibitor, 100µg/mL cycloheximide; DTT, Protease inhibitor, RNAse inhibitor and cycloheximide were added fresh before use)

Equipment:
Bioanalyzer 2100, Agilent Technologies
Centrifuge 5424R, Eppendorf
Heraeus Pico 17 Centrifuge, Thermo Fisher Scientific
Overhead Stirrer RZR2021, Heidolph
Qubit 2.0 Fluorometer, Thermo Fisher Scientific
Rotator SB2, Stuart
Thermomixer Compact, Eppendorf
Vortex Genie I Touch Mixer, Scientific Industries

Reagents and materials:
Agilent RNA 6000 Nano Kit, Agilent Technologies
Agilent RNA 6000 Pico Kit, Agilent Technologies
Anti-HA 12CA5, Roche Life Science
Cycloheximide (C7698), Sigma-Aldrich
Dynabeads Protein G for Immunoprecipitation (10004D), Thermo Fisher Scientific
Magna GrIP Rack (8 well), Merck Millipore
Qubit RNA HS Assay Kit, Thermo Fisher Scientific
RNAase inhibitor (N8080119), Thermo Fisher Scientific
RNeasy Mini Kit, Qiagen
SIGMAFAST Protease Inhibitor Tablets (S8820), Sigma-Aldrich
Tissue Grinder (5ml), Wheaton

3.8 RNA-sequencing library preparation and RNA-sequencing

Library preparation and RNA-sequencing was done at the DZNE in Göttingen (AG Bonn). 300ng of total RNA or 150ng of immunoprecipitated mRNA (higher concentrated IP replicate) was used for RNA-sequencing run. Each individual RNA sample was checked again for quality and RNA integrity number using Nanodrop 2000 and Agilent 2100 Bioanalyzer respectively. For each condition (five Rtag/Cre lines, injected with RML or NBH, sacrificed at 10 or 18 wpi) we used four individual samples (exception: SST RML 10 wpi: n=3; PV NBH 10 wpi: n=3; Astro RML 18 wpi: n=2).
RNA was converted to cDNA using the Transcriptor High Fidelity cDNA synthesis Kit. RNA-sequencing libraries were prepared using the TruSeq RNA Sample

Preparation 2 Kit. The library quality was checked using an Agilent 2100 Bioanalyzer and concentration was measured by a Qubit dsDNA HS Assay Kit and adjusted to 2nM before sequencing (single end, 50 bp) on a HiSeq 2000 Sequencer using TruSeq SR Cluster Kit 3-cBot-HS and TruSeq SBS Kit 3-HS according to the manufacturer's instructions.

Equipment:
Agilent 2100 Bioanalyzer, Agilent Technologies
HiSeq 2000 Sequencer, Illumina
Nanodrop 2000, Thermo Fisher Scientific
Qubit 2.0 Fluorometer, Thermo Fisher Scientific

Reagents and materials:
Qubit dsDNA HS Assay Kit, Thermo Fisher Scientific
Transcriptor High Fidelity cDNA synthesis Kit, Roche Applied Science
TruSeq RNA Sample Preparation 2 Kit, Illumina
TruSeq SBS Kit 3-HS, Illumina
TruSeq SR Cluster Kit 3-cBot-HS, Illumina

3.9 RNA-sequencing data analysis

RNA-sequencing data analysis was done in two different ways based on the same raw data from the RNA-sequencing run. One analysis was done by Vikas Bansai (AG Bonn, DZNE Göttingen) based on total gene reads, the other analysis was done by myself (Melvin Schleif, AG Jackson, DZNE Bonn) based on unique exon reads (UER).

AG Jackson analysis: Raw RNA-Sequencing data was imported to CLC Genomics Workbench (7.5.2), quality checked, trimmed and mapped to the mouse reference genome (NCBI GRCm38.88). Trimming parameters: ambiguous trim limit = 2; quality trim limit = 0.05; minimum number of nucleotides in reads = 30. Mapping parameters: maximum number of hits for a read = 1; strand specific = both; similarity fraction = 0.8; length fraction = 0.9; mismatch cost = 2; insertion cost = 3; deletion cost = 3. Thereafter, mapped sequence data was compared to each other with CLC in the following manner: IP (for each cell type) vs. total RNA (pool of all available total RNA data) and RML vs. NBH [Treatment vs. control]. Differential

expression analysis was carried out using UER counts from CLC with the DESeq2 package (1.6.3) (Love et al. 2014) in R-Project Bioconductor (3.1.2) (Dessau and Pipper 2008). Genes with less than five reads (baseMean) were filtered out.

DESeq2 commands [XXX = file name, sample name, condition, …]:

```
> datafile = system.file("Data/XXX.txt", package="XXX")
> datafile
> CountTable = read.table(datafile, header = TRUE, row.names=1)
> head(CountTable)
> samples <- data.frame(row.names=c("XXX", " XXX.1", ….),
condition=as.factor(c("XXX", “XXX", ...)))
> samples
> library("DESeq2")
> CDS <- DESeqDataSetFromMatrix(countData = CountTable, colData=samples,
design=~condition)
> CDS <- DESeq(CDS)
> res <- results(CDS)
> head(res)
> write.csv(res,file="XXX.csv")
```

DESeq2 commands example (Glut, 10 wpi, RML vs. NBH, 4 replicates / condition):

```
> datafile = system.file("Data/Glut 10 wpi.txt", package="DESeq2")
> datafile
[1] "C:/…/R/R-3.1.2/library/DESeq2/Data/Glut 10wpi.txt"
> CountTable = read.table(datafile, header = TRUE, row.names=1)
> samples <- data.frame(row.names=c("NBH","NBH.1","NBH.2","NBH.3",
"RML","RML.1","RML.2","RML.3"),
condition=as.factor(c("NBH","NBH","NBH","NBH", "RML","RML","RML","RML")))
> samples     condition
NBH           NBH
NBH.1         NBH
NBH.2         NBH
NBH.3         NBH
RML           RML
RML.1         RML
RML.2         RML
RML.3         RML
> library("DESeq2")
> CDS <- DESeqDataSetFromMatrix(countData = CountTable, colData=samples,
design=~condition)
> CDS <- DESeq(CDS)
estimating size factors
estimating dispersions
gene-wise dispersion estimates
mean-dispersion relationship
```

final dispersion estimates
fitting model and testing
> res <- results(CDS)
> head(res)
log2 fold change (MAP): condition RML vs NBH
Wald test p-value: condition RML vs NBH
DataFrame with 6 rows and 6 columns
BaseMean log2FoldChange lfcSE stat pvalue padj
<numeric> <numeric> <numeric> <numeric> <numeric> <numeric>
Snap25 228790.35 0.023463 0.069340 0.338372 0.735083 0.914074
Calm1 105952.42 -0.005734 0.063530 -0.090253 0.928087 0.977285
> write.csv(res,file="Glut 10 wpi.csv")

AG Bonn analysis: Quality assessment was based on the raw reads using the FastQC (0.10.1) quality control tool. The sequence reads (single-end, 50 bp) were aligned to the mouse reference genome (mm10) with Bowtie2 (2.0.2) (Langmead and Salzberg 2012) using RSEM (1.2.29) (Li and Dewey 2011) with default parameters. First, the mouse reference genome was indexed using the Ensembl annotations (84.38) with rsem-prepare-reference from RSEM software. Next, rsem-calculate-expression was used to align the reads and quantify the gene abundance. Differential expression analysis was carried out using total gene read counts with DESeq2 package (1.12.4) (Love et al. 2014). Genes with less than five reads (baseMean) were filtered out and false discovery rate (padj) was recalculated with Benjamini-Hochberg procedure for the remaining genes.

3.10 Pathway and gene ontology analysis

For canonical pathway and gene ontology (GO) term analysis of differentially expressed genes Ingenuity Pathway Analysis (IPA, Qiagen Bioinformatics) and DAVID Bioinformatics Resources 6.8 (National Institute of Allergy and Infectious Diseases) were used (Huang et al. 2007, Huang da et al. 2009a, Huang da et al. 2009b).

3.11 Immunohistochemistry

For immunohistochemistry (IHC) formalin fixed brain tissues were treated with 98% formic acid and then postfix for more than four days in formalin. Brains were then embedded in paraffin with cassettes containing both NBH and RML injected brains,

ensuring that controls and diseased samples are stained identically. Cassettes were cut into 4µm thick sections. Sections were dewaxed in xylene and rehydrated in graded dilutions of ethanol (each 5min). Sections stained for prion aggregates were further treated with 98% formic acid (3min). This step was excluded for all other stainings. Epitope retrieval was performed with a steamer in 0.01M citrate buffer (PrP: pH = 6; Iba1, GFAP: pH = 8; 30min). Endogenous peroxidase was removed with H_2O_2 treatment (3%, 5min). For PrP and GFAP staining Mouse on Mouse Elite Peroxidase Kit was used according to the manufacturer's instructions. For Iba1 staining 2,5% donkey normal serum was used for blocking (30min), followed by incubation with the primary antibody (30-60min), biotinylated secondary antibody (30min) and AB-Complex (30min). Staining of the epitope was done with DAB with Nickel for all stainings (5-10min). A counterstain with hematoxylin was performed (10s) and sections were dehydrated with graded dilutions of ethanol and xylene (each 5min).

For each time point, NBH and RML infected brain sections were on the same slide twice and all brain sections were treated at the same time with the same solutions and materials. For taking IHC staining pictures a Zeiss AXIO Observer.A1 microscope with Zen 2012 software was used. IHC staining pictures of NBH and RML infected brain sections were taken with the same microscope imaging parameters.

Buffer:

Citrate buffer (0.01M; pH = 6: 0.242g citric acid, 2.57g sodium citrate; pH = 8: 4mg citric acid, 2.935g sodium citrate; adjust to exact required pH with sodium hydroxide)

Primary antibodies:

Anti-GFAP Clone GA5 (MAB360), 1:5000, Merck Millipore

Prion Protein Monoclonal Antibody SAF84, 1:200, Cayman Chemical

Rabbit Anti Iba1 for ICC, 1:200, Waco

Secondary antibodies:

Biotin-SP-conjugated AffiniPure Donkey Anti-Rabbit IgG, 1:500, Jackson ImmunoResearch

Equipment:

Benchtop Tissue Processor Leica TP1020, Leica Biosystems

Flattening Table Leica HI1220, Leica Biosystems
Microscope Zeiss AXIO Observer.A1, Carl Zeiss Microscopy
Modular Tissue Embedding Center Leica EG1150, Leica Biosystems
Rotary Microtome Leica RM2255, Leica Biosystems
Steamer DG552, AEG
Tissue-Tek Manual Slide Staining Set, Sakura Finetek
Water Bath Leica HI1210, Leica Biosystems

Reagents and materials:
DAB Peroxidase (HRP) Substrate Kit with Nickel, Vector Laboratories
Donkey Serum (S30), Merck Millipore
Hematoxylin QS (H-3404), Vector Laboratories
Menzel-Gläser Cover Slips, Thermo Fisher Scientific
Menzel-Gläser Microscope Slides Superfrost Ultra Plus, Thermo Fisher Scientific
Mouse on Mouse Elite Peroxidase Kit, Vector Laboratories
Proteinase K (P8044), Sigma-Aldrich
Richard Allan Scientific Cytoseal XYL, Thermo Fisher Scientific
Vectastain Elite ABC HRP Kit, Vector Laboratories

3.12 Polyacrylamide gel electrophoresis and western blot

RiboTag IP was done like described with changes of certain parameters. Samples for polyacrylamide gel electrophoresis (PAGE) and western blot were collected during the whole procedure (inputs, supernatants, washing steps and bead samples). HA tagged ribosomes were eluted from the beads with 1x LDS sample buffer on a Thermomixer (50µl, 700rpm, 5min, RT). The other samples were also prepared for western blotting by adding the LDS sample buffer on a Thermomixer (700rpm, 5-10min, 70°C).
Prepared PAGE samples (10-20µl) and standard protein ladder (5µl) were loaded on a NuPAGE 10% Bis-Tris Protein Gel and PAGE run was performed in a XCell4 SureLock Midi-Cell Chamber with NuPAGE MES SDS Running Buffer (100-120V, ~2-3h). Electrophoresis separated proteins from the gel were transferred to a nitrocellulose membrane with help of a wet tank Criterion Blotter and cooled 1x Transfer buffer (1 gel: 60min, 0.6A; 2 gels: 70min, 0.7A). After blotting nitrocellulose membrane was blocked with skim dry milk (5%/PBS, 30 min, RT) and incubated with anti-HA antibody (1h, RT, in 1% skim dry milk/PBS) followed by the secondary

antibody (1h, RT, in 1% skim dry milk/PBS). Washing steps in between and after second antibody incubation were performed three times with PBS (each 5min). Detection was done with SuperSignal West Chemiluminescent Substrate and Stella 3200 imaging system.

Primary antibodies:
Monoclonal Anti-HA antibody clone HA-7, 1:1000, Sigma-Aldrich

Secondary antibodies:
Peroxidase AffiniPure Goat Anti-Mouse IgG (115-035-174), 1:5000, Jackson ImmunoResearch

Buffer:
10x Transfer buffer 10x (0.25M Tris base, 1.9M glycine)
1x Transfer buffer (10% 10x Transfer buffer, 10% methanol)

Equipment:
Criterion Blotter, Bio-Rad
Orbital Shaker PSU-10i, Biosan
PowerPac HC, Bio-Rad
STELLA 3200, Raytest
Thermomixer Compact, Eppendorf
VARIOMAG Magnetic Stirrer Mono Direct, Thermo Fisher Scientific
XCell4 SureLock Midi-Cell, Invitrogen

Reagents and material:
Nitrocellulose Membrane Roll (0.2µm), Bio-Rad
NuPAGE 10% Bis-Tris Protein Gels, Thermo Fisher Scientific
NuPAGE LDS Sample Buffer 4x (NP0007), Thermo Fisher Scientific
NuPAGE MES SDS Running Buffer 20x, Thermo Fisher Scientific
Precision Plus Protein WesternC Standard Ladder (1610376), Bio-Rad
SuperSignal West Femto Chemiluminescent Substrate, Thermo Fisher Scientific
SuperSignal West Pico Chemiluminescent Substrate, Thermo Fisher Scientific
Thick Blot Absorbent Filter Paper, Bio-Rad

3.13 Dot blot

Different anti-HA antibodies in various concentrations were incubated with magnetic beads (50µl, 45min, RT). Supernatants were saved for dot blot analysis and bead-coupled antibody was eluted from the three times High salt buffer (500µl) washed magnetic beads with 1x LDS sample buffer on a Thermomixer (50µl, 700rpm, 5-10min, RT). Nitrocellulose membrane with one underlying blot absorbent filter paper was placed into the Minifold Dot Blot system, washed three times with PBS, loaded with the supernatant and eluted bead samples in a 1:2 serial dilution and washed again tree times with PBS. Nitrocellulose membrane was blocked with skim dry milk (5%/PBS, 30 min, RT) and incubated with suitable secondary antibodies for the different loaded primary anti-HA antibodies (1h, RT). Detection was done with SuperSignal West Chemiluminescent Substrate and Stella 3200 imaging system.

Buffer:
High salt buffer (50mM Tris pH = 7.5, 300mM KCl, 12mM $MgCl_2$, 1% Nonidet P-40)

Primary antibodies:
Anti-HA 12CA5, Roche Life Science
Covance Anti-HA.11 Epitope Tag Antibody, BioLegend
Monoclonal Anti-HA antibody clone HA-7, Sigma-Aldrich
Rabbit Anti-HA antibody (H6908), Sigma Aldrich

Secondary antibodies:
Goat Anti-Rabbit IgG–Peroxidase antibody (A9169), 1:500, Sigma-Aldrich
Peroxidase AffiniPure Goat Anti-Mouse IgG (115-035-174), 1:5000, Jackson ImmunoResearch

Equipment:
Mini Laboratory Pump VP 86, VWR
Minifold Dot-Blot System 96 Well, Whatman
Orbital Shaker PSU-10i, Biosan
STELLA 3200, Raytest
Thermomixer Compact, Eppendorf

Reagents and material:
Dynabeads Protein G for Immunoprecipitation (10004D), Thermo Fisher Scientific
Nitrocellulose Membrane Roll (0.2µm), Bio-Rad
NuPAGE LDS Sample Buffer 4x (NP0007), Thermo Fisher Scientific
SuperSignal West Femto Chemiluminescent Substrate, Thermo Fisher Scientific
SuperSignal West Pico Chemiluminescent Substrate, Thermo Fisher Scientific
Thin Blot Absorbent Filter Paper, Bio-Rad

3.14 Reverse transcription and real-time quantitative PCR

Cell-type-specific mRNA and IP input total RNA was used for reverse transcription (RT) and real-time quantitative PCR (qPCR). To prepare complementary DNA (cDNA) TaqMan Reverse Transcription Reagents were used. The following reverse transcription reaction was set up: RNA (IP mRNA: ~10µl; total RNA: ~1µl), 5µl 10x RT Buffer, 3.5µl $MgCl_2$ (25mM), 10µl dNTP mix (10mM, each 2.5mM), 2.5 MultiScribe RT (50/µl), 2.5µl RNase inhibitor (20U/µl), 2.5µl Oligo $d(T)_{16}$ primer, add water to a total volume of 50µl. The following reaction conditions were used: 65°C for 5min, 4°C for 2min, 37°C for 30min and 95°C for 5min.
Prepared cDNA was used for qPCR on a 384-well plate using Power SYBR Green PCR Master Mix and a 7900HT Fast Real-Time System Cycler. One sample was added to the plate as triplet. The following qPCR reaction was set up: 4µl cDNA (RT reaction diluted to the needed amount for the qPCR plate), 6µl 2x Power SYBR Green PCR Master Mix, 2µl Primer mix (For + Rev primer; each 5µM), total volume of 12µl. The following reaction conditions were used: 50°C for 2min, 95°C for 10min followed by 40 cycles of 95°C for 15s and 60°C for 1min.
For set up of the qPCR run and calculation of cycle threshold (CT) values of housekeeping genes and cell type marker genes provided SDS 2.4 software was used. Fold changes (enrichment or depletion of marker genes, IP vs. total RNA) were calculated from the CT values via ΔΔCT method (Livak and Schmittgen 2001).

Primer - housekeeping genes:
Actb For: 5‘-GTTACAGGAAGTCCCTCACC-3‘
Actb Rev: 5’-ACCAAAGCCTTCATACATCAAGT- 3’
Gapdh For: 5’-CAACAGGGTGGTGGACCT-3’
Gapdh Rev: 5’-TGTGAGGGAGATGCTCAGTG-3’

HPRT For: 5’-CTCTGGTAGATTGTCGCTTATC-3’
HPRT Rev: 5’-CTCTTAGATGCTGTTACTGATAG-3’
Pgk1 For: 5’-TAGTGGCTGAGATGTGGCAC-3’
Pgk1 Rev: 5’-GCTGAGTCAAGAACAGTGAG-3’

Primer – neuron marker genes:
Gap43 For: 5’-ATCCCAAGTCCAACAGTGTG-3’
Gap43 Rev: 5’-GGAACAGAGAGAAATAGAGAGG-3’
Syn1 For: 5’-CTCCTCCAGAAACCCCTC-3’
Syn1 Rev: 5’-GCCACTGTACGCATTACCACA-3’

Primer – glutamatergic neuron marker genes:
Vglut1 For: 5’-GCACTTTATTCTCCTGGGTGG-3’
Vglut1 Rev: 5’-CAGAGACAGACACCAAGACAC-3’
Vglut2 For: 5’-GCTTGTGGTAGCAGTGATTTC-3’
Vglut2 Rev: 5’-AGTCAAGAGCACAGGACACC-3’

Primer – GABAergic neuron marker genes:
Gad2 For: 5’-TCACCCTTTCACCCAGTCC-3’
Gad2 Rev: 5’-CACCTTCTCCAAGACCCTG-3’
Pvalb For: 5’-ATCAAGAAGGCGATAGGAGC-3’
Pvalb Rev: 5’-GCCAGAAGCGTCTTTGTTTC-3’
SST For: 5’-TGAGCAGGACGAGATGAGG-3’
SST Rev: 5’-TATGGGGTTTGGGGGAGAG-3’
Vgat For: 5’-GTCTGCGTTTCTGTCGTCC-3’
Vgat Rev: 5’-CGAACTTTCCCTCCCTTCC-3’

Primer – neuroglia and astrocyte marker genes:
AldH1L1 For: 5’-TGCGGATCAAGACTGTGACT-3’
AldH1L1 Rev: 5’-GTGTCCTGTCACCAGCAG-3’
GFAP For: 5’-CGAGTCCCTAGAGCGGCA-3’
GFAP Rev: 5’-GCCCTCCAGCAATTTCCTG-3’
S100b For: 5’-GTTAGTTGTATCTTCCTTGCTCC-3’
S100b Rev: 5’-CAAGTTAGAAAGCCTCAAGTCC-3’

Equipment:
7900HT Fast Real-Time System Cycler, Apllied Biosystems

DNA Engine Tetrad2 Peltier Thermal Cycler, Bio-Rad
PowerPac HC, Bio-Rad
Vortex Genie I Touch Mixer, Scientific Industries

Reagents and material:
MicroAmp Optical 384-Well Reaction Plate, Applied Biosystems
MicroAmp Optical Adhesive Film, Applied Biosystems
Power SYBR Green PCR Master Mix, Apllied Biosystems
TaqMan Reverse Transcription Reagents (N8080234), Applied Biosystems

3.15 Chemicals and consumable goods

Used chemicals were either bought from Carl Roth or Sigma-Aldrich. Consumable goods like reaction tubes were ordered from Sarstedt or Eppendorf. Pipette tips for used Eppendorf and Gilson pipettes were produced by Nerbe Plus, Starlab and Eppendorf. Ready to use solutions like balanced salt solutions were purchased from Gibco (Thermo Fisher Scientific). Custom DNA primers were ordered from Sigma-Aldrich.

3.16 Software and web applications

2100 Expert Software, Agilent Technologies
Adobe Illustrator CS5.1, Adobe Systems
Bowtie2 2.0.2, Ben Langmead / Steven Salzberg
CLC Genomics Workbench 7.5.2, Qiagen Bioinformatics
DAVID 6.8, National Institute of Allergy and Infectious Diseases
DESeq2 1.6.3, Michael Love / Simon Anders / Wolfgang Huber
DQ ART, DSI
EndNote X7, Thomson Reuters
FastQC 0.10.1, Babraham Bioinformatics
GraphPad Prism 7, GraphPad Software
Ingenuity Pathway Analysis, Qiagen Bioinformatics
Mausoleum 6.4.6, Hanns-Eugen Stöffler
Matlab R2013b, MathWorks
Microsoft Office 2010, Microsoft
NeuroScore 3.0, DSI

SPSS Statistics, IBM

R-Project Biocunductor 3.1.2, R Foundation for Statistical Computing

RSEM 1.2.29, Bo Li / Colin Dewey / Peng Liu

SDS 2.4, Apllied Biosystems

ZEN 2012, Carl Zeiss Microscopy

4. Results

4.1 Selection of mouse genetic background

The mouse genetic background has an influence on the activity levels of the animals. For our study we sought a genetic background that has a very consistent activity state. To determine the mouse genetic background for the RiboTag mice and the mice for EEG recordings data from video-based behavior-recognition were analyzed to detect behavior features and possible abnormalities of the commonly used C57Bl/6N (B6; n=24) and 129S4/SvJae (S4; n=16) inbred mouse strains (Figure 4.1). This work was done by Walker Scot Jackson (AG Jackson, DZNE Bonn) at MIT. Analyzed behavior features included distance travelled (Figure 4.1A), eating (Figure 4.1B), grooming (Figure 4.1C), hanging related (Figure 4.1D), jumping (Figure 4.1E) and sleeping (Figure 4.1F). Measurements were performed at an age of six months.

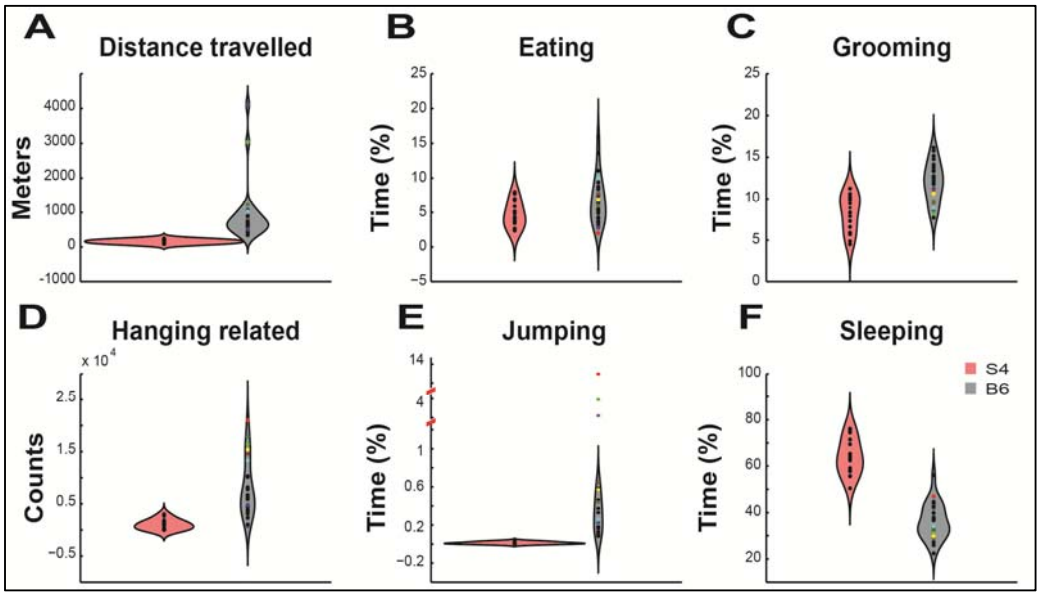

Figure 4.1: Violin plots of behavior features (A. Distance travelled; B. Eating; C. Grooming; D. Hanging related; E. Jumping; F. Sleeping) from video-based behavior-recognition data of six month old C57Bl/6N (B6; n=24) and 129S4/SvJae (S4; n=16) mice. Dots represent individual mice. Colored dots of B6 group in the different behavior feature panels represent a given individual mouse. Shaded areas depict probability density estimates calculated using the Matlab function ksdensity. In panel E. the three B6 mice with the highest values were excluded as outliers from the calculation of the probability density. Vertical axis is interrupted in panel E. at the locations indicated by red lines.

The B6 inbred mouse strain shows highly variable behaviors within the group of individual animals, especially for distance travelled, eating, hanging related and jumping. Only in the B6 group are really outstanding individuals detectable for these behavioral features. Note that it is not consistently the same individuals that exhibit the highest scores across different behavioral measures. For example, one mouse of the B6 group travelled over 4000m within the limited confines of the animal holding cage while another mouse jumped for 14% of a 24h period. Therefore, the spread of the B6 group is not merely driven by a small number of abnormally behaving animals. Distribution of the two groups for grooming is similar, even B6 mice spend more time grooming. Presumably because of the extensive instigation of other behaviors, B6 mice sleep a lot less.

Such drastically different behavioral activities will clearly have an impact on metabolism and physiology and finally also on gene expression. Based on these results, to avoid a widely variable group of individual mice and thereby possible effects on gene expression, we decided to use the RiboTag mice in the S4 genetic background.

4.2 Selection of disease time points

After selection of the suitable mouse genetic background, disease time points for the gene expression analysis by next generation sequencing and the neuropathological analysis by IHC had to be chosen. It was planned to analyze two disease time points, a disease onset time point and an early preclinical time point. The disease onset was defined as the earliest time point in which a clinically relevant detectable difference between our control and RML group could be detected in living mice. For the preclinical time point we would pick the last time point at which the above sought after metric was exactly the same in both groups. To this end we recorded the EEG and EMG of S4 mice during wake and sleep at multiple time points after the RML injection as disease progressed. EEG and EMG recordings were performed by Lars Dittrich (AG Jackson, DZNE Bonn). Because we employed an EEG recording system that transmits data telemetrically the mice were able to roam untethered throughout the course of the experiment. Simultaneously, body weight of the animals as a disease marker was measured weekly during the experiment. Our S4-RML model consistently causes mice to become terminally ill at an average of 22.5 wpi within a very small time frame.

ANOVA tests demonstrate significant differences between the two groups in four measurements, theta frequency (5-10Hz) in wake (Figure 4.2A), deep slow wave sleep (NREM) (Figure 4.2B) and paradoxical sleep (REM) (Figure 4.2C) and body weight (Figure 4.2D). The significant difference detected was an increase in EEG theta frequency in RML injected mice starting at 16 wpi and this difference became stronger at 18 wpi. However, it began to decline by our last time point of 20 wpi (Figure 4.2A-C). Importantly, even at 20 wpi the mice appear healthy by passive observation. Only a trained experimenter could detect that the RML injected mice are not healthy by using specific tests. Thus, at 18 wpi the mice have a clinically relevant measurement that indicates animals are at the beginning of clinical disease. Therefore, 18 wpi time point was chosen as the disease onset for our planned analysis.

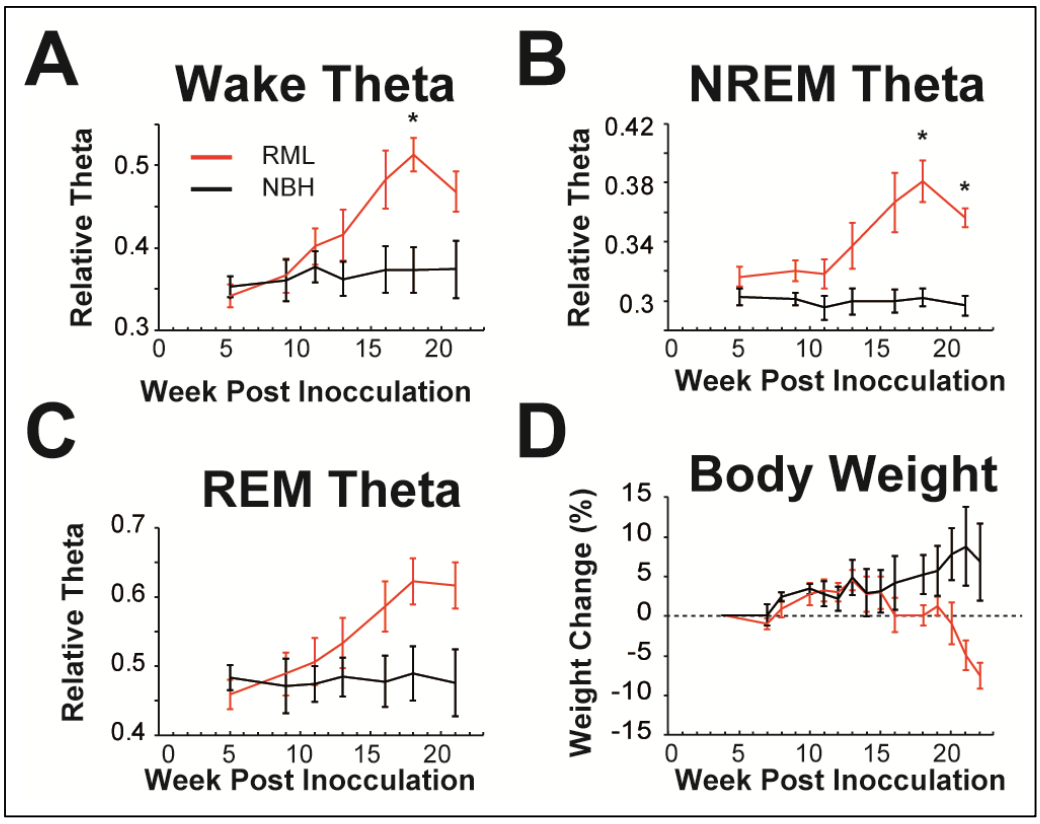

Figure 4.2: A., B., and C. EEG data of wake (A), NREM sleep (B) and REM sleep (C) from normal (black) or RML (red) brain homogenate injected mice. D. Weekly percentage body weight change from initial weight of the same mouse cohorts. Two-factor mixed ANOVA tests demonstrate significant difference in all four measurements. A. $F(6,48)=8.3$, $pval<0.001$; B. $F(6,48)=6.9$, $pval<0.001$; C. $F(6,48)=8.9$, $pval<0.001$; D. $F(14,98)=4.8$, $pval<0.001$; asterisks indicate $pval\leq0.05$ (Holm-Šídák test).

We determined an earlier time point by examining the evolution of differences in recorded EEG theta frequency and found that theta frequency for both groups is overlapping up to 10 wpi in disease progression. After 10 wpi the two groups slowly begin to separate. Therefore, 10 wpi was chosen as our pre-onset disease time point. The body weight of the animals is another widely used indicator for decline in health of diseased humans and mouse models with neurodegeneration. The two groups still overlap at 15 wpi (Figure 4.2D), indicating that the 10 wpi time point is well before clinical disease. Therefore, based on these results mice were sacrificed at 10 or 18 wpi and the brain dissected for the further planned analysis.

4.3 Experimental setup

4.3.1 Improvement of RiboTag immunoprecipitation

To analyze gene expression changes caused by RML induced neurodegeneration in a cell-type specific manner the RiboTag method was used. At first, cell-type-specific isolation of ribosome associated mRNA from Rtag/Cre mice by RiboTag IP had to be established in our laboratory and at the beginning it was done as described in the original publication (Sanz et al. 2009). However, the achieved cell-type-specific mRNA yields and cell type specificity compared to input total RNA were not satisfactory. Therefore, we tested several changes to the original protocol including incubation times, buffer ingredients, reaction volumes, order of reaction steps and anti-HA antibody isolates or clones, testing each parameter one at a time. To verify the impact of the changed parameters yields of cell-type-specific immunoprecipitated mRNA (Agilent 2100 Bioanalyzer and Qubit Fluorometer) and the cell type specificity (RT followed by qPCR; enrichment or depletion of cell type marker genes) were analyzed. Western blot was used to analyze the disposition of the HA tagged ribosomes during the IP, for example whether the ribosomes were bound and remained coupled to the beads during the procedure or dispersed in the supernatant or washing steps. Western blot was also informative about input volumes and amount of magnetic beads by checking abundance of tagged ribosomes bound to beads versus remaining in the supernatant. Dot blot was used to test different antibodies, their affinity to the magnetic beads and the needed antibody concentration. At the end, an improved RiboTag IP protocol was developed and thereafter IPs were done as described in the material and method section for this study (Section 3.7).

One important example is we discontinued the use of heparin in the brain homogenate. Although, the addition of heparin in the polysome buffer leads to a higher yield of immunoprecipitated mRNA, these mRNAs are less cell-type-specific. The enrichment or depletion of marker genes was more significant compared to preparations made with heparin (data not shown).

In detail, additional to the exclusion of heparin in the brain homogenate changes to the original protocol are as follows. Instead of 200U/ml RNase inhibitor only 100U/ml was used. The reduction of RNase inhibitor to this concentration did not lead to any difference of yields and cell type specificity (data not shown).

We also tested whether the order in which antibodies and beads are added to the supernatant affects the IPs (direct vs. indirect IP method). In the direct method from the original protocol antibody-coupled beads are incubated with the brain homogenate. In the indirect method brain homogenate is first incubated with the antibody and this mixture is then added to the magnetic beads. Because the indirect method is prone to background contamination since the magnetic beads are not saturated with antibody and unspecific binding of ingredients from the brain homogenate supernatant to the beads can occur, brain homogenates were pre-cleared in advance with fresh, non-reusable magnetic beads. Elimination of the pre-clearing step within the indirect IP method led to contaminations in the mRNA and therefore to less cell-type specificity (data not shown). Changing the IP from the direct to the indirect method with addition of a pre-clearing step of the brain homogenate resulted in an increase of immunoprecipitated mRNA with constant cell type specificity (data not shown).

We also tested different anti-HA antibodies for our RiboTag IP. In our experiments anti-HA 12CA5 worked the best. Other tested antibodies led to less yields of immunoprecipitated mRNA even with high concentrations or did not even stay coupled to the beads (data not shown). The ideal antibody concentration was determined by a dot blot assay. The amount of anti-HA 12CA5 antibody bound to the beads and the amount of antibody left in the supernatant was analyzed with different antibody concentrations. The antibody concentration in which the beads were saturated with antibody but no or little antibody was left in the supernatant was used. This determined concentration for the anti-HA 12CA5 antibody was 10µl / 200µl supernatant (data not shown).

Furthermore, different IP reaction volumes were tested. In our experiment half of the input volume compared to the original protocol for RiboTag IP was used, so 200µl instead of 400µl. With less input we proportionately harvested more immunoprecipitated mRNA, especially for very abundant cell types (data not

shown). We assume that this effect is caused by oversaturated magnetic beads and RNA isolation columns. If higher input volumes were used we harvested more cell-type-specific mRNA when the material was split on two RNA isolation columns than loading all material on one column (data not shown).
In addition, different incubation times were given a trial. Incubation times were tried to be done as short as possible to lower the risk of RNA degradation without any decrease in mRNA yields or less significant cell type specificity. The final developed procedure includes pre-clearing of supernatant for 30min, incubation of pre-cleared supernatant with antibody for 45min and incubation of all components together for 1-2h. To avoid additional risk of RNA degradation most steps of the IP protocol were performed at 4°C. Longer incubation times or extending the IP overnight like described in the original protocol had no advantages in immunoprecipitated mRNA yields or cell type specificity (data not shown).
In summary, our improved RiboTag IP protocol differs from the original in six ways: elimination of heparin, concentration of RNase inhibitor, change to indirect IP method with pre-clearing, use of anti-HA 12CA5 antibody, change of IP reaction volumes and IP reaction incubation times.

4.3.2 RNA-sequencing sample generation

After the selection of mouse genetic background, disease time points for planned analysis and improvement of the RiboTag IP, needed Rtag/Cre mice were bred to isolate actively translated mRNA from specific cell types of the brain to analyze effects on gene expression caused by intracranial RML injection (Sanz et al. 2009). To study the response to RML induced neurodegeneration, mice were intracranially injected with brain homogenate from either normal or prion infected (RML) mice. Homogenates were injected into the right brain hemisphere through the bregmatic suture (Figure 4.3.2.1C). Mice in a 129S4 genetic background expressing the epitope-tagged ribosomes in astrocytes (Astro, Cre driver: Cnx43) or subsets of neurons, including glutamatergic (Glut, Cre driver: Vglut2), GABAergic (GABA, Cre driver: Gad2), parvalbumin (PV, Cre driver: Pvalb) or somatostatin neurons (SST, Cre driver: SST) were used to study a wide range of cell types (Figure 4.3.2.1B). Mice were sacrificed after 10 or 18 wpi.
To harvest cell-type-specific mRNA, dissected, frozen mouse brain tissue was homogenized followed by an immunoprecipitation and RNA isolation. Cell-type-specific mRNA and total mRNA from brain homogenate IP input were

analyzed by next generation sequencing (RNA-sequencing) (Figure 4.3.2.1A). Changes to gene expression were analyzed for the selected disease time points, at a stage when clinical signs first become apparent (18 wpi) and at a much earlier stage (10 wpi) in the disease process (Figure 4.3.2.1C). Neuropathological changes (microglia activation, astrogliosis, proteinase K resistant prion aggregates and spongiosis) were analyzed by different IHC stainings.

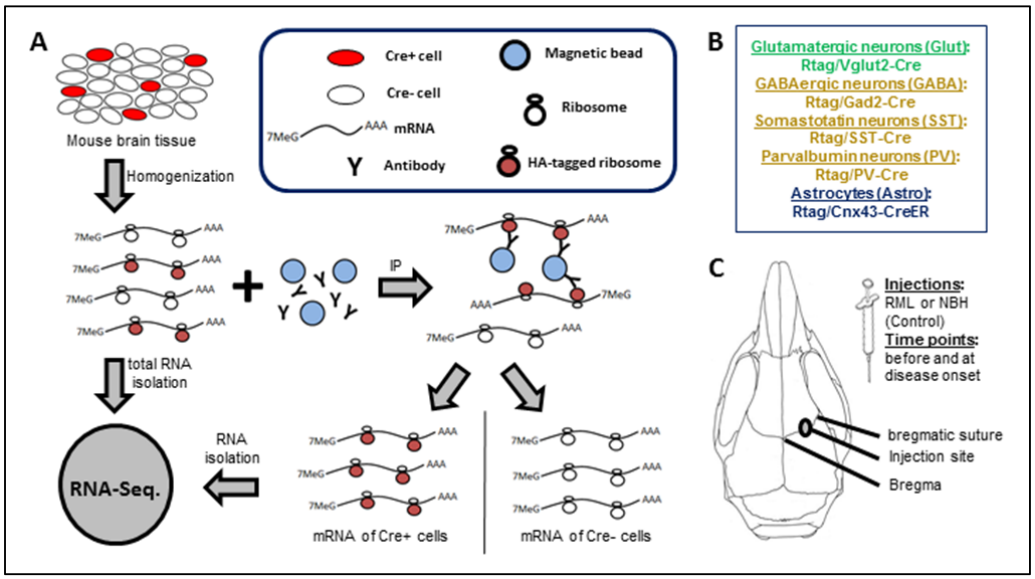

Figure 4.3.2.1: Outline of experimental plan. A. Conceptual summary of the RiboTag method. Frozen mouse brain tissue was homogenized. Cell-type-specific, ribosome associated mRNA was isolated by RiboTag IP with magnetic beads and anti-HA antibody. Total RNA and mRNA from Cre+ cells were used for RNA-sequencing. B. Cell types to study and corresponding mouse lines. RiboTag mice were crossed to cell-type-specific Cre driver mice to express HA tagged ribosomes only in specific cell types. C. Neurodegeneration is induced by intracranial injections with 20µl 0.1% RML or normal brain homogenate (NBH, Control) into the right brain hemisphere at the bregmatic suture.

Table 4.3.2.1 (total RNA samples) and table 4.3.2.2 (IP mRNA samples) list all samples used for RNA-sequencing with information about conditions (cell type, time points, NBH or RML injection, IP mRNA or total RNA) and RNA concentration (n=101). 300ng of total RNA or 150ng of immunoprecipitated mRNA (higher concentrated IP replicate) was used for RNA-sequencing. For samples under a total amount of 150ng RNA all available RNA material from the higher concentrated of the two technical IP replicates was provided for RNA-sequencing. Before RNA-sequencing each individual RNA sample was checked for RNA quality and quantity using a Qubit Fluorometer and an Agilent 2100 Bioanalyzer. At the DZNE in Göttingen RNA quality and quantity was again analyzed, here with help of Agilent 2100 Bioanalyzer and Nanodrop 2000.

Table 4.3.2.1: Partially pooled total RNA samples with conditions (5 cell types, 2 time points, NBH or RML injection, RNA type) and RNA concentration for RNA-sequencing.

Sample number	Mouse	Cell Type	Time Point	Injection	RNA Type	Concentration [ng/µl]
5	U37, U45	Glut	10 wpi	NBH	total RNA	26.0
6	U38, U39	Glut	10 wpi	NBH	total RNA	31.0
11	U11, U12	Glut	10 wpi	RML	total RNA	51.0
12	U13, U14	Glut	10 wpi	RML	total RNA	43.0
17	U53, U54	Glut	18 wpi	NBH	total RNA	30.0
18	U57, U58	Glut	18 wpi	NBH	total RNA	32.0
23	U68, U69	Glut	18 wpi	RML	total RNA	34.0
24	U77, U96	Glut	18 wpi	RML	total RNA	37.0
46	Z27, Z29	SST	10 wpi	NBH	total RNA	32.0
47	Z32, Z33	SST	10 wpi	NBH	total RNA	41.0
51	Z38, Z39	SST	10 wpi	RML	total RNA	28.0
52	Z24, 25	SST	10 wpi	RML	total RNA	52.0
57	Z35, Z36	SST	18 wpi	NBH	total RNA	54.0
58	Z37, Z42	SST	18 wpi	NBH	total RNA	49.0
63	Z44, Z45	SST	18 wpi	RML	total RNA	38.0
64	Z46, Z47	SST	18 wpi	RML	total RNA	29.0
84	S176, S177	Astro	10 wpi	NBH	total RNA	33.0
85	S179, S18	Astro	10 wpi	NBH	total RNA	31.0
90	S5, S7	Astro	10 wpi	RML	total RNA	29.0
91	S11, S13	Astro	10 wpi	RML	total RNA	35.0
96	S16, S21	Astro	18 wpi	NBH	total RNA	29.0
97	S23, S30	Astro	18 wpi	NBH	total RNA	47.0
100	S45	Astro	18 wpi	RML	total RNA	38.0
101	S49	Astro	18 wpi	RML	total RNA	23.0

Table 4.3.2.2: Individual IP mRNA samples with conditions (5 cell types, 2 time points, NBH or RML injection, RNA type) and RNA concentration for RNA-sequencing.

Sample number	Mouse	Cell Type	Time Point	Injection	RNA Type	Concentration [ng/µl]
1	U37	Glut	10 wpi	NBH	IP	19.3
2	U45	Glut	10 wpi	NBH	IP	18.3
3	U38	Glut	10 wpi	NBH	IP	18.1
4	U39	Glut	10 wpi	NBH	IP	21.8
7	U11	Glut	10 wpi	RML	IP	19.2
8	U12	Glut	10 wpi	RML	IP	23.3
9	U13	Glut	10 wpi	RML	IP	16.5
10	U14	Glut	10 wpi	RML	IP	17.5
13	U53	Glut	18 wpi	NBH	IP	18.8
14	U54	Glut	18 wpi	NBH	IP	16.7
15	U57	Glut	18 wpi	NBH	IP	13.8
16	U58	Glut	18 wpi	NBH	IP	19.4
19	U68	Glut	18 wpi	RML	IP	12.3
20	U69	Glut	18 wpi	RML	IP	14.5
21	U77	Glut	18 wpi	RML	IP	11.3
22	U96	Glut	18 wpi	RML	IP	13.8
25	D203	GABA	10 wpi	NBH	IP	33.0
26	D204	GABA	10 wpi	NBH	IP	37.0
27	D175	GABA	10 wpi	NBH	IP	29.3
28	D176	GABA	10 wpi	NBH	IP	32.3
29	D687	GABA	10 wpi	RML	IP	33.6
30	D688	GABA	10 wpi	RML	IP	39.0
32	D689	GABA	10 wpi	RML	IP	33.4
33	D690	GABA	10 wpi	RML	IP	30.8
34	D198	GABA	18 wpi	NBH	IP	7.5
35	D213	GABA	18 wpi	NBH	IP	7.0
36	D214	GABA	18 wpi	NBH	IP	5.1
37	D215	GABA	18 wpi	NBH	IP	6.0
38	D692	GABA	18 wpi	RML	IP	13.2
39	D693	GABA	18 wpi	RML	IP	16.7
40	D694	GABA	18 wpi	RML	IP	20.0
41	D695	GABA	18 wpi	RML	IP	17.0
42	Z27	SST	10 wpi	NBH	IP	2.7
43	Z29	SST	10 wpi	NBH	IP	2.6
44	Z32	SST	10 wpi	NBH	IP	3.2
45	Z33	SST	10 wpi	NBH	IP	3.6
48	Z39	SST	10 wpi	RML	IP	2.9
49	Z24	SST	10 wpi	RML	IP	4.4
50	Z25	SST	10 wpi	RML	IP	3.4
53	Z35	SST	18 wpi	NBH	IP	2.0
54	Z36	SST	18 wpi	NBH	IP	2.7
55	Z37	SST	18 wpi	NBH	IP	3.3
56	Z42	SST	18 wpi	NBH	IP	2.9

59	Z44	SST	18 wpi	RML	IP	3.7
60	Z45	SST	18 wpi	RML	IP	5.8
61	Z46	SST	18 wpi	RML	IP	3.6
62	Z47	SST	18 wpi	RML	IP	5.0
65	E190	PV	10 wpi	NBH	IP	14.1
66	E191	PV	10 wpi	NBH	IP	15.4
67	E192	PV	10 wpi	NBH	IP	17.3
68	E674	PV	10 wpi	RML	IP	14.7
69	E675	PV	10 wpi	RML	IP	17.6
70	E678	PV	10 wpi	RML	IP	18.9
71	E679	PV	10 wpi	RML	IP	13.4
72	E208	PV	18 wpi	NBH	IP	5.4
73	E211	PV	18 wpi	NBH	IP	7.7
74	E223	PV	18 wpi	NBH	IP	6.7
75	E224	PV	18 wpi	NBH	IP	5.8
76	E677	PV	18 wpi	RML	IP	5.8
77	E680	PV	18 wpi	RML	IP	7.1
78	E681	PV	18 wpi	RML	IP	2.6
79	E682	PV	18 wpi	RML	IP	2.8
80	S176	Astro	10 wpi	NBH	IP	2.9
81	S177	Astro	10 wpi	NBH	IP	4.0
82	S179	Astro	10 wpi	NBH	IP	3.8
83	S18	Astro	10 wpi	NBH	IP	4.3
86	S5	Astro	10 wpi	RML	IP	2.3
87	S7	Astro	10 wpi	RML	IP	4.6
88	S11	Astro	10 wpi	RML	IP	3.2
89	S13	Astro	10 wpi	RML	IP	2.6
92	S16	Astro	18 wpi	NBH	IP	2.3
93	S21	Astro	18 wpi	NBH	IP	2.6
94	S23	Astro	18 wpi	NBH	IP	2.6
95	S30	Astro	18 wpi	NBH	IP	2.6
98	S45	Astro	18 wpi	RML	IP	3.4
99	S49	Astro	18 wpi	RML	IP	2.7

One representative immunoprecipitated mRNA electropherogram from Bioanalyzer run for each cell type, time point and NBH or RML injected sample is given in figure 4.3.2.2 showing good RNA quality profiles. The profiles show the internal Bioanalyzer marker peak at 25 nucleotides, a broad hump of mRNA with different length and the two ribosomal RNA peaks. Thus, the RiboTag IPs and RNA isolation resulted in good quality RNA samples for next generation sequencing.

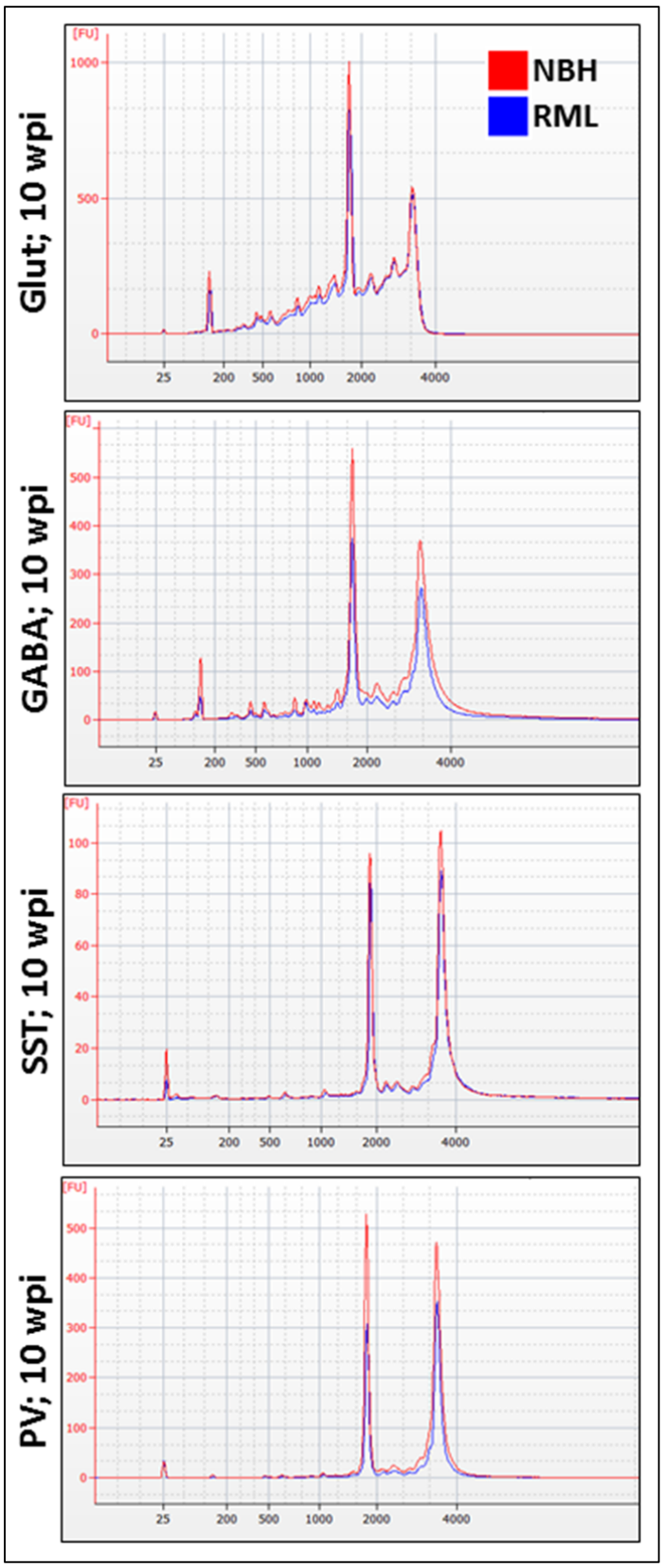

Figure 4.3.2.2: Continued on the next page.

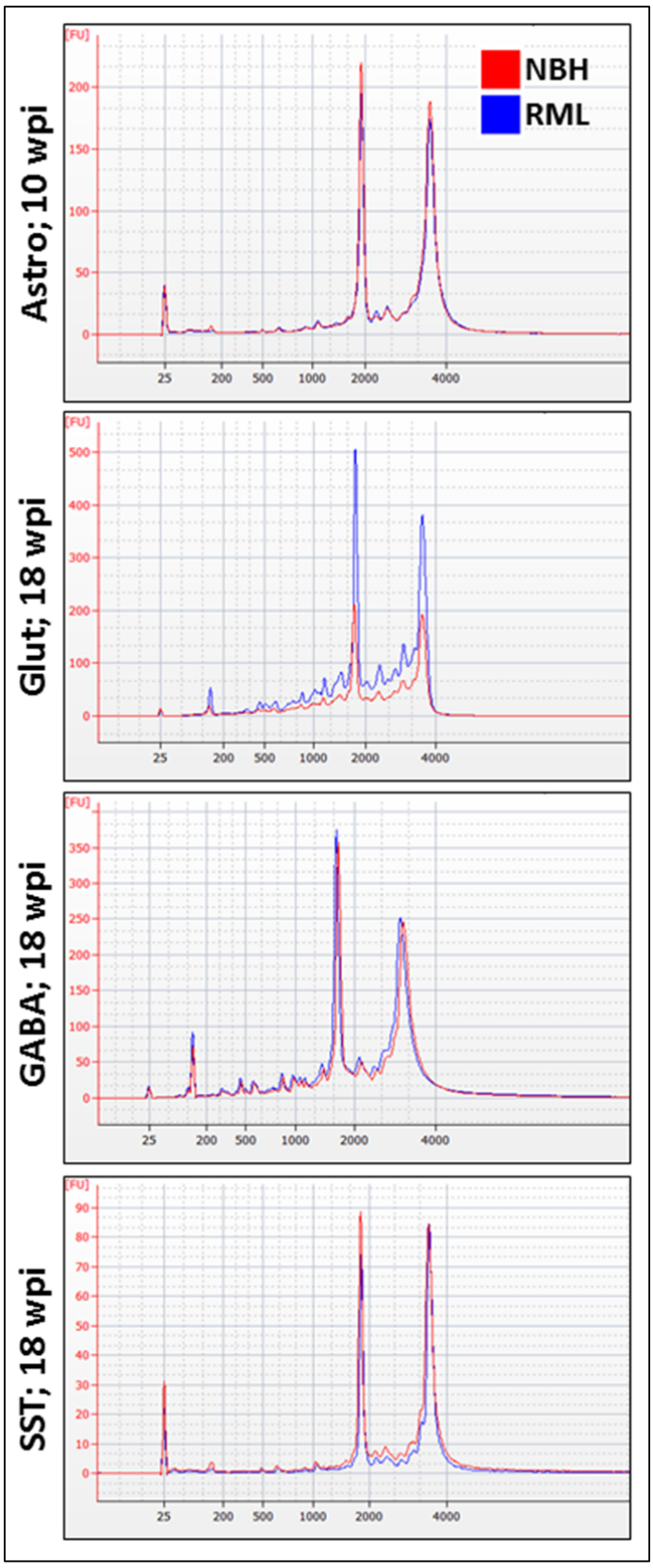

Figure 4.3.2.2: Continued on the next page.

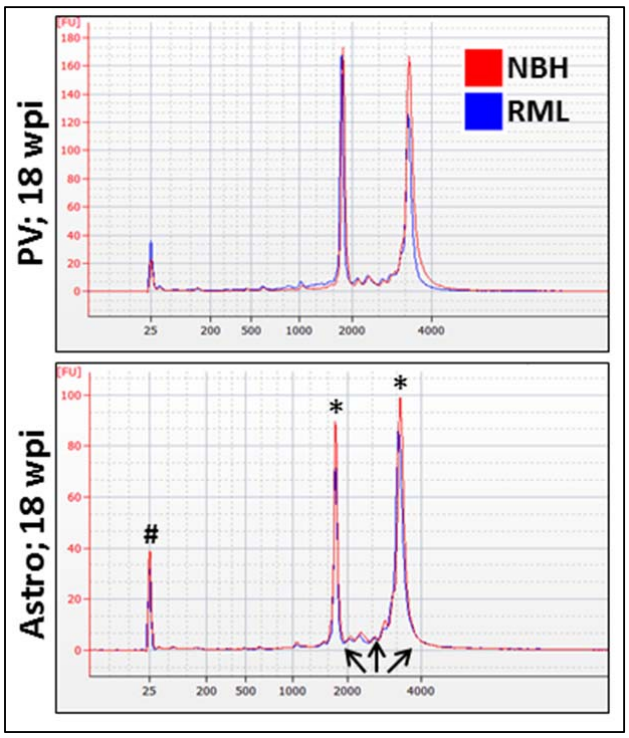

Figure 4.3.2.2: Agilent 2100 Bioanalyzer electropherograms for representative immunoprecipitated mRNA for each cell-type, time point and NBH or RML injected sample (horizontal axis: number of nucleotides; vertical axis. fluorescence units). The Astro 18 wpi panel shows important features of the RNA profile (pound (#): internal Bioanalyzer marker peak; arrows (→): broad hump of mRNA; asterisks (*): two ribosomal RNA peaks).

4.3.3 RNA-sequencing quality control

To analyze the RNA-sequencing data and for differentially expressed gene (DEG) analysis a good quality of the RNA-sequencing run is required. Therefore, a quality control of the RNA-sequencing run was performed. RNA-sequencing (AG Bonn, DZNE Göttingen) resulted in 3,098,782,483 reads with an average of 31,000,000 reads for each individual sequenced sample (n=101). 100% of the reads were 50 bp long (Figure 4.3.3.1). 99.83% of the reads had no ambiguous base content (Figure 4.3.3.1). 72.98% of the reads had a PHRED quality score of minimum 38 (in CLC given maximum PHRED score = 40; low quality: ≤19; medium quality: 20-39; high quality: ≥40; PHRED score 38: 700,129,924 (22.59%); 39: 1,154,171,275 (37.25%); 40: 394,711,679 (12.74%)) (Figure 4.3.3.1). The PHRED quality score is a measure for the quality of the identification of nucleobases of a DNA-sequencing run (base calling accuracy). It indicates the probability that a given base is not correctly detected by the sequencing machine.

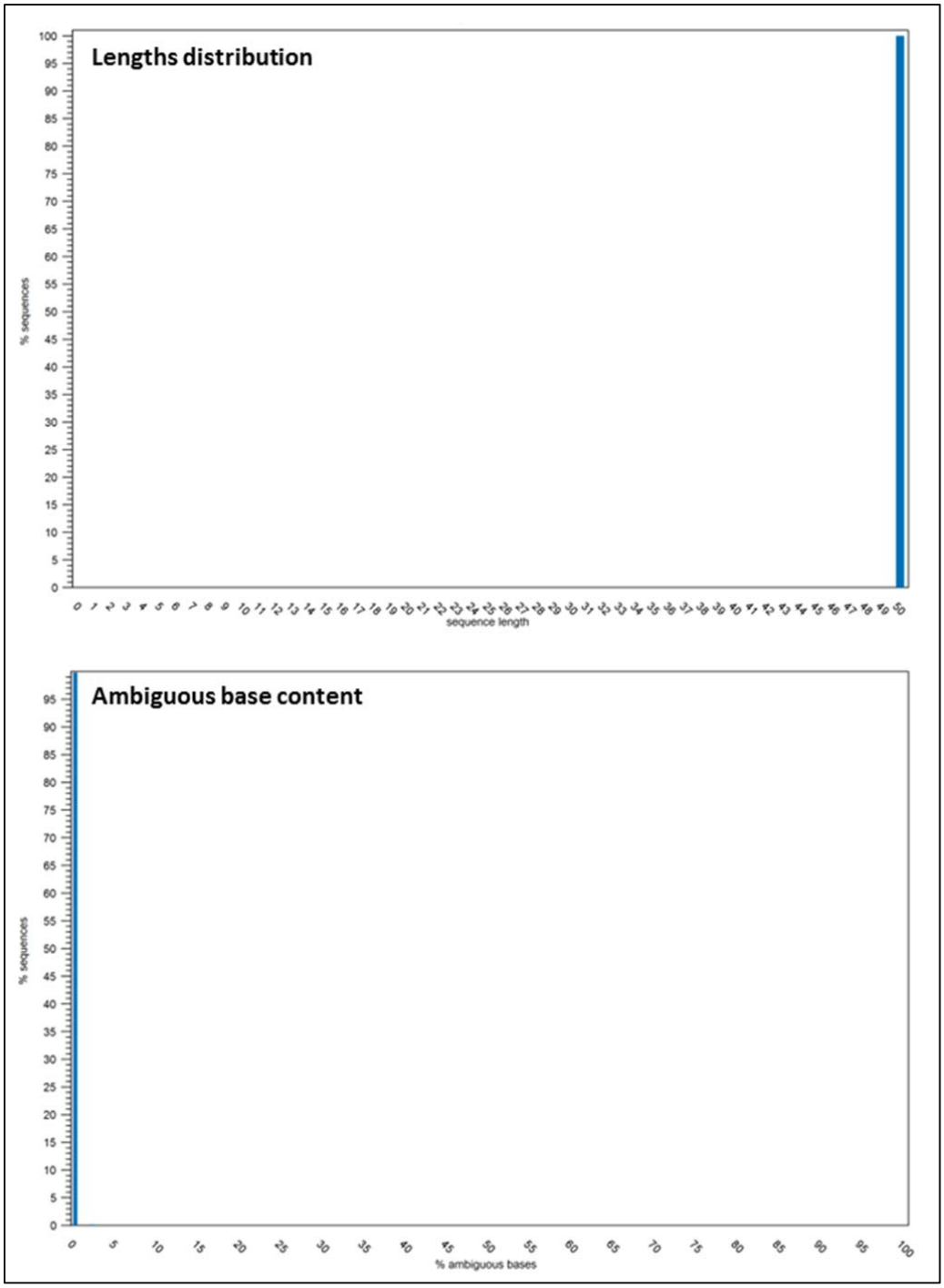

Figure 4.3.3.1: Continued on the next page.

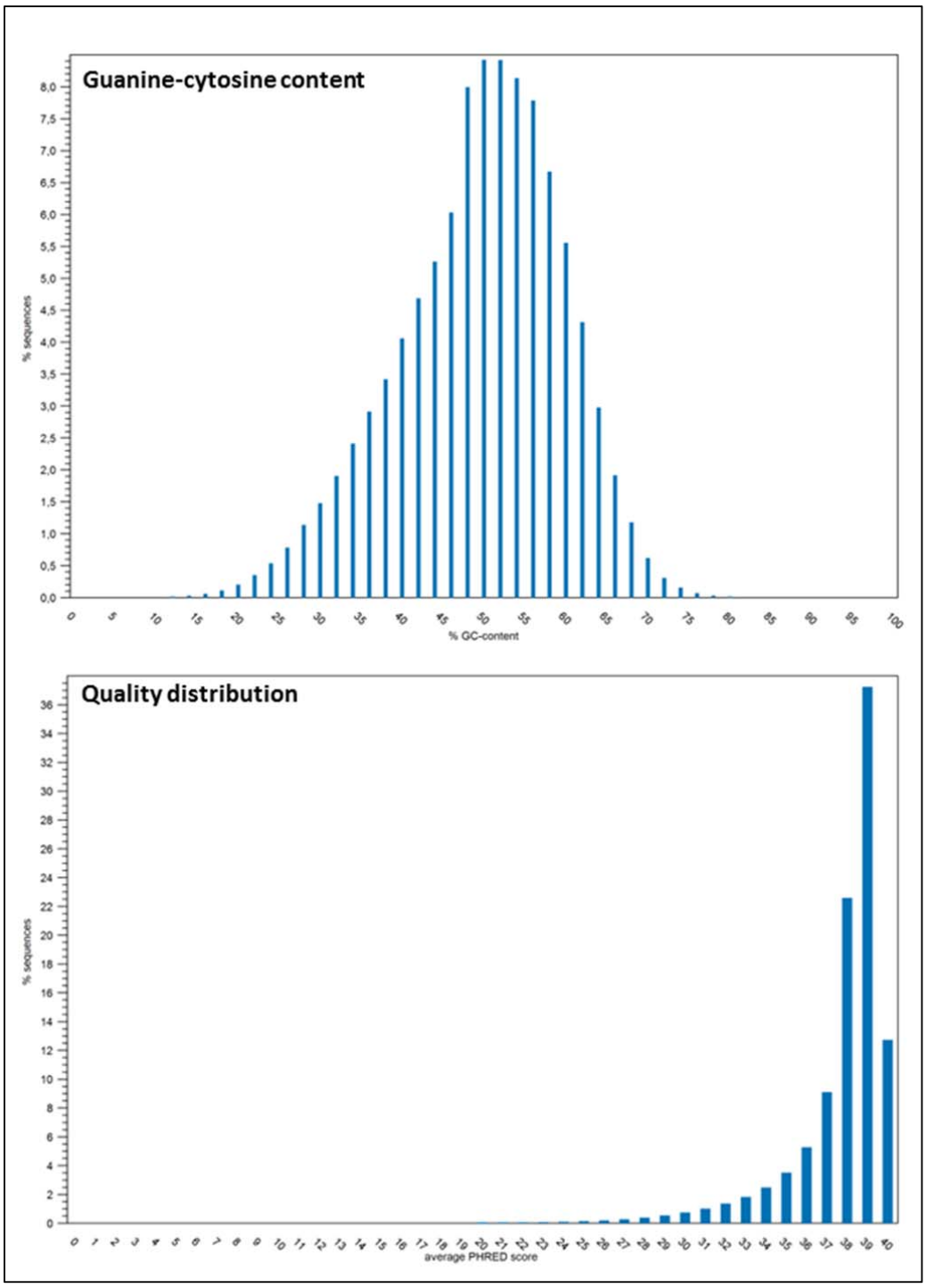

Figure 4.3.3.1: CLC Genomics Workbench lengths distribution (sequence lengths against percentage of sequences), ambiguous base content (percentage of ambiguous base content against percentage of sequences), guanine-cytosine content (percentage of guanine-cytosine content against percentage of sequences) and quality distribution (average PHRED score against percentage of sequences) of all RNA-sequencing reads.

After trimming 3,085,708, 304 reads were left (99.58%). 96.84% of the reads consist still of 50bp (Figure 4.3.3.2). 99.99% of the remaining reads have no ambiguous

base content after trimming (Figure 4.3.3.2). 73.17% of the reads show a PHRED quality score of minimum 38 (PHRED score 38: 704,302,282 (22.82%); 39: 1,158,107,331 (37.53%); 40: 395,648,638 (12.82%)) (Figure 4.3.3.2). Thus, the RNA-sequencing resulted in excellent data quality.

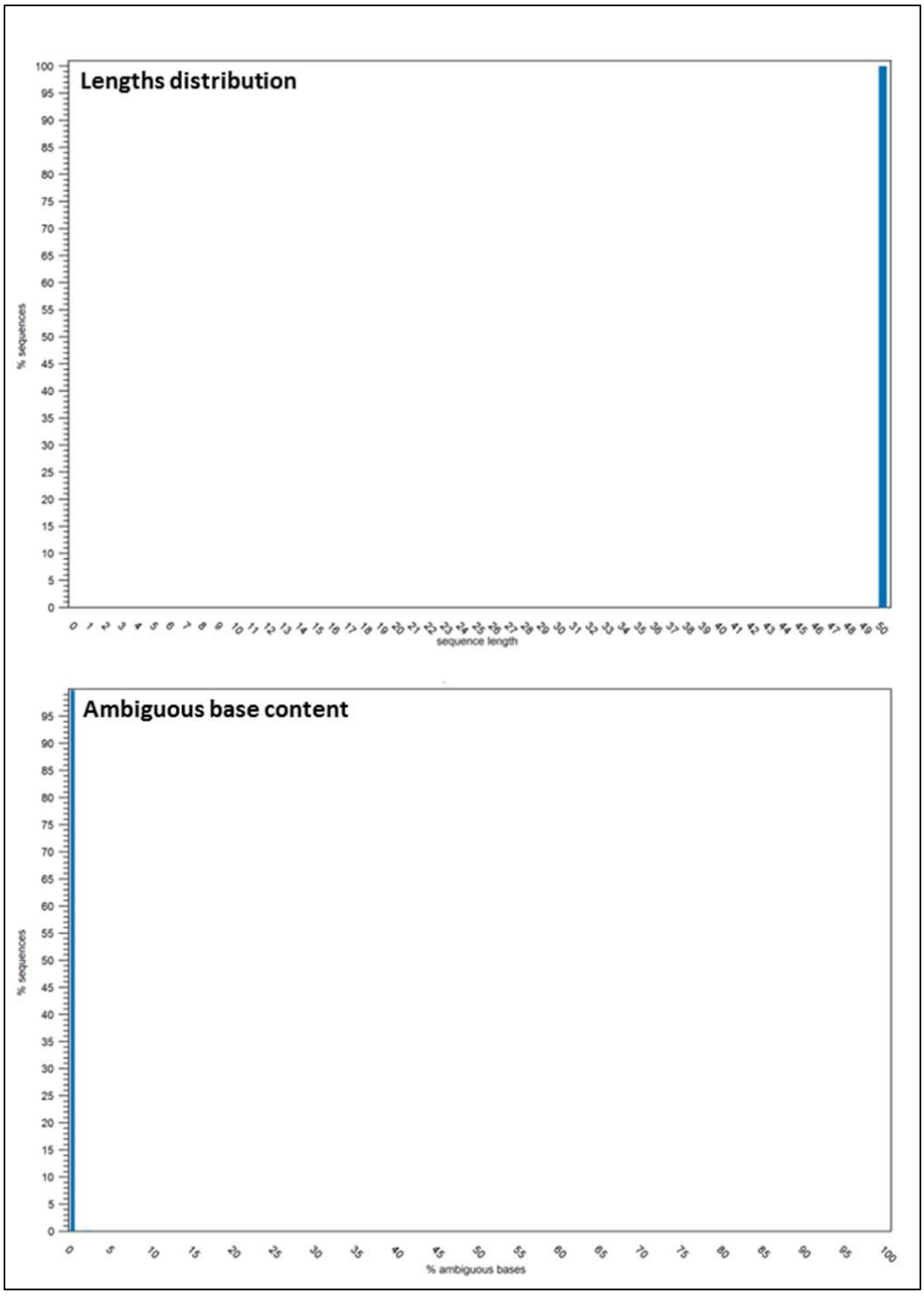

Figure 4.3.3.2: Continued on the next page.

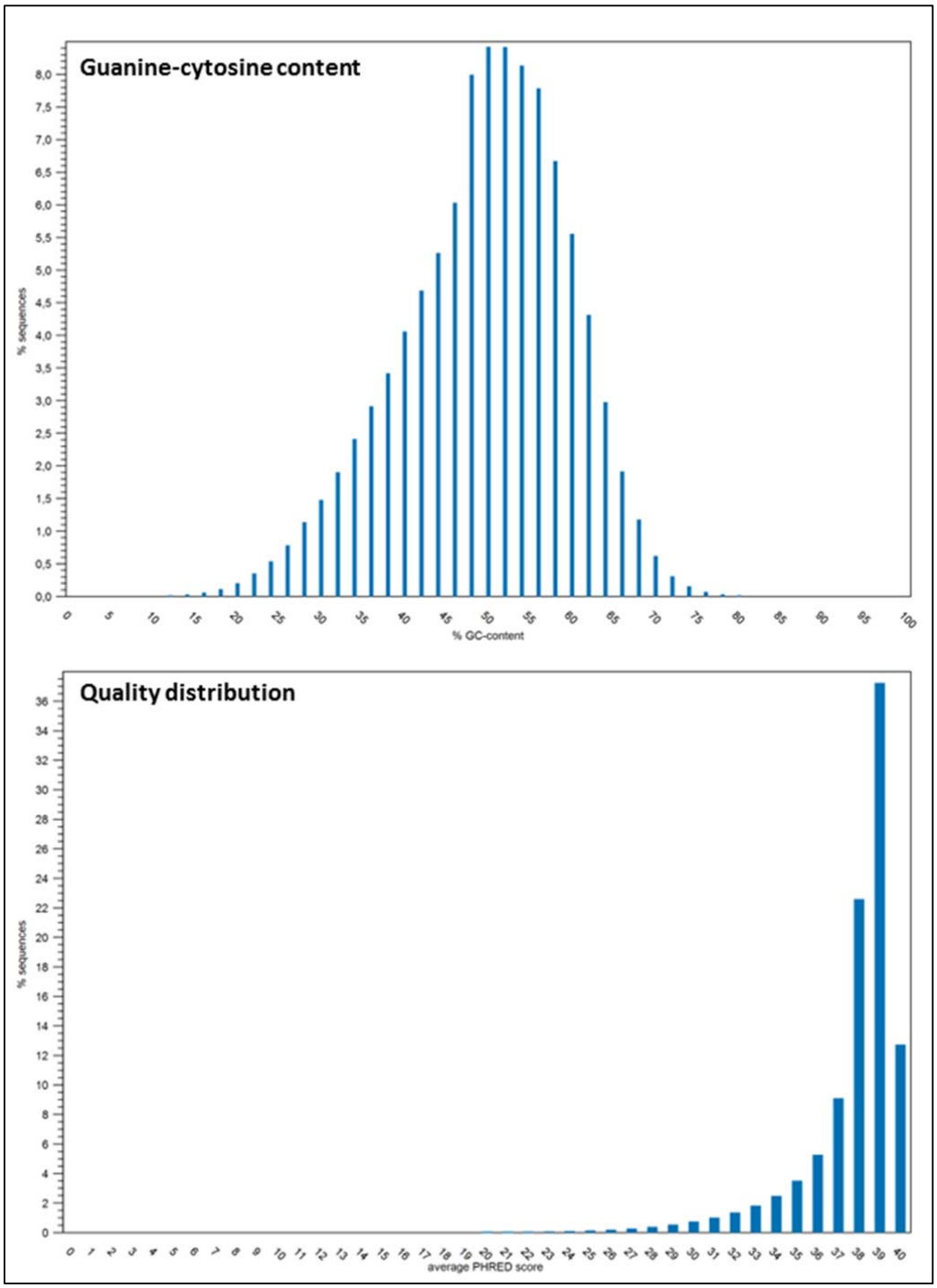

Figure 4.3.3.2: CLC Genomics Workbench lengths distribution (sequence lengths against percentage of sequences), ambiguous base content (percentage of ambiguous base content against percentage of sequences), guanine-cytosine content (percentage of guanine-cytosine content against percentage of sequences) and quality distribution (average PHRED score against percentage of sequences) of all RNA-sequencing reads after trimming.

4.4 Neuropathological changes

Neuropathological changes are a hallmark of NDs and are commonly used as indicators of disease severity in individual samples. Therefore, potential neuropathological changes in the RML injected RiboTag mice were studied by IHC. Staining with SAF84 prion protein antibody after proteinase K treatment to detect proteinase K resistant aggregated prions, staining with GFAP antibody to detect astrogliosis and staining with Iba1 antibody to detect microglia activation were done (Figure 4.4.1). Abnormal staining of Iba1 and GFAP are typical for NDs. Proteinase K resistant prion aggregates are specific for TSEs (Figure 4.4.1, Figure 4.4.2). These abnormal stainings are present only in the clinical disease onset time point of RML injected mice (18 wpi) demonstrating activated microglia, astrogliosis and proteinase K resistant prion aggregates in these samples.

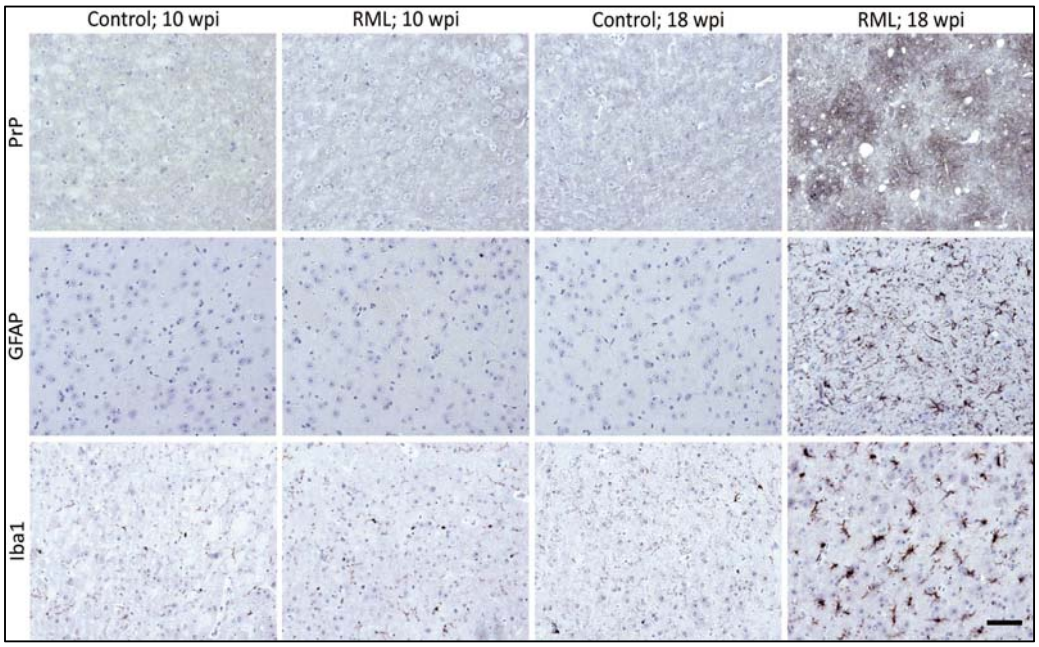

Figure 4.4.1: IHC staining of RML infected and control 4µm brain sections at 10 and 18 wpi to detect potential neuropathological changes. Staining with SAF84 prion protein antibody (black) after proteinase K treatment to detect aggregated prions, staining with GFAP antibody (black) to detect astrogliosis and staining with Iba1 antibody (black) to detect microglia activation (brain region: thalamus; counterstain: hematoxylin; bar: 50 µm).

The Iba1 antibody stained microglia in the 18 wpi RML infected sections are activated cells showing swollen, truncated processes and large cell bodies. In contrast, the Iba1 antibody stained some microglia of controls at the 10 and 18 wpi time points equally well as the RML 10 wpi samples (Figure 4.4.1). These stained

microglia differ in their morphology, they are resting microglia with long, ramified processes and small cell bodies. The similar morphology of microglia in control and RML 10 wpi samples indicates that the 10 wpi time point is very early in disease.

Another eponymous hallmark of TSEs, namely spongiosis, can be seen at the 18 wpi disease time point of RML injected mice (Figure 4.4.1, Figure 4.4.2). None of these neuropathological changes were detected in the early time point (10 wpi), again confirming that these samples were well before clinical disease, or in any of the control samples, confirming that these mice show no neuropathological characteristics of prion disease like expected. In summary, neuropathological changes were exclusively detected in the RML infected mice at the 18 wpi disease time point.

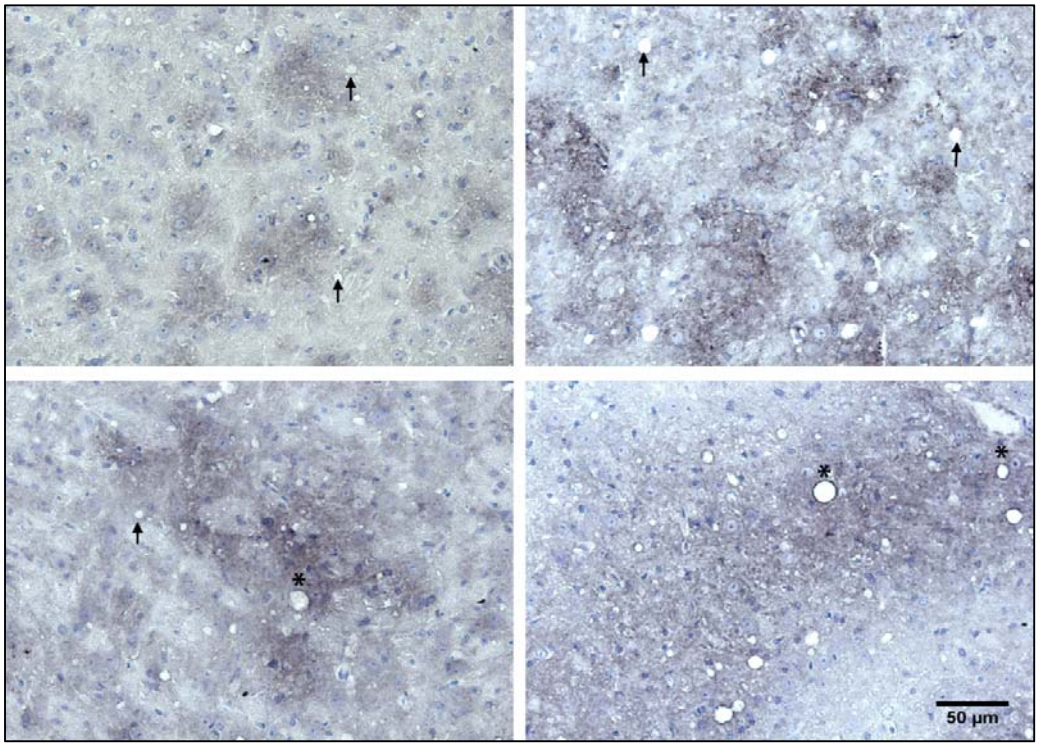

Figure 4.4.2: IHC staining of 4µm thick brain sections of RML infected mice at 18 wpi showing aggregated prions (SAF84 prion protein antibody staining after proteinase K treatment, black) and spongiosis. Spongiosis is exemplary indicated by arrows (→) and possible blood vessels are exemplary indicated by asterisks (*) for differentiation (brain region: thalamus; counterstain: hematoxylin; bar: 50 µm).

4.5 RNA-sequencing data analysis methods

There are many ways to analyze next generation sequencing data (Conesa et al. 2016). We predicted that if our results were robust, the overall results would be similar when using different analysis methods und we thus tried two. For both analysis methods the same raw reads from the same RNA-sequencing run were used. Moreover, for both analyses the DESeq2 package for DEG analysis was used because it is commonly used (Kukurba and Montgomery 2015).

The analyses mainly differ in the expression values for the DEG analysis. The analysis done in Bonn (Melvin Schleif, AG Jackson, DZNE Bonn) is based on unique exon reads. This expression value is the number of reads that match uniquely to the exons including the exon-exon and exon-intron junctions. If a read could be matched to more than one specific gene because there are genes with very similar nucleotide sequences, this read would be excluded for counting of the expression value. The analysis done in Göttingen (Vikas Bansai, AG Bonn, DZNE Göttingen) is based on total gene reads. This expression value is the number of all the reads that are mapped to this gene (reads that map uniquely to the gene plus reads that match to more positions in the reference genome if parameter maximum number of hits for a read > 1). In the case a read would map to multiple genes, this read is shared between the corresponding genes based on their relative abundance.

UER and total gene reads are both absolute, not normalized expression values. Normalization is later done by the DESeq2 package. Furthermore, the two analyses differ in the software and web applications used for quality control, trimming and mapping of the RNA-sequencing reads. In addition, the mouse reference genome was not exactly the same version, though they were closely related. The following sections describe the results received from the two different analysis methods based on either UER or total gene reads.

4.6 RNA-sequencing analysis based on unique exon reads

4.6.1 Cell type specificity

To analyze gene expression changes caused by RML induced neurodegeneration in a cell-type specific manner the immunoprecipitated mRNA has to be cell-type-specific. To demonstrate the specificity of the RiboTag method, enrichment or depletion of known cell type marker genes compared to the total RNA input was investigated based on unique exon reads (Figure 4.6.1). Because the comparison is against the total RNA input the RNA of the cell type of interest is always present in this sample. Thus, the more a cell type is abundant, the less is the enrichment of known marker genes of this cell type, but the greater the depletion of other cell type markers.

As expected, mice expressing the epitope-tagged ribosomes in glutamatergic neurons show enrichment in glutamatergic marker genes and depletion in GABAergic and astrocyte marker genes. GABAergic and GABAergic subtype mouse lines show GABAergic marker enrichment and depletion in glutamatergic and astrocyte markers. The GABAergic subtypes differ like expected in expression pattern of their marker genes SST and Pvalb and the marker gene Homer3, a PV neuron marker. The astrocyte mouse line samples show enrichment in astrocyte marker genes. Thus, the immunoprecipitation harvested mRNA is cell-type-specific and cell-type-specific response of RML induced neurodegeneration can be analyzed.

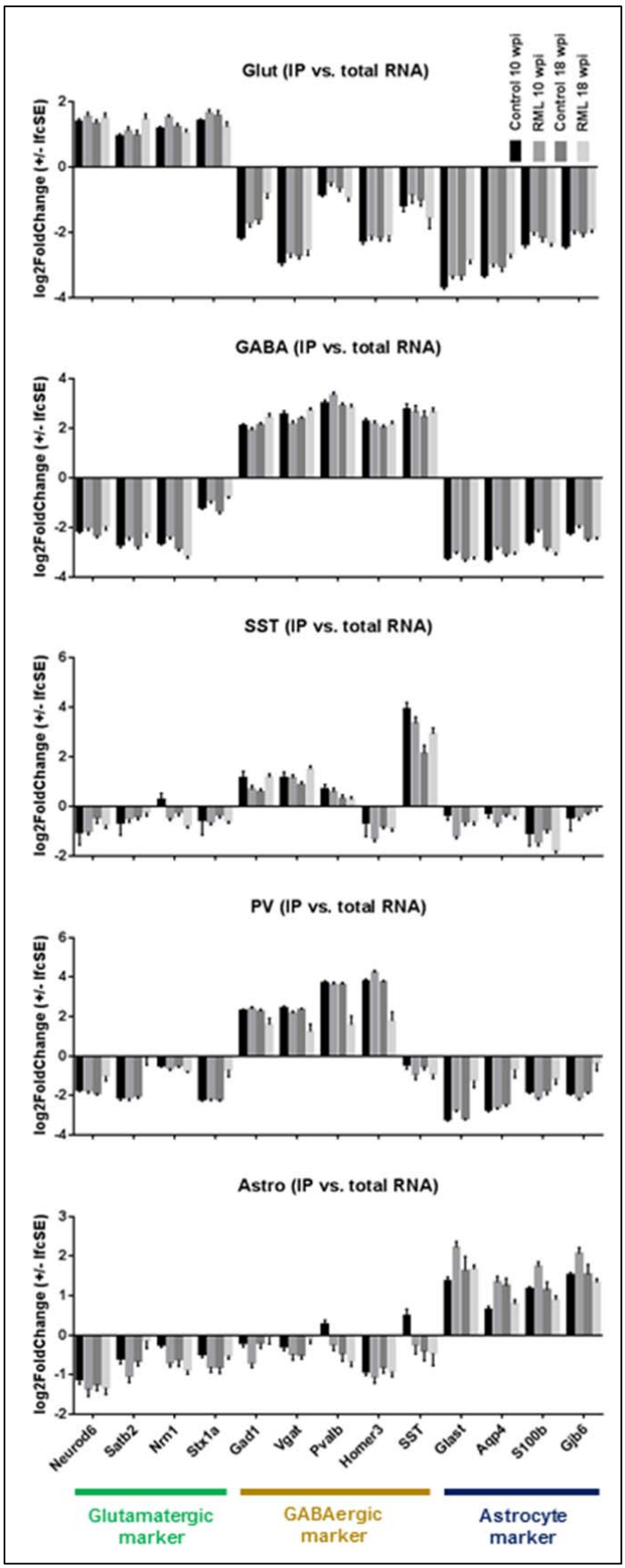
Glut (IP vs. total RNA)
GABA (IP vs. total RNA)
SST (IP vs. total RNA)
PV (IP vs. total RNA)
Astro (IP vs. total RNA)
log2FoldChange (+/- lfcSE)
Control 10 wpi
RML 10 wpi
Control 18 wpi
RML 18 wpi
Neurod6
Satb2
Nrn1
Stx1a
Gad1
Vgat
Pvalb
Homer3
SST
Glast
Aqp4
S100b
Gjb6
Glutamatergic marker
GABAergic marker
Astrocyte marker

4.6.2 Comparison of cell-type-specific gene expression regulation

With the RiboTag system and RNA-sequencing of our samples we detected around 14,500 – 16,000 genes to be expressed in each cell type (expression value: unique exon reads; expression BaseMean ≥ 5; analyzed by Melvin Schleif, AG Jackson, DZNE Bonn). The commonly used expression value UER is the number of reads that match uniquely to the exons including the exon-exon and exon-intron junctions. A summary of the number of genes detected for each cell type at each time point and the number and percentage of differentially expressed genes with chosen statistical cutoffs (pval<0.05 and padj<0.1) is given in table 4.6.2.1. The statistical values for the cutoffs are calculated by the DEseq2 package. The pval is based on a gene by gene t-test (Wald test). Since multiple t-tests were done the padj is calculated to reduce and control for false positive DEGs (Benjamini-Hochberg).
We found that although the 18 wpi time point represented the very beginning of clinical disease, the gene expression changes in the mouse brain were really drastic with too many changes for an in-depth gene expression analysis of which cells were most affected and what were the most changed molecular pathways. However, using the statistical cutoff of padj<0.1 the 10 wpi samples were quite interesting. First, we found glutamatergic neurons were changing. In contrast, GABA neurons, PV neurons and SST neurons were unaltered. Interestingly, we found that astrocytes are highly altered.

Table 4.6.2.1: Number of total and differentially expressed cell-type-specific genes (BaseMean unique exon reads ≥ 5) at 10 and 18 wpi with pval<0.05 and padj<0.1 (NBH vs. RML).

Time point	Cell type	Genes total	pval<0.05	padj<0.1
10 wpi	Glut	15435	1262 (8.2%)	106 (0.7%)
	GABA	15460	327 (2.1%)	2 (0.0%)
	SST	14635	163 (1.1%)	1 (0.0%)
	PV	15763	456 (2.9%)	1 (0.0%)
	Astro	15584	1417 (9.1%)	195 (1.3%)
18 wpi	Glut	15503	6648 (42.9%)	6414 (41.4%)
	GABA	15989	5972 (37.4%)	5681 (35.5%)
	SST	14961	5206 (34.8%)	4643 (31.0%)
	PV	15824	5176 (32.7%)	3387 (21.4%)
	Astro	14512	2195 (15.1%)	987 (6.8%)

To identify and quantify the directions of variability in the data sets a principal component analysis was done. This mathematical analysis can be used for quality control to identify outlying samples and shows principal causes of variation in a dataset. Every dot represents an individual RNA-sequencing sample. Also the principal component analysis with CLC Genomics Workbench based on reads per kilobase per million mapped reads (RPKM) values at 10 wpi indicates that astrocytes are the most altered cell type. The RPKM value is a normalized expression value, in which feature-length and library-size effects were removed. RPKM is the most reported RNA-sequencing expression values (Conesa et al. 2016). All astrocyte control samples cluster very well, showing their similar gene expression. The RML infected samples are not clustering with the control samples, showing the detected gene expression changes induced by RML infection. However, glutamatergic neurons are relatively unchanged, similar to the GABAergic neurons and GABAergic subtypes. The close clustering of NBH and RML groups in GABAergic, somatostatin and PV neurons reflects the small number of gene expression changes at 10 wpi in these cell types (Figure 4.6.2.1).

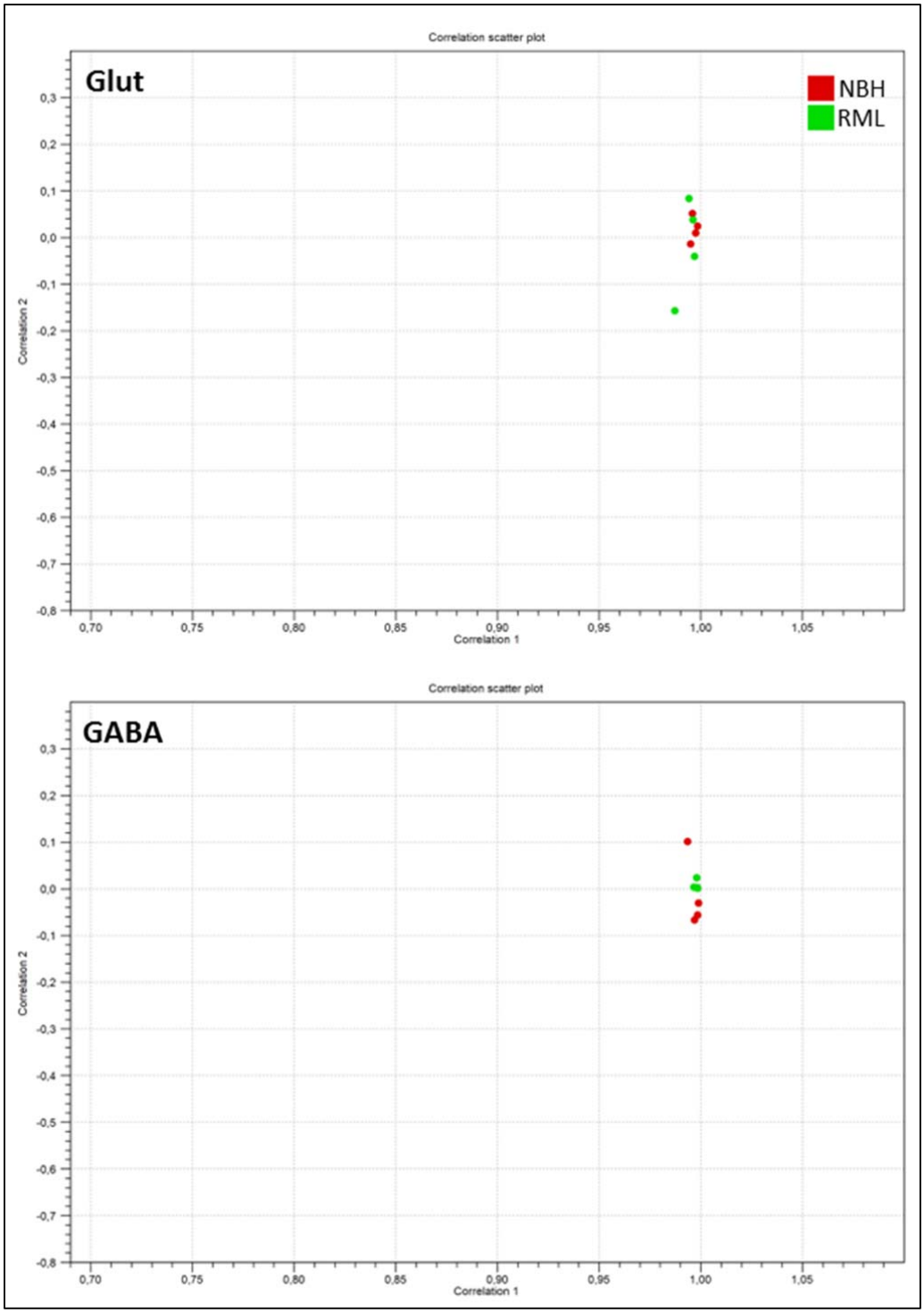

Figure 4.6.2.1: Continued on the next page.

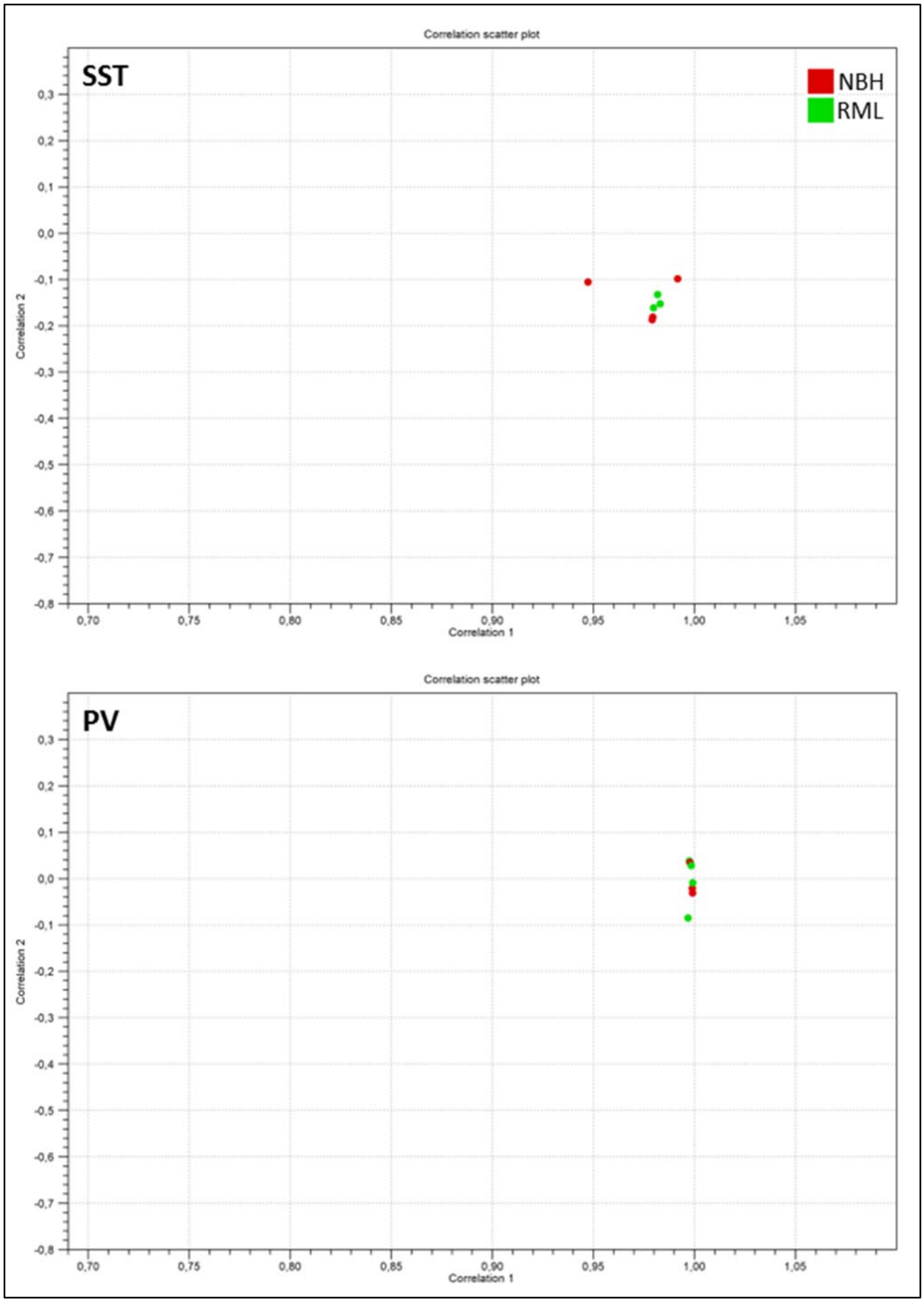

Figure 4.6.2.1: Continued on the next page.

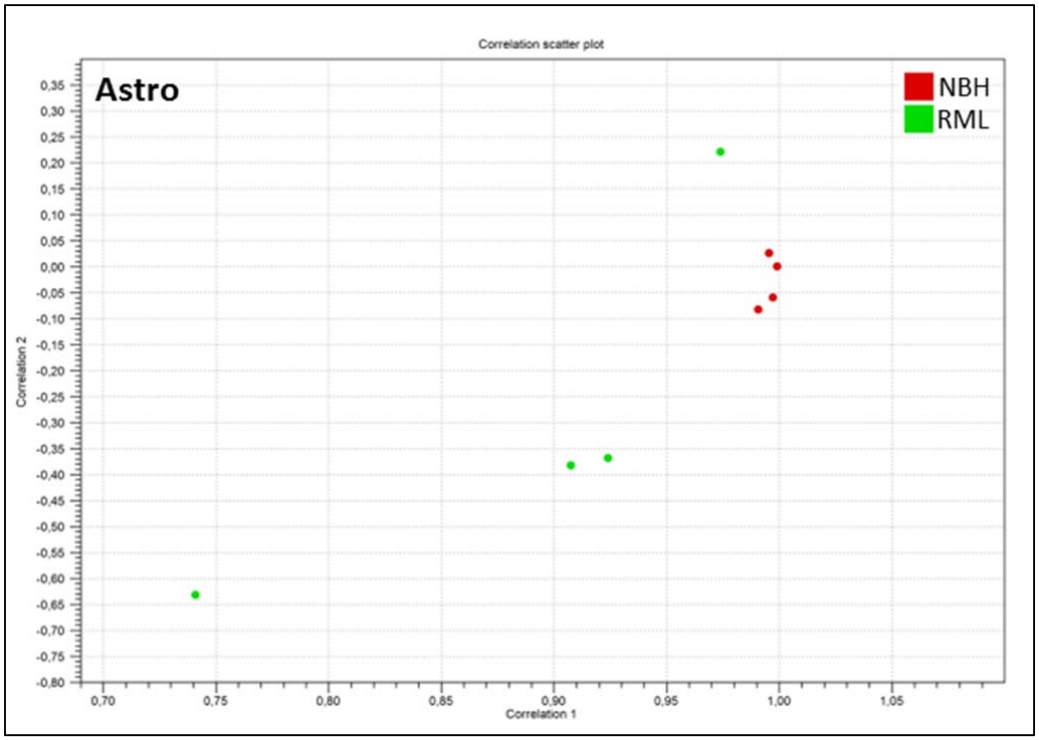

Figure 4.6.2.1: CLC Genomics workbench principal component analysis with correlation scatter plot of the individual samples (NBH and RML) for the different cell types at 10 wpi (horizontal axis range (correlation 1): 0.7 - 1.1; vertical axis range (correlation 2): -0.8 - 0.4).

CLC Genomics Workbench volcano plots based on RPKM values with an empirical analysis of differentially expressed genes (NBH vs. RML; EDGE test based on tagwise dispersions) is used to quickly identify changes in big data sets. Every dot represents a detected gene. The horizontal axis plots the 2logFC of detected genes; the vertical axis plots the –log10 pval. The further away a point on the horizontal axis is from the center (X = 0; unregulated genes), the stronger the gene is regulated. The higher a gene is on the vertical axis, the more significant is the gene regulation. The fold change is a measurement describing the quantity change between two values, here the expression value between the NBH and RML groups (=1: no change of gene expression between the groups; <1: gene down regulated caused by RML infection; >1: gene up regulated caused by RML infection). The fold change can also be given as a logarithmic value (here as 2logFC; (=0: no change of gene expression between the groups; <0: gene down regulated caused by RML infection; >0: gene up regulated caused by RML infection).

Volcano plots show that astrocytes are highly altered. This cell type shows a high distribution of fold changes. A lot of these gene expression changes in astrocytes are also significant with a cutoff of pval 0.05 (pval 0.05 = pval -log10 1.3). Most DEGs of astrocytes are down regulated. GABAergic neurons and PV neurons show

less distribution of DEGs within fold changes and also fewer genes with pval<0.05. SST neurons show in the volcano plot a high distribution within fold changes. A lot of genes are regulated with very high or low fold changes. However, these fold changes are less significant compared to other cell types. Only a small number of genes are regulated with pval<0.05. Glutamatergic neurons show gene expression changes with moderate changes. However, a lot of these changes are significant. Most DEGs in glutamatergic neurons show an up regulation (Figure 4.6.2.2).

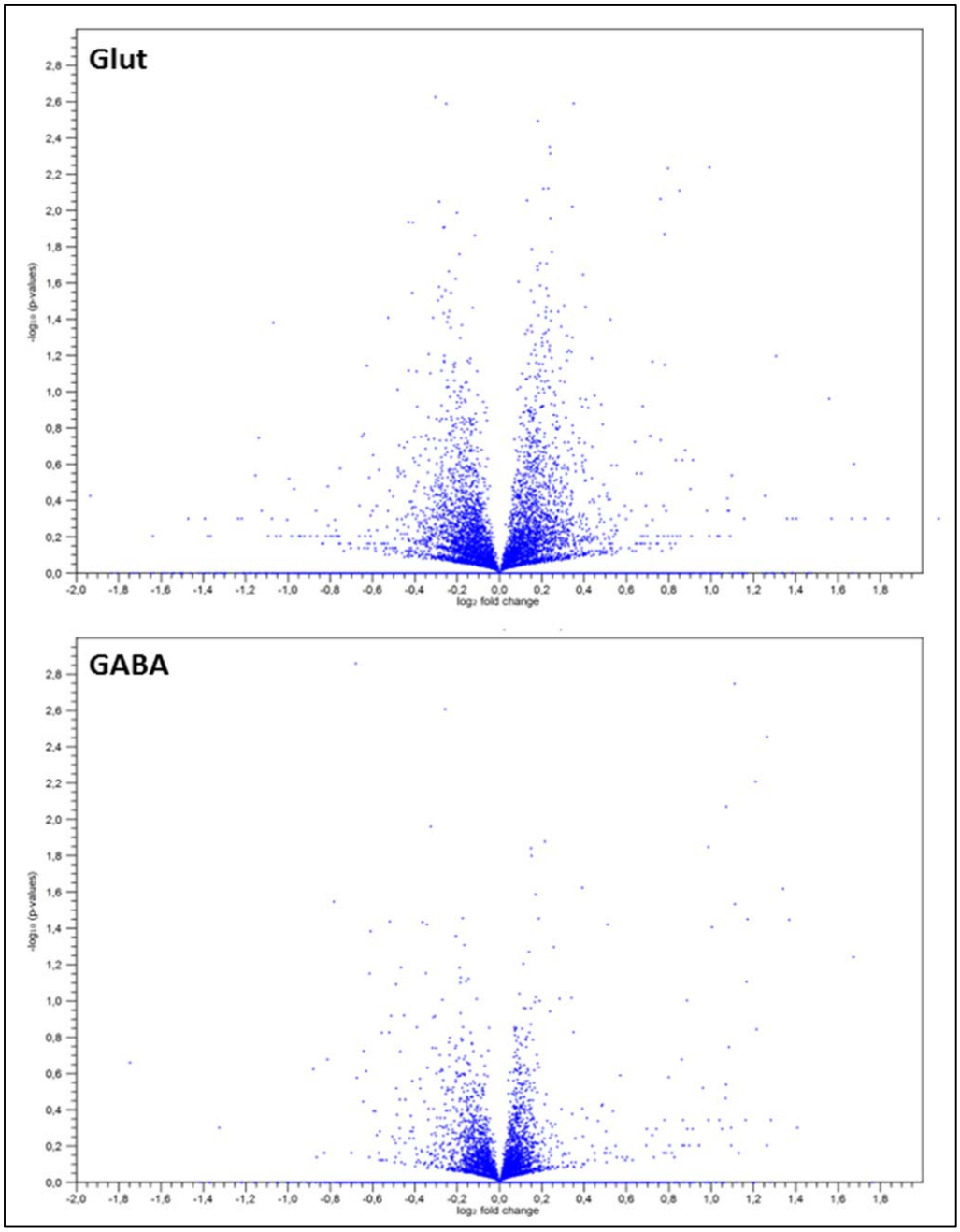

Figure 4.6.2.2: Continued on the next page.

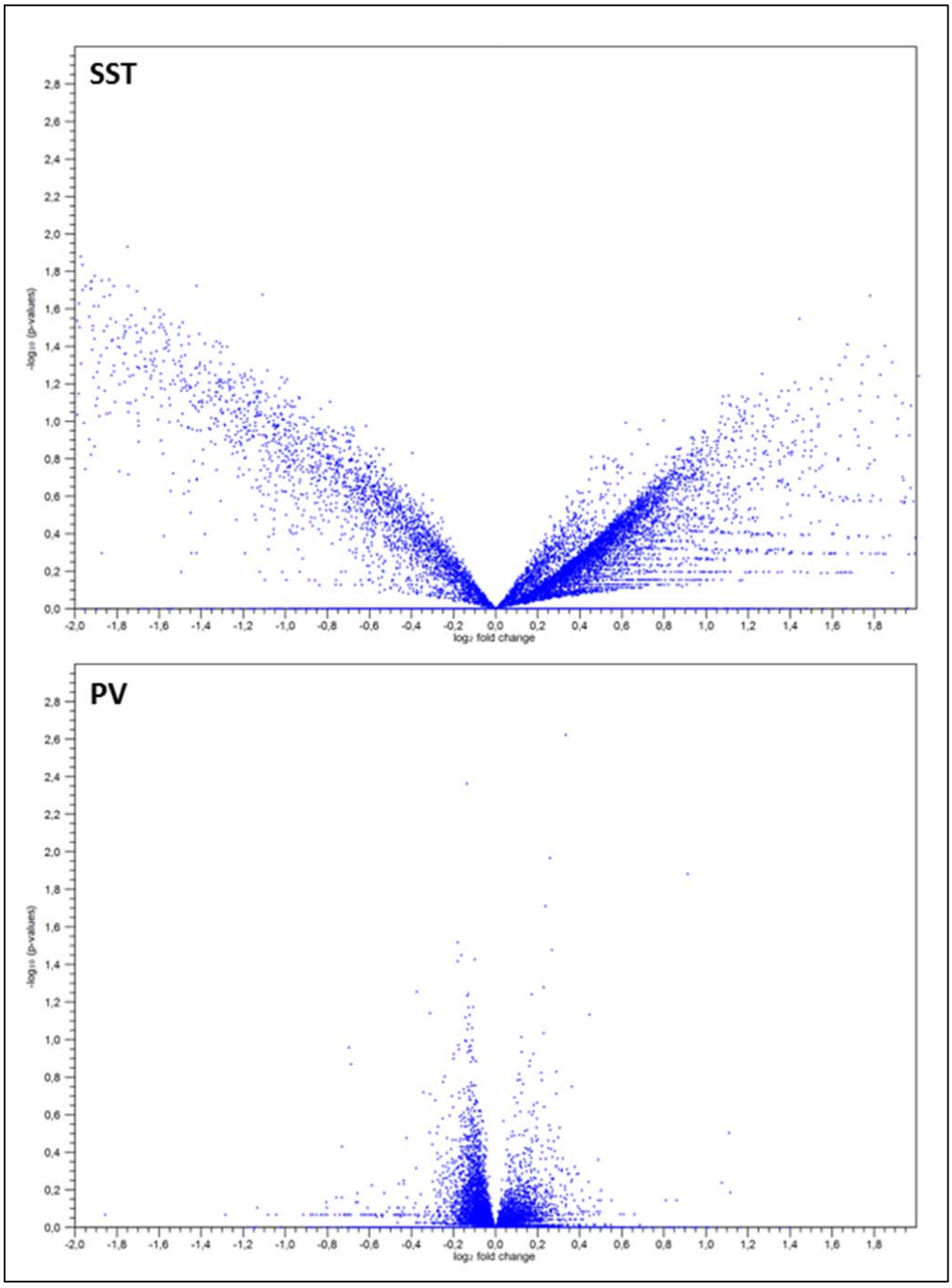

Figure 4.6.2.2: Continued on the next page.

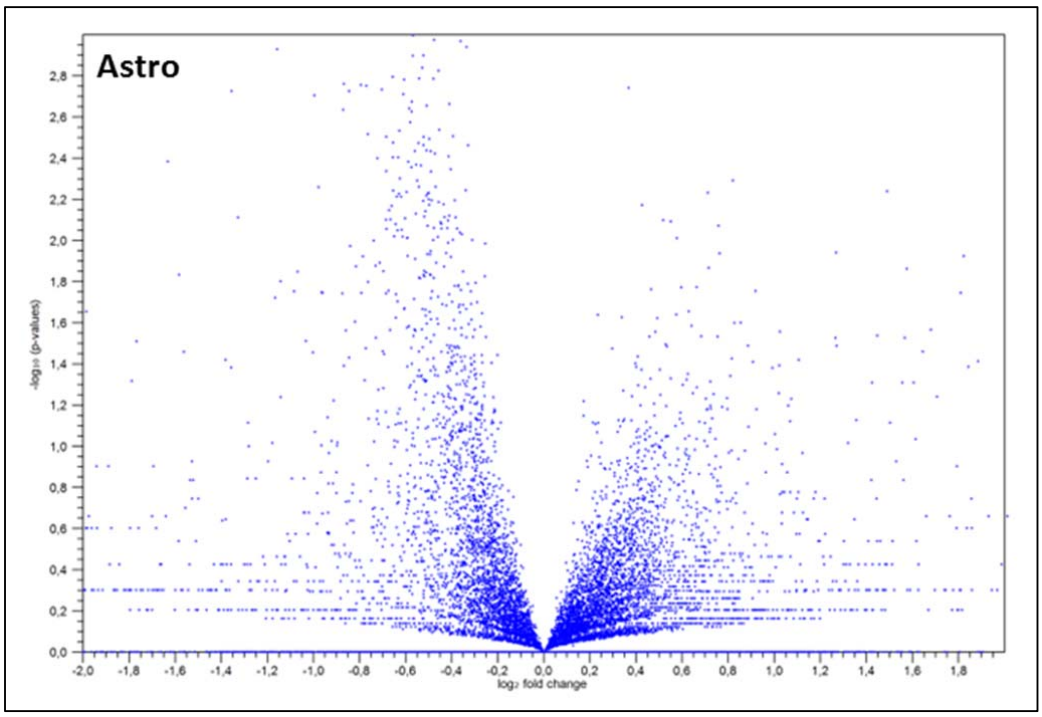

Figure 4.6.2.2: CLC Genomics workbench volcano plots (empirical analysis of differentially gene expression test, NBH and RML) for the different cell types at 10 wpi (horizontal axis range (2logFC): -2 - 2; vertical axis range (-log10 pval): 0 - 3)

Glutamatergic neurons have more up regulation within differentially expressed genes based on unique exon reads, whereas astrocytes show more down regulation within the DEGs (padj<0.1) at the 10 wpi time point (Figure 4.6.2.3A). Comparing glutamatergic neuron and astrocyte DEGs (padj<0.1) at the early time point demonstrate little overlap of differentially expressed genes between these cell types, showing that individual cell types respond to the same ND differently (Figure 4.6.2.3B, Table 4.6.2.2).

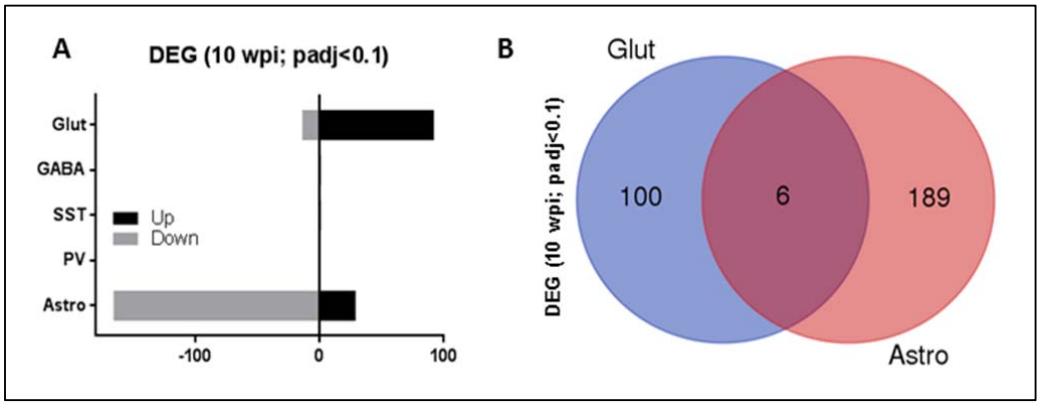

Figure 4.6.2.3: A. Cell-type-specific up and down regulated DEGs at 10 wpi with padj<0.1. B. Overlap of glutamatergic neuron and astrocyte DEGs at 10 wpi with padj<0.1.

Table 4.6.2.2: Comparison of cell-type-specific DEGs (gene input: padj<0.1, RML vs. NBH, 10 wpi).

Cell type	Gene count	Genes
Glut + Astro	6	Lhfpl4 Gas5 Arc Nr4a1 Rpl41 Erc1
Glut	100	Ctss Dusp1 Fth1 Ighm Gm15440 Kcnip2 Ormdl3 1500009C09Rik March8 Pik3ip1 Agpat4 Ank2 Fxyd6 Mprip Taf15 Matn2 Mmd2 Rian Trpm2 Gabrb2 Sox8 Golgb1 Kcnj2 Lamtor4 Crcp Limd2 Atp1a2 Sirt3 Scg5 Sptbn1 Lmbrd2 Tmem50a Klf10 Fgf11 Zcchc24 Slc6a7 Nucb2 Arl4d Trib1 Snrpd2 Apol8 BC026585 Tet2 Lin7a Cacnb4 Gsn Macf1 Rapgef3 Btg2 Zic2 Myo5a Aqp11 Arl2bp Lrrc61 Ppp1r9a Necab1 Plec Tmed9 Pmch Clk1 St6galnac6 Nfrkb Sptb Gsg1l Tceal5 Serinc5 Prdm2 Snn Rasl10b Tma7 Slc25a18 Borcs8 Mllt6 Limch1 Snrnp35 5031439G07Rik Zkscan16 Bloc1s1 Myo6 Lamtor2 Mapk8ip2 Spry4 Zbtb18 S100a1 Tceal6 Zfp831 Tnnt2 Fkbp2 Mcfd2 Sptbn2 Lrrc41 Etnk1 Polr2m Gm11613 Sfxn5 Nr2c2 Zmat2 Clu Amot Sptan1
GABA	2	Sf3b1 Dbp
SST	1	Lgals3
PV	1	Hddc3
Astro	189	Ap2s1 Arl6ip4 Nat14 Plxnb2 Nrgn Rprml Plat Dnajc21 Arl2 Rplp2 Daam2 Stmn3 Ndufb9 Palm Cabp1 Rpl26 Cox6a1 Elob Mrpl18 Slc25a35 Hprt Snx21 Atp5e Abhd8 Uqcr11 Hnrnpa3 Rps4x Ly6h Kcnh1 C130074G19Rik Frzb Tbcc Rps24 Rnaseh2c C1qtnf4 Tox2 Pfdn2 Jund Prr7 Eid2 Mrpl57 Kcnj4 Gm13889 Nr2f2 Rps20 Mapre3 Myo1c Caly Gm10073 Sms Unc79 Rpl13a Lgals3bp Tmsb10 Rps5 Calb2 1500011K16Rik Mrps12 Usmg5 Diras1 6030419C18Rik Ccdc124 Arpc5l Ppp3ca C4b Rps19 Cox7a2l St14 Ppp1r16a Fbxo45 Akap12 Dynll1 Fkbp8 Rps16 Sst Cltb Ccdc92 Ap1s2 Uqcrq Gm31166 Gas2l3 Frat1 Tpgs1 Mrpl43 Rpl14 Tmem191c Krt9 Myh7 Rps21 Epn1 Scand1 Ndufa12 Ctsd Dohh Rps29 Nbeal2 Tmem240 Znhit2 Lsm4 Uqcc2 Abca1 Tnnt1 Smyd2 Bag1 Ccdc85b Eif5b Mcrs1 Bola2 Sncb Zfp871 Hmga1-rs1 Ramp3 Ndufa2 Dynll2 Abhd11os Rnf208 Stmn1 Cd9 Hipk2 Golga4 Pcp2 Rps26 Lypla2 Mvb12a Gabarapl1 Ctxn1 Uqcr10 Stard10 Denr Snhg8 Selenom Pigyl Itga7 Rfxap Rprm Ube2m Uchl1 Zrsr2 Wasf1 Cycs Use1 Ndufaf8 Bola1 Tcirg1 Acbd6 Fxyd7 Polr2f Egln2 Tbr1 Vti1b Cck Rpl28 Calm2 Lars2 Rnf123 Cox17 Rps8 Kcnh3 Camk2n2 Epha5 Upf2 Rplp1 Cdr1 Rpl38 Coa3 Ywhah Nog Pcp4 Nhp2 Glrx5 Matk Fcor Plekho1 Cxx1b Sik2 Nfkbil1 Romo1 Pkig Hspbp1 Ssbp4 Pfdn5 Ubald1 Htt Rpl19 Gm1673 Serpina3n Zfp160 Pcsk1n Arhgdig

4.6.3 Gene expression regulation in glutamatergic neurons

We next wondered if specific molecular pathways or gene ontology terms were changed in the specific cell types caused by RML induced neurodegeneration. We therefore used the IPA software and the DAVID Bioinformatics Resources web application. The canonical pathway analysis (IPA) shows the cell-type-specific disease response of the individual cell types at 10 wpi (padj<0.1). The most prominent IPA canonical pathway in the glutamatergic neurons is “Sertoli Cell - Sertoli Cell Junction Signaling”, which included only spectrins (cytoskeletal proteins; SPTAN1, SPTB, SPTBN1 and SPTBN2). Molecular and cellular functions analysis shows significant changes in molecular transport, cellular assembly and organization, cell morphology, signaling and cell death and survival (Table 4.6.3.1).

Table 4.6.3.1: IPA top canonical pathways and molecular and cellular functions altered in glutamatergic neurons (gene input: padj<0.1, RML vs. NBH, 10 wpi; list filter: pval<0.05, molecule hits>1)

Canonical pathway	**pval**	**Overlap**
Sertoli Cell-Sertoli Cell Junction Signaling	1.40E-02	2.3% (4/172)
Molecular and cellular functions	**pval**	**Molecules**
Molecular Transport	4.74E-02 – 2.54E-05	28
Cellular Assembly and Organization	4.92E-02 – 2.87E-05	23
Cell Morphology	4.92E-02 – 1.06E-04	29
Cell-To-Cell Signaling and Interaction	4.74E-02 – 3.41E-04	25
Cell Death and Survival	4.88E-02 – 4.65E-04	26

The gene ontology analysis (DAVID) resulted in even more genes associated with actin, actin binding and cytoskeleton. Next to cytoskeleton associated gene ontology terms several transport, binding and protein binding gene ontology terms are detectable. Many genes within the cellular compartment analysis are also associated to actin and cytoskeleton, but also to cell organelles and synapses (Table 4.6.3.2).

Table 4.6.3.2: DAVID top gene ontology terms (CC: Cellular compartment, BP: Biological process, MF: Molecular function) altered in glutamatergic neurons (gene input: padj<0.1, RML vs. NBH, 10 wpi; list filter: pval<0.05, molecule hits>1)

GO	GO number + GO term name	pval
CC	GO:0043229 Intracellular organelle	2.01E-07
	GO:0015629 Actin cytoskeleton	3.01E-07
	GO:0043226 Organelle	6.60E-07
	GO:0030864 Cortical actin cytoskeleton	7.12E-07
	GO:0030863 Cortical cytoskeleton	6.27E-06
	GO:0097458 Neuron part	7.08E-06
	GO:0044424 Intracellular part	1.73E-05
	GO:0045202 Synapse	1.89E-05
	GO:0043227 Membrane-bounded organelle	2.19E-05
	GO:0044456 Synapse part	3.00E-05
BP	GO:1902578 Single-organism localization	1.84E-08
	GO:0065008 Regulation of biological quality	1.18E-07
	GO:0044765 Single-organism transport	1.52E-07
	GO:0051179 Localization	1.64E-07
	GO:0032412 Regulation of ion transmembrane transporter activity	3.61E-07
	GO:0022898 Regulation of transmembrane transporter activity	4.90E-07
	GO:0032409 Regulation of transporter activity	8.37E-07
	GO:0034765 Regulation of ion transmembrane transport	2.67E-06
	GO:0034762 Regulation of transmembrane transport	4.04E-06
	GO:0006811 Ion transport	5.96E-06
MF	GO:0003779 Actin binding	6.36E-07
	GO:0008092 Cytoskeletal protein binding	9.78E-05
	GO:0005200 Structural constituent of cytoskeleton	7.06E-04
	GO:0005509 Calcium ion binding	3.18E-03
	GO:0098641 Cadherin binding involved in cell-cell adhesion	3.21E-03
	GO:0098632 Protein binding involved in cell-cell adhesion	3.69E-03
	GO:0098631 Protein binding involved in cell adhesion	4.02E-03
	GO:0045296 Cadherin binding	4.58E-03
	GO:0030506 Ankyrin binding	5.19E-03
	GO:0005515 Protein binding	7.99E-03

If changes of gene expression are coordinated the IPA upstream regulator analysis can identify the upstream transcriptional regulators responsible for the observed gene expression regulation. After applying this method top candidate upstream regulators in glutamatergic neurons are displayed in table 4.6.3.3. They are sorted by pval or z-score and their significantly changed target molecules within our statistical cutoff of padj<0.1 in the dataset are also listed. The purpose of the activation z-score is to conclude the activation state of a predicted transcriptional regulator, so if the upstream regulator is activated or inhibited. If it is an activating regulator and the target genes are up regulated, the predicted activation state of this regulator is “activated”. If the target genes are down regulated the predicted activation state is “inhibited”. If it is an inhibiting regulator and the target genes are

down regulated, the predicted activation state of this regulator is “activated”. If the target genes are up regulated the predicted activation state is “inhibited”.

Table 4.6.3.3: IPA top upstream regulators sorted by pval or activation z-score in glutamatergic neurons with 2logFC, predicted activation state and significantly changed target molecules (gene input: padj<0.1, RML vs. NBH, 10 wpi).

Regulator	2logFC	z-score	Activation	Target molecules
PSEN1	0.08	0.38	---	ARC ATP1A2 CTSS DUSP1 GAS5
ADORA2A	0.05	-1.07	---	ATP1A2 DUSP1 NR4A1 SPTBN1
Regulator	**2logFC**	**pval**	**Activation**	**Target molecules**
EPB41	-0.14	4.43E-04	---	Ank2 SPTAN1
GNB2	0.05	7.14E-04	---	ARC DUSP1 NR4A1
GNB1	0.01	7.14E-04	---	ARC DUSP1 NR4A1
PSEN1	0.08	9.30E-04	---	ARC ATP1A2 CTSS DUSP1 GAS5
miR-122-5p	---	1.59E-03	---	Ank2 ATP1A2 TRIB1

4.6.4 Gene expression regulation in GABAergic neurons and subtypes

With the standard cutoff of padj<0.1 there are only one or two genes significantly changed in GABAergic neurons, SST neurons and PV neurons based on unique exon read analysis. Therefore, the number of DEGs is too small for an in-depth gene expression analysis with changed canonical pathways and gene ontology terms, showing that the used cutoff is very stringent to detect early changes in gene expression in these cell types and confirming that the 10 wpi time point is well before clinical disease.

4.6.5 Gene expression regulation in astrocytes

Astrocytes also show a cell-type-specific disease response at 10 wpi (padj<0.1). Actively translated mRNAs changed in this cell type are mainly down regulated ribosomal proteins (IPA canonical pathways: “EIF2 Signaling”, “Regulation of eIF4 and p70S6K Signaling”, “mTOR Signaling”) and down regulated members of the electron transport chain (IPA canonical pathways: “Oxidative Phosphorylation”, “Mitochondrial Dysfunction”). Altered molecular and cellular functions are cell death and survival, lipid metabolism, small molecule biochemistry, gene expression and protein synthesis (Table 4.6.5.1).

Table 4.6.5.1: IPA top canonical pathways and molecular and cellular functions altered in astrocytes (gene input: padj<0.1, RML vs. NBH, 10 wpi; list filter: pval<0.05, molecule hits>1)

Canonical pathway	pval	Overlap
EIF2 Signaling	2.23E-13	9.2% (19/207)
Oxidative Phosphorylation	3.89E-09	11.1% (11/99)
Mitochondrial Dysfunction	5.33E-07	6.9% (11/159)
Regulation of eIF4 and p70S6K Signaling	2.34E-06	6.7% (10/149)
mTOR Signaling	2.01E-05	5.3% (10/190)
Molecular and cellular functions	**pval**	**Molecules**
Cell Death and Survival	4.85E-02 – 7.19E-07	46
Lipid Metabolism	2.94E-02 – 9.73E-05	7
Small Molecule Biochemistry	3.90E-02 – 9.73E-05	13
Gene Expression	1.97E-02 – 1.18E-04	9
Protein Synthesis	4.44E-02 – 5.87E-04	10

The changed mRNAs of proteins building the electron transport chain are integrated in cytochrome c or complex I, III, IV and V. No member of complex II is significantly altered. All of these electron transport chain associated DEGs found by IPA are down regulated (Figure 4.6.5.1). The differentially expressed ribosomal proteins are listed in table 4.6.5.2. Moreover, all significantly changed ribosomal proteins are down regulated demonstrating the massive down regulation of DEGs in astrocytes.

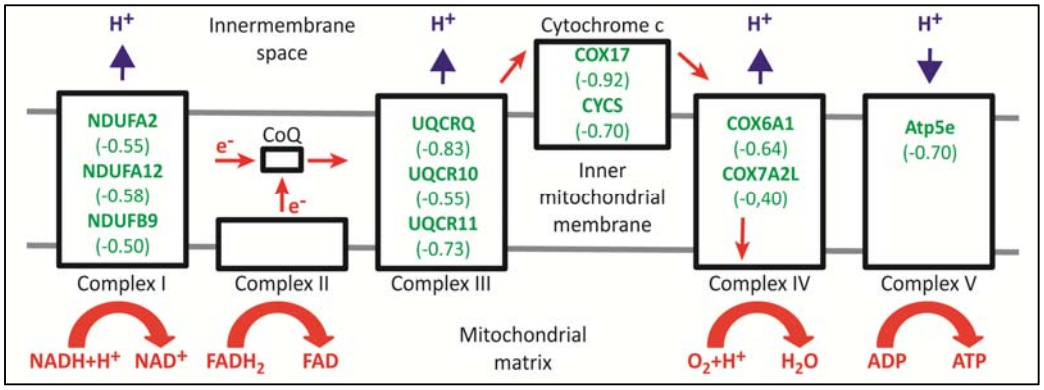

Figure 4.6.5.1: Electron transport chain with DEGs in astrocytes and their 2logFC in green. Negative 2logFCs indicate genes are all down regulated (gene input: padj<0.1, RML vs. NBH, 10 wpi).

Table 4.6.5.2: Regulated ribosomal proteins in astrocytes with 2logFC and padj (gene input: padj<0.1, RML vs. NBH, 10 wpi).

Regulated ribosomal proteins	2logFC	padj
Mrpl18	-0.56	7.48E-02
Mrps12	-0.94	2.11E-03
Rpl13a	-0.43	7.90E-02
Rpl14	-0.54	2.89E-02
Rpl19	-0.63	5.32E-03
Rpl26	-0.66	2.82E-02
Rpl28	-0.66	1.87E-02
Rpl38	-0.72	2.57E-02
Rpl41	-0.59	5.24E-02
Rplp1	-0.93	3.83E-05
Rplp2	-0.91	4.39E-06
Rps16	-1.05	1.84E-03
Rps19	-0.61	4.66E-02
Rps20	-0.65	3.86E-04
Rps21	-0.66	2.85E-02
Rps24	-0.58	7.90E-02
Rps26	-0.74	6.16E-03
Rps29	-0.74	1.77E-02
Rps4x	-0.46	8.21E-02
Rps5	-0.37	6.31E-02
Rps8	-0.49	4.44E-02

DAVID gene ontology analysis with cellular compartments, biological processes and molecular functions confirms the IPA results. Most gene ontology terms detected are associated with the down regulated ribosomal proteins and the changed genes of the electron transport chain (Table 4.6.5.3).

Table 4.6.5.3: DAVID top gene ontology terms (CC, BP and MF) altered in astrocytes (gene input: padj<0.1, RML vs. NBH, 10 wpi; list filter: pval<0.05, molecule hits>1)

GO	GO number + GO term name	pval
CC	GO:0005840 Ribosome	1.41E-16
	GO:0022626 Cytosolic ribosome	3.16E-15
	GO:0044391 Ribosomal subunit	9.05E-15
	GO:0044445 Cytosolic part	6.84E-12
	GO:0030529 Intracellular ribonucleoprotein complex	3.68E-10
	GO:1990904 Ribonucleoprotein complex	3.78E-10
	GO:0022627 Cytosolic small ribosomal subunit	1.10E-09
	GO:0015935 Small ribosomal subunit	4.69E-09
	GO:0005737 Cytoplasm	9.28E-09
	GO:0005829 Cytosol	2.50E-08
BP	GO:0006412 Translation	2.57E-13
	GO:0043043 Peptide biosynthetic process	5.52E-13
	GO:0043604 Amide biosynthetic process	1.12E-12
	GO:0006518 Peptide metabolic process	8.96E-12
	GO:1901566 Organonitrogen compound biosynthetic process	9.11E-12
	GO:1901564 Organonitrogen compound metabolic process	1.70E-11
	GO:0043603 Cellular amide metabolic process	1.61E-10
	GO:0044271 Cellular nitrogen compound biosynthetic process	4.56E-06
	GO:0034641 Cellular nitrogen compound metabolic process	8.37E-06
	GO:0044267 Cellular protein metabolic process	8.63E-06
MF	GO:0003735 Structural constituent of ribosome	3.01E-17
	GO:0005198 Structural molecule activity	6.11E-10
	GO:0019843 rRNA binding	8.64E-05
	GO:0003723 RNA binding	8.71E-05
	GO:0070180 Large ribosomal subunit rRNA binding	2.65E-04
	GO:0015078 Hydrogen ion transmembrane transporter activity	3.39E-04
	GO:0044822 Poly(A) RNA binding	7.01E-04
	GO:0009055 Electron carrier activity	7.48E-04
	GO:0008092 Cytoskeletal protein binding	8.32E-04
	GO:0016681 Oxidoreductase activity, acting on diphenols…	1.75E-03

The top upstream regulator of the IPA analysis is RICTOR (RPTOR independent companion of MTOR complex 2). This regulator is associated with most of the down regulated ribosomal proteins and most of the proteins altered in the electron transport chain. RICTOR itself is slightly up regulated (2logFC: 0.16065; activation z-score: 4.71; not significant) and it is responsible for the down regulation of these proteins. Therefore, IPA predicts an activation of RICTOR. Genes regulated by RICTOR are listed in table 4.6.5.4.

Table 4.6.5.4: DEGs regulated by RICTOR in astrocytes with 2logFC and padj (gene input: padj<0.1, RML vs. NBH, 10 wpi).

RICTOR regulated genes	2logFC	padj
Atp5e	-0.70	3.11E-02
Cox17	-0.92	4.70E-04
Cox6a1	-0.64	8.80E-03
Cox7a2l	-0.40	7.90E-02
Ndufa2	-0.55	7.79E-02
Ndufb9	-0.50	8.89E-02
Rpl13a	-0.43	7.90E-02
Rpl14	-0.54	2.89E-02
Rpl26	-0.66	2.82E-02
Rpl28	-0.66	1.87E-02
Rpl38	-0.72	2.57E-02
Rpl41	-0.59	5.24E-02
Rplp1	-0.93	3.83E-05
Rplp2	-0.91	4.39E-06
Rps19	-0.61	4.66E-02
Rps21	-0.66	2.85E-02
Rps24	-0.58	7.90E-02
Rps26	-0.74	6.16E-03
Rps29	-0.74	1.77E-02
Rps4x	-0.46	8.21E-02
Rps5	-0.37	6.31E-02
Rps8	-0.49	4.44E-02
Tcirg1	0.64	7.47E-02
Uqcr10	-0.55	8.65E-02
Uqcr11	-0.73	7.19E-03
Uqcrq	-0.83	6.99E-03

In addition to RICTOR there are other upstream regulators responsible for the gene expression changes in astrocytes caused by RML induced neurodegeneration. Table 4.6.5.5 lists other upstream regulators and their target molecules highlighted by activation z-score and pval. A lot of the target molecules are again ribosomal proteins or members of the electron transport chain.

Table 4.6.5.5: IPA top upstream regulators (without RICTOR) sorted by pval or activation z-score in astrocytes with 2logFC, predicted activation and significantly changed target molecules (gene input: padj<0.1, RML vs. NBH, 10 wpi).

Regulator	2logFC	z-score	Activation	Target molecules
RB1	0.23	-2.65	Inhibited	COA3 COX17 COX6A1 MYH7 NDUFA2 TNNT1 UQCRQ
FOXO1	0.11	-2.00	Inhibited	Atp5e MRPL57 MRPS12 NDUFA12
PAX6	0.10	-1.98	---	PALM PCSK1N SST TBR1
NOS2	-0.05	2.00	Activated	CYCS LGALS3BP MYH7 SERPINA3
KDM5A	0.181	2.65	Activated	COA3 COX17 COX6A1 MYH7 NDUFA2, TNNT1 UQCRQ
Regulator	**2logFC**	**pval**	**Activation**	**Target molecules**
POLG	0.01	9.37E-10	---	COX7A2L RPL14 RPS16 RPS19 RPS24 RPS5 USE1
RRP1B	-0.01	6.89E-06	---	RPL13A RPL14 RPL19 Rplp1 RPS19 RPS26 RPS5 RPS8
ZFHX3	-0.36	1.32E-05	---	DOHH ROMO1 Rplp1 RPLP2 SST TBR1 UQCR10
LMX1A	0.08	1.13E-04	---	COX6A1 NDUFA2 UQCRQ
KDM5A	0.18	1.60E-04	Activated	COA3 COX17 COX6A1 MYH7 NDUFA2 TNNT1 UQCRQ

4.6.6 Summary of unique exon read data analysis

Using the first analysis we found that at disease onset (18 wpi) a drastic regulation of gene expression is detectable. To detect which cells are affected earliest and how they respond to the emerging disease the early disease time point (10 wpi) was most informative. First, we found glutamatergic neurons were changing. However, GABAergic neurons, PV neurons and SST neurons were unaltered. Moreover, we found that astrocytes are highly altered. Glutamatergic neurons have more up regulation within DEGs, whereas astrocytes show more down regulation within the DEGs. Comparison of the DEGs of the different cell types with little overlap demonstrate that individual cell types respond to the same RML induced neurodegeneration differently. Canonical pathway analysis show actively translated mRNAs changed in the astrocytes are mainly ribosomal proteins and members of the electron transport chain. Glutametergic gene ontology analysis possesses genes associated to actin, actin binding, cytoskeleton, cellular transport and signaling.

4.7 RNA-sequencing analysis based on total gene reads

4.7.1 Cell type specificity

To demonstrate the specificity of the RiboTag method and the resulting immunoprecipitated cell-type-specific mRNA, enrichment or depletion of known cell type marker genes compared to the total RNA was also investigated for the second next generation sequencing analysis (Figure 4.7.1). This analysis was based on total gene read counts of the RNA-sequencing analysis done in Göttingen (Vikas Bansai, AG Bonn, DZNE Göttingen). Once again, the total gene read data analysis shows that immunoprecipitated mRNA is cell-type-specific. Moreover, results of both methods to analyze cell type specificity are highly similar.

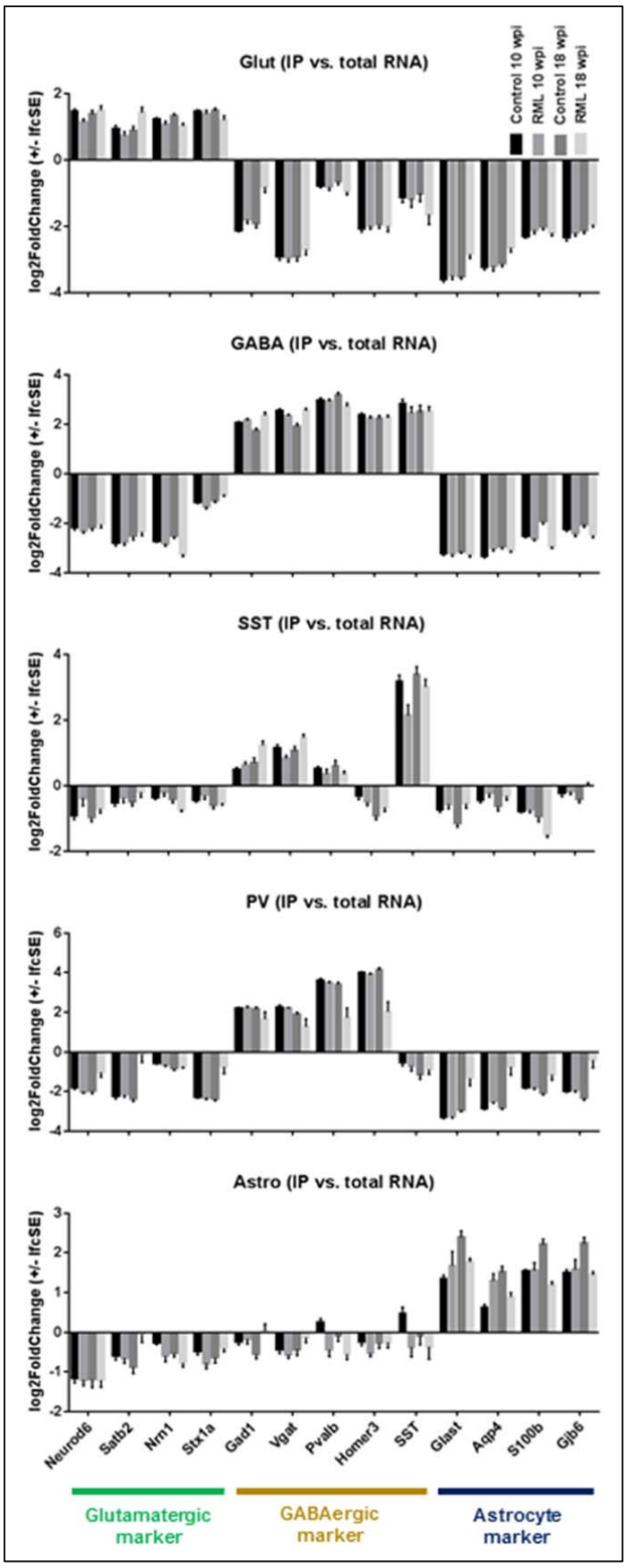
Glut (IP vs. total RNA)
GABA (IP vs. total RNA)
SST (IP vs. total RNA)
PV (IP vs. total RNA)
Astro (IP vs. total RNA)
Control 10 wpi
RML 10 wpi
Control 18 wpi
RML 18 wpi
log2FoldChange (+/- lfcSE)
Neurod6
Satb2
Nrn1
Stx1a
Gad1
Vgat
Pvalb
Homer3
SST
Glast
Aqp4
S100b
Gjb6
Glutamatergic marker
GABAergic marker
Astrocyte marker

4.7.2 Comparison of cell-type-specific gene expression regulation

With RNA-sequencing analysis based on total gene reads we detected around 17,000 – 18,000 genes expressed in each brain cell type (expression value: total gene reads; expression BaseMean ≥ 5; analyzed by Vikas Bansai, AG Bonn, DZNE Göttingen). A summary of the number of genes detected for each cell type at each time point and the number and percentage of differentially expressed genes (padj<0.1) is given in figure 4.7.2A.

Gene expression changes based on total gene reads at the 18 wpi time point in the mouse brain were still drastic with too many changes for an in-depth gene expression analysis. At the 10 wpi time point we found glutamatergic and GABAergic neurons were changing. Again, PV neurons and SST neurons were unaltered. Astrocytes were again highly altered.

Glutamatergic neurons had more up regulation within differentially expressed genes, whereas GABAergic neurons and astrocytes had more down regulation within the differentially expressed genes (padj<0.1) at the 10 wpi time point (Figure 4.7.2B). Comparing the differentially expressed genes (padj<0.1) of the different cell types at the early time point demonstrate again little overlap of differentially expressed genes between the lines, showing that individual cell types respond to the same ND differently (Figure 4.7.2C). Also the canonical pathway analysis (IPA) shows the cell-type-specific disease response of the individual cell types (Figure 4.7.2D).

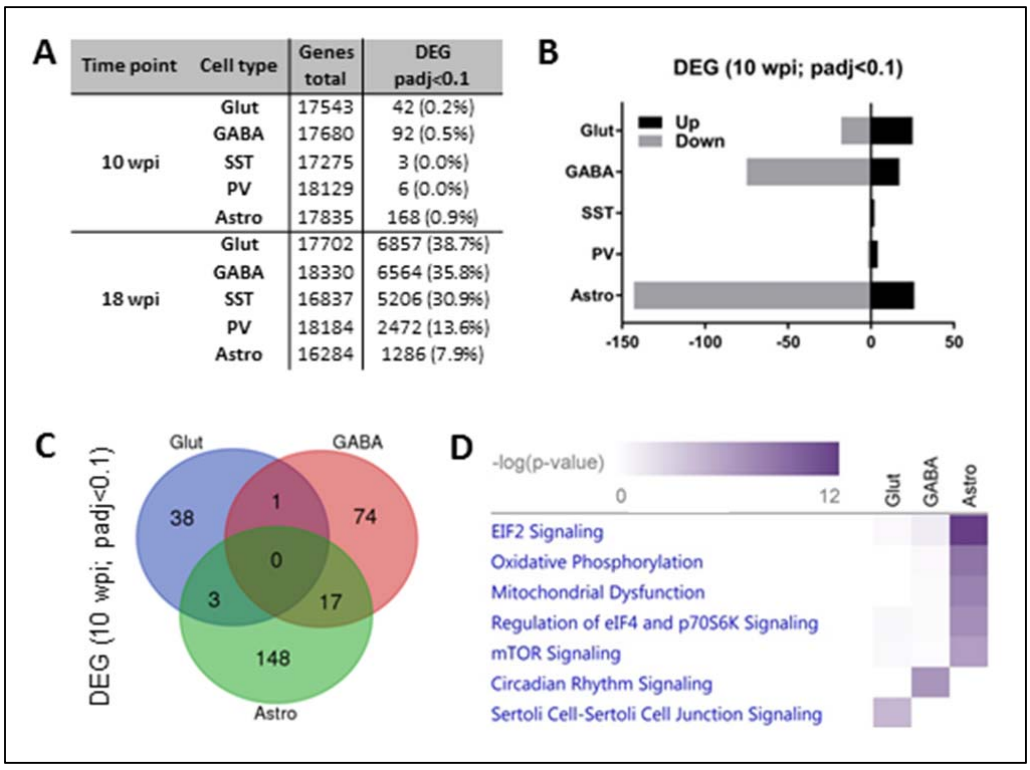

Figure 4.7.2: A. Number of total (base mean reads ≥ 5) and differentially expressed cell-type-specific genes at 10 and 18 wpi with padj<0.1 (NBH vs. RML). B. Up and down regulated genes at 10 wpi with padj<0.1. C. Overlap of regulated genes within different cell types at 10 wpi with padj<0.1. D. IPA heatmap of top hits (-log(pval)) of canonical pathways regulated in the different cell types at 10 wpi.

4.7.3 Gene expression regulation in glutamatergic neurons

The most prominent IPA canonical pathway in the glutametergic neurons was again “Sertoli Cell – Sertoli Cell Junction Signaling” with the included spectrins at 10 wpi. Furthermore, the IPA molecular and cellular functions “Cellular Assembly and Organization” and “Cell-To-Cell Signaling and Interactions” were revealed.

DAVID gene ontology analysis revealed again genes associated with actin, cytoskeleton, binding, protein binding and genes localized at organelles and synapses. However, with total gene read analysis no transport gene ontology terms are detectable. Instead, gene ontology terms associated with transcription, transcription factors and nervous system development were revealed. DEGs in glutamatergic neurons are displayed in table 4.7.3.

Table 4.7.3: DAVID gene ontology categories altered in glutamatergic neurons with included genes and their 2logFC. Red colored box indicates up regulation, green colored box indicates down regulation (gene input: padj<0.1, RML vs. NBH, 10 wpi).

Genes	2logFC	Gene ontology category				
		Actin / Cytoskeleton	Transcription / Transcription factor	Binding / Protein binding	Nervous system development	Synapse
ARC	0.50	X		X	X	X
ARL4D	0.48			X		
BTG2	0.39		X	X	X	
C4B	0.42			X		X
CLK1	0.39			X		
DLG1	-0.25			X	X	X
DUSP1	0.50			X		
ETV1	-0.36		X	X	X	
FZD7	-0.34			X		
GABRB2	-0.47			X	X	X
GFAP	0.58	X		X	X	
GSN	0.40	X		X	X	
HNRNPLL	-0.31			X		
LIMCH1	0.48	X		X		
MAPK8IP2	0.32	X		X	X	X
MPRIP	0.35	X		X		
NECAB1	-0.31			X		
NR2C2	-0.44		X	X	X	
NR4A1	0.83		X	X		
PAX6	-0.31		X	X	X	
PCDHGB2	-0.42			X		
PPP1R9A	0.43	X		X		X
RGS4	-0.24			X		
RPS28	0.35			X		
SIRT3	0.27			X		
SOX8	0.40		X	X	X	
SPTAN1	0.37	X		X		
SPTB	0.36	X		X		
SPTBN1	0.54	X		X		X
SPTBN2	0.46	X		X	X	X
TSHZ2	-0.42		X	X		
ZBTB18	-0.28			X	X	
ZIC1	-0.33		X	X	X	
ZIC2	-0.37		X	X	X	
ZXDB	-0.37		X	X		

4.7.4 Gene expression regulation in GABAergic neurons and subtypes

Analysis based on total gene reads shows changes in genes involved in the IPA canonical pathway “Circadian Rhythm Signaling” in GABAergic neurons at 10 wpi (Figure 4.7.4). All these circadian rhythm genes are known to be involved in oxidative stress response (Musiek et al. 2013, Mendez et al. 2016, Musiek and Holtzman 2016). With a less stringent cutoff the canonical pathway can also be found in the DEG analysis based on unique exon reads. The order of regulated genes is similar when sorted by pval and padj. However, the absolute calculated values for statistics do not pass our stringent cutoff (padj<0.1) in the UER analysis. Nonetheless, the similarities of the results from both analysis methods are clear.

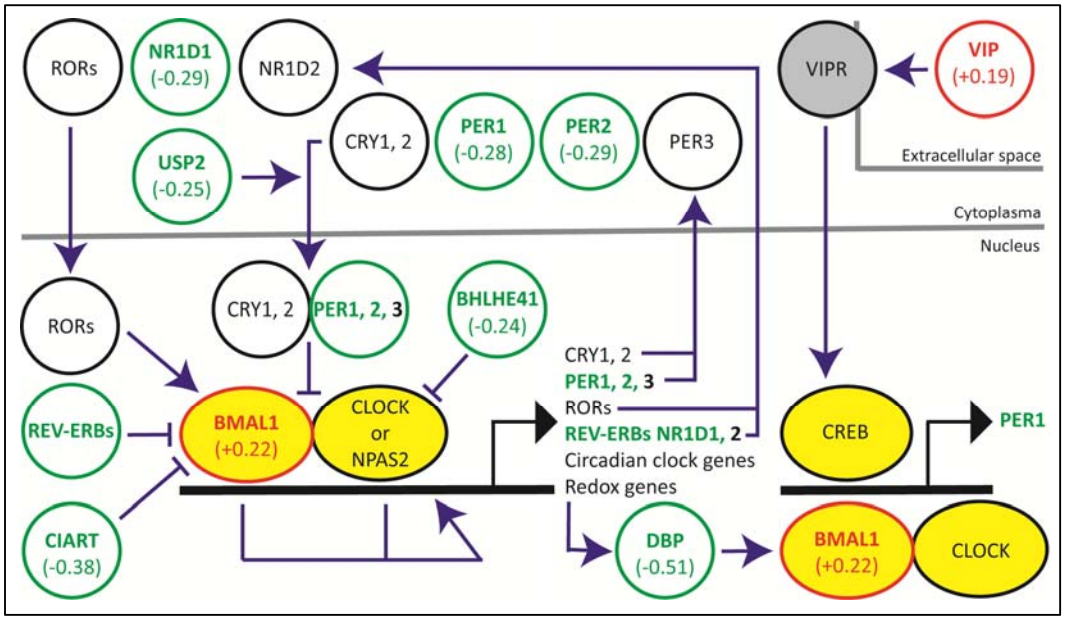

Figure 4.7.4: Regulation of DEGs involved in circadian rhythm and oxidative stress response in GABAergic neurons und their 2logFC based on total gene reads. Green genes are down regulated, red genes are up regulated and black genes are not significantly regulated (gene input: padj<0.1, RML vs. NBH, 10 wpi).

The complexes of BMAL1/Clock or BMAL1/NPAS2 function as transcription factors. They drive expression of circadian clock genes and redox genes (Figure 4.7.4). All genes inhibiting these transcription factors are down regulated. BMAL1 itself is up regulated. USP2, responsible for the transport of PER1 to the nucleus is also down regulated. Therefore, even less PER1 is transferred into the nucleus to inhibit transcription of target genes. Only VIP, leading to more expression of PER1, is up

regulated. However, VIP functions transcellularly and its increased gene expression may come from healthy cells attempting to regulate the circadian clock pathway in sick cells. In addition, VIP has more cellular functions and is involved in other pathways. Surprisingly, with activation of these BMAL1 associated transcription factor complexes, the target genes themself are not up regulated. Analyzed redox genes are unchanged or, like DBP, significantly down regulated.

4.7.5 Gene expression regulation in astrocytes

Actively translated mRNAs changed at 10 wpi in the astrocytes are again mainly down regulated ribosomal proteins (pathways: “EIF2 Signaling”, “Regulation of eIF4 and p70S6K Signaling”, “mTOR Signaling”) and down regulated members of the electron transport chain (pathways: “Oxidative Phosphorylation”, “Mitochondrial Dysfunction”) similar to the results of the unique exon reads analysis. The changed mRNAs of proteins building the electron transport chain are integrated again in cytochrome c or complex I, III, IV and V and the DEGs of both analysis are highly overlapping (Figure 4.7.5). However, non-overlapping DEGs in the UER analysis were close to but not within our stringent statistical cutoff. This is also true for differentially expressed ribosomal proteins. A comparison of changed ribosomal proteins in astrocytes caused by RML with the two analyses is shown in table 4.7.5. The top upstream regulator in the IPA analysis is again RICTOR with a predicted activation.

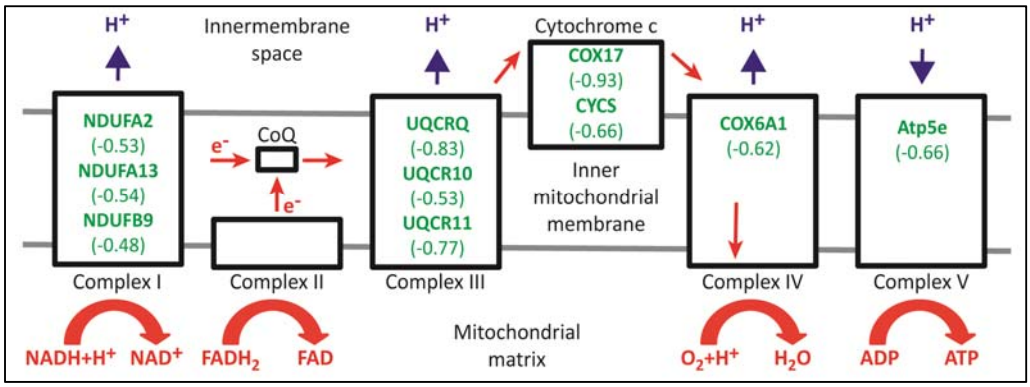

Figure 4.7.5: Electron transport chain with DEGs in astrocytes und their 2logFC based on total gene reads in green. Negative 2logFCs indicate genes are all down regulated (gene input: padj<0.1, RML vs. NBH, 10 wpi).

Table 4.7.5: Comparison of regulated ribosomal proteins in astrocytes between the two analysis (gene input: padj<0.1, RML vs. NBH, 10 wpi).

Analysis	Gene count	Ribosomal proteins
UER + Total gene reads	16	Rpl38 Mrps12 Rps26 Rpl14 Rps16 Rplp2 Rps21 Rps8 Rpl13a Rps19 Mrpl18 Rps29 Rpl41 Rplp1 Rps24 Rps20
UER	5	Rpl28 Rps4x Rpl26 Rpl19 Rps5
Total gene reads	11	Rpl35 Rps25 Rpl36 Rpl34-ps1 Rpl10a Rpl13 Rpl24 Rps27a Rpl37rt Rpl9 Rpl11

4.7.6 Summary of total gene read data analysis

Using the second analysis we found gene expression changes similar to the first analysis based on unique exon reads except for GABAergic neurons. To detect which cells are affected earliest and how they respond to the emerging disease the early disease time point (10 wpi) was again chosen for analysis. The gene expression changes of the 18 wpi time point were too drastic. First, we found glutamatergic neurons and GABAergic neurons were changing. However, PV neurons and SST neurons were unaltered. Moreover, we found that astrocytes are highly altered. Glutamatergic neurons have again more up regulation within DEGs, whereas GABAergic neurons and astrocytes show more down regulation within the DEGs. Comparison of the DEGs of the different cell types with little overlap demonstrate that individual cell types respond to the same RML induced neurodegeneration differently.

Canonical pathway analysis shows actively translated mRNAs changed in the astrocytes are mainly ribosomal proteins and members of the electron transport chain. Glutametergic gene ontology analysis possesses genes associated with actin, actin binding, cytoskeleton, signaling and transcription. GABAergic neurons show changes in genes involved in circadian rhythm signaling. All these circadian rhythm genes are also known to be involved in oxidative stress response (Musiek et al. 2013, Mendez et al. 2016, Musiek and Holtzman 2016).

5. Discussion

Why neurodegenerative diseases target specific brain regions is poorly understood. We hypothesize that this selective vulnerability is caused by specific brain cells in these regions having unique strategies and capacities to cope with various disease related protein conformers that ultimately fail.

To study the phenomenon of selective vulnerability of NDs and how specific cell types in the mouse brain respond to a neurodegenerative disease, prion infection with RML scrapie strain was used in this study as a model of neurodegenerative disease. RML infection was combined with the RiboTag method to isolate ribosome associated mRNA from specific brain cell types for gene expression analysis. Mice expressing the epitope-tagged ribosomes specifically in astrocytes or subsets of neurons, including glutamatergic, GABAergic, parvalbumin and somatostatin neurons, were injected with brain homogenate from either normal or prion infected mice. Changes to gene expression were analyzed by next generation sequencing at disease onset and at a preclinical time point in the disease process. Neuropathological changes in the brain were analyzed with several ND typical IHC stainings. This study was performed to give clues into which cells are affected earliest and how they respond to the emerging disease.

5.1 Selection of a disease model

5.1.1 RML as a model of neurodegenerative prion disease

An advantage of studying prion disease in mice is its high precision in regards to time to clinical illness and the neuropathological changes. The transmission of scrapie as a model of prion disease into various animal models, especially rodents, has led to a better understanding of prion diseases and disease mechanism in the prion field (Foster et al. 2001). The mouse adapted RML scrapie strain is a well-known and commonly used model of prion disease. RML is highly precise and, although it is a slowly progressing disease, all mice become terminally ill within a very small time frame (Di Bari et al. 2012). Therefore, RML infection as a model of neurodegenerative prion disease was chosen in our study. In our laboratory the S4-RML model showed behavioral changes around 18 wpi and was terminally down around 22.5 wpi.

5.1.2 Selection of S4 genetic background

The advantage of high precision in regards to the clinical disease time course and the neuropathological changes in prion diseases could be compromised if changes to gene regulation unrelated to the ongoing disease process occur. Two major contributors to the gene regulation changes in normal mice are circadian rhythm and activity levels. To control for circadian rhythm mice were always killed at the same time of the day (12:00-13:00). To control for activity levels we sought a genetic background that has a very consistent activity state. To this end, behavioral features of two common used inbred mouse strains were studied, B6 and S4 from archived data (Section 4.1). The B6 inbred mouse strain showed more penetrance of variable behavior within the group of individual animals. Importantly, it is not consistently the same individuals that exhibit the highest scores across different behavioral measures. Therefore, the spread of the B6 group is not merely driven by a small number of abnormally behaving animals. Based on these results, to avoid a widely variable group of individual mice and thereby possible effects on gene expression, we decided to use the RiboTag mice in the S4 genetic background. Of course, for other studies the B6 strain or other available inbred mouse strains might be the better choice. All inbred mouse strains have special features and differ in their genotype and phenotype, giving benefits for certain research questions (Crawley et al. 1997, Bothe et al. 2005, Casellas 2011). However, the high number of abnormally behaving individuals in the B6 group was a criterion for exclusion of the B6 genetic background for our study to avoid gene expression changes because of widely variable activity levels.

5.1.3 Selection of 10 and 18 wpi disease time points

It was planned to analyze two disease time points, a disease onset time point and an early preclinical time point (Section 4.2). The disease onset was defined as the earliest time point in which a clinically relevant detectable difference between our control and RML groups could be detected in living mice. We found that a great biomarker was a significant increase of theta frequency in wake, deep slow wave sleep and paradoxical sleep in RML injected mice starting at 16 wpi and becoming stronger at 18 wpi. Thus, 18 wpi time point was chosen as the disease onset.

For the preclinical time point the last time point at which EEG theta power was exactly the same in both groups was picked. By examining the evolution of

differences in recorded EEG theta frequency we found that theta frequency for both groups is overlapping until 10 wpi, after which the two groups slowly begin to separate. Therefore, 10 wpi was chosen as our preclinical disease time point. In retrospect, it would have been interesting to have analyzed more disease time points, especially with regard to the drastic gene expression regulation at the 18 wpi time point with too many changes for an in-depth gene expression analysis.

Nonetheless, at the outset of the project it was unknown if the RiboTag method could provide any useful insight into mechanisms of NDs. This project clearly shows it does. This insight into mechanisms of NDs and selective vulnerability is needed to develop therapies. If these therapies should be able to stop or slow the disease progress, it is important to identify the disease at an early stage and to understand what happens at the very beginning of the disease. Therefore, an early disease time point, even before clinical disease, is important for identification of these early disease changes, finding biomarkers and eventually therapies. Although, the 18 wpi time point represents the very beginning of clinical disease, neuropathological changes and really drastic changes in gene expression were detectable. Thus, at this time point the disease would be difficult to treat.

5.2 Neuropathological changes

Neuropathological changes in the RML injected RiboTag mice were studied by IHC stainings with Iba1, GFAP and SAF84 prion protein antibodies (Section 4.4). Abnormal staining of Iba1 and GFAP could be detected at 18 wpi in RML infected brains, detecting ongoing astrogliosis and activated microglia. These abnormal Iba1 and GFAP stainings are typical for NDs, showing that these brains are abnormal and are developing a neurodegenerative disease already at this disease onset time point (18 wpi). The similar morphology of microglia stained in control and RML 10 wpi samples indicates that the 10 wpi time point is very early in disease. These stained microglia are not activated cells. They are resting microglia with long, ramified processes and small cell bodies.

Proteinase K resistant prion aggregates are specific for TSEs and could also be detected at the 18 wpi time point in RML infected mice, again confirming that these mice are abnormal and developing a neurodegenerative prion disease. Also spongiosis, another hallmark of prion diseases, was detectable in the 18 wpi time point of RML infected mice. These results demonstrate that at disease onset time point (18 wpi) the brain has detectable neurophatological changes, namely activated

microglia, astrogliosis, proteinase K resistant prion aggregates and spongiosis showing that these animals are clearly diseased. None of these neuropathological changes were detected in the control groups and in the 10 wpi RML group, confirming that the 10 wpi time point is well before clinical disease and that these samples show no neuropathological characteristics of prion disease.

These results also show that the intracranial injections were successfully performed and that infectious material was present in the injected RML brain homogenate to inoculate prions into the mouse brains of the RML group leading to a mouse adapted scrapie infection. Because control group animals show no hallmarks of prion disease, injections of NBH worked as expected and the disease was not simply an adverse reaction to foreign brain homogenate invading the immune privileged brain. These results also show that gene expression changes are detectable much earlier in the emerging disease than neuropathological changes and neurodegeneration.

5.3 Quality of RNA samples and RNA-sequencing run

To analyze the RNA-sequencing data and for DEG analysis a good quality of the RNA samples and the RNA-sequencing run is required. After purification each individual RNA sample was checked for RNA quality and quantity using a Qubit Fluorometer, an Agilent 2100 Bioanalyzer and a Nanodrop 2000. Bioanalyzer electropherograms from samples later used for RNA-sequencing showed the expected RNA quality profiles with internal Bioanalyzer marker peak, broad hump of mRNA and the two ribosomal RNA peaks, confirming that our improved RiboTag IP protocol and RNA isolation of immunoprecipitated mRNA and isolation of total RNA from IP input worked well (Section 4.3.2). Also the RNA yields were proportional to the number of RiboTag expressing cells and were like expected from previous RiboTag experiments for the different Rtag/Cre mouse lines (Section 4.3.2).

With an average of around 31,000,000 reads for each sample a good RNA-sequencing run was performed with enough reads to study gene expression changes within our different conditions. Quality control of all individual reads also showed that the RNA-sequencing run was well performed. No read had to be discarded because of its length, 100% of all reads had a length of 50 bp. Only a small number of reads had a bad quality score or more than two ambiguous nucleotides within the 50 bp reads. After trimming of these reads with a bad quality

score or too high ambiguous base content even more than 99.5% of all reads were left and could be used for DEG analysis, confirming the good RNA-sequencing performance (Section 4.3.3).

5.4 Comparison of the two RNA-sequencing data analyses

RNA-sequencing is used to estimate gene and transcript expression and became the standard method for transcriptome analysis. It is based on the number of reads that can be mapped to a genome sequence. There is no optimal analysis method for RNA-sequencing data. Every RNA-sequencing experiment can have different optimal methods for expression value quantification, normalization and DEG analysis (Conesa et al. 2016).

The raw read counts are not sufficient to compare expression levels between different samples to identify expression changes since raw read values are affected by many factors like transcript length, library size and sequencing biases. The RPKM value is a normalized expression value, in which feature-length and library-size effects were removed. RPKM is the most reported RNA-sequencing expression values (Conesa et al. 2016). The DESeq2 package has its own read count normalization and needs an absolute gene expression value as input. Therefore, RPKM value can not be used as input. The DESeq2 normalization corrects for library size and RNA composition bias (Love et al. 2014). Therefore, UER and total gene reads as absolute, not normalized expression values were taken in the two different RNA-sequencing analyses.

We predicted that if our RNA-sequencing data analysis results were robust, the overall results would be similar when using different analysis methods (Section 4.5). The analyses mainly differ in the method expression values are counted for the DEG analysis, unique exon reads and total gene reads. Furthermore, the two analyses differ in the software and web applications used for quality control, trimming, mapping of the RNA-sequencing reads and the mouse reference genome used.

Overall, the results of the two types of analyses are quite similar except for absolute statistical value differences (for example in the GABAergic neuron dataset at 10 wpi). The different absolute statistical values were unexpected, because the DESeq2 package calculating the statistical values was used for both analysis methods. However, in the analysis based on total gene reads the padj value was

recalculated using the Benjamini-Hochberg procedure after filtering of the DEG output list. This recalculating can make a difference if the DESeq2 output results in a lot of genes with a significant pval but have a not available padj value. If padj value is taken for the DEG cutoff, these genes with the not available padj value would be eliminated from the pathway and gene ontology analysis. Therefore, recalculating the padj was also tested for the analysis based on unique exon reads. Nevertheless, recalculated padj values after filtering of the list and the DESeq2 calculated padj values were identical up to the third decimal place. Thus, the number of DEGs in analyses with recalculated and DESeq2 calculated padj value with the same statistical cutoff stayed more or less the same since not many genes with a significant pval had a not available padj value. The differences we detect in the two RNA-sequencing data analyses tested in this study have to be caused by the different expression values used for DEG analysis and the different processing (trimming and mapping) of the sequencing reads.
The lists of DEGs for each cell type sorted by pval or padj are highly overlapping in both analyses. Altered canonical pathways and GO terms are also similar or identical for the different cell types. Of course, the DEG lists of the two analyses are not 100% identical. Genes detected as differentially expressed in one analysis are often close to but not within our stringent statistical cutoff in the other analysis, again confirming that both types of analysis are similar with highly overlapping results.

Since the two DEG analyses of the RNA-sequencing data are similar but not identical shows that the use of different expression values, different analyzing tools and different analysis parameters has a strong influence on the results. It is to be expected that the accordance of results obtained from different RNA-sequencing analysis tools is sometimes low and that the results are affected by different parameter settings. This is especially true for low expressed genes (Conesa et al. 2016). Therefore, it is difficult to decide which method is the better choice. UER and total gene read counts differ in the case if reads can be mapped to different genes. There are two possibilities if reads can be mapped to different annotated genes. The first strategy is to discard these reads, keeping only uniquely mapping reads for expression estimation or doing the DEG analysis directly with the UER value. A second strategy is to count these reads to genes in proportion to coverage by uniquely mapping reads. Indeed, the second strategy was reported to show expression values that are more comparable with microarray results and it is better for genes lacking unique exons (Li et al. 2010, Kukurba and Montgomery 2015).

5.5 Cell-type specificity

To demonstrate the cell type specificity of the RiboTag method and the resulting immunoprecipitated cell-type-specific mRNA, enrichment or depletion of known cell type marker genes compared to the total RNA input was investigated (Section 4.6.1, Section 4.7.1). The results based on the RNA-sequencing data show that IP harvested mRNA was cell-type-specific since expected enrichment or depletion of specific cell type markers was detected, again demonstrating that the RiboTag IP and mRNA isolation worked well. Noteworthy, because the comparison is against the total RNA input the RNA of the cell type of interest is always present in this input sample. Thus, the more abundant a cell type is, the less is the enrichment of known marker genes of this cell type, but the greater the depletion of other cell type markers. Conversely, the less abundant a cell type is, the higher the enrichment of marker genes, but the lesser the depletion of cell type specific marker genes.

However, it has to be mentioned that most cell type markers are not completely unique for just one brain cell type. It is often just more abundant in a specific cell type compared to other cells to make it a cell type marker. With RNA-sequencing we also detect astrocyte marker mRNA in neurons and neuronal marker mRNA in astrocytes. The RNA-sequencing expression value is often not so little that it could be just background contamination within the RiboTag IP method; often the expression value is in the two-digit range and therefore not only expressed or detected by chance. To eliminate genes that are probably not expressed a minimum UER filter was used (baseMean UER ≥5). GFAP is a very good example; it is highly expressed in our astrocyte samples but it is also expressed to a lesser extent in our neuron samples (RML vs. NBH; Glut base mean UER: 65.4; Astro base mean UER: 668.3). This mRNA is well known as an astrocyte and ependymocyte marker in the central nervous system, but GFAP mRNA can also be detected in mature neuronal cells (Zhang et al. 2014). In our study we detected a significant up regulation caused by RML induced neurodegeneration at 18 wpi for all cell types. At 10 wpi glutamatergic neurons, PV neurons and astrocytes show an up regulation of GFAP with a statistical cutoff of pval<0.05 (not with padj<0.1) caused by RML. Nonetheless, this was surprising since GFAP was not increased in IHC experiment at the 10 wpi time point. This up regulation of GFAP in neurons was also reported for other NDs (Hol et al. 2003). In another transcriptome study using a system similar to RiboTag, GFAP was also found to be expressed in motor neurons and it was up regulated upon induction by mutant superoxide dismutase 1 in a mouse model of amyotrophic lateral sclerosis (Sun et al. 2015).

5.6 Gene expression regulation

With both RNA-sequencing analyses we found thousands of genes expressed in the brain (even with a minimum expression value filter). We found that although the 18 wpi time point represented the beginning of clinical disease, the gene expression changes in the mouse brain were really drastic. Differential gene expression analysis at 18 wpi resulted in too many changes for an in-depth gene expression analysis of which cells were most affected and what were the most changed molecular pathways and gene ontology terms (Section 4.6.2, Section 4.7.2). That the gene expression changes were so drastic at the 18 wpi disease time point was unexpected, since the freely moving mice appeared normal by passive observation at this time point, showing that the RiboTag method and RNA-sequencing is really sensitive to detect early gene expression changes in disease process. However, using the statistical cutoff of padj<0.1 the 10 wpi disease time point was quite interesting for in-depth gene expression analysis.

First, with the analysis based on unique exon reads we found glutamatergic neurons were changing. However, GABA neurons, and the GABAergic subtypes (PV neurons and SST neurons) were unaltered. Moreover, we found that astrocytes are highly altered (Section 4.6.2, Section 4.7.2). Finding three cell types were not altered with these standard cutoff of padj<0.1 shows that this cutoff is very stringent, enabling detection of very early changes in gene expression and confirming that the 10 wpi time point is well before clinical disease.

With the analysis based on total gene reads the GABAergic neurons were also found to be altered (Section 4.7.2). In both analyses the top changed genes sorted by pval and padj were mainly the same in GABAergic neurons. However, the absolute calculated statistical values of both analyses were different. With a less stringent cutoff the same canonical pathways and GO terms can be found in the DEG analysis based on unique exon reads, showing that both kinds of RNA-sequencing data analysis are providing similar results.

Glutamatergic neurons have more up regulation within differentially expressed genes, whereas GABAergic neurons (in the total gene read analysis) and astrocytes show more down regulation within the differentially expressed genes (Section 4.6.2, Section 4.7.2). A higher proportion of up regulation is more likely to be an active response to the emerging disease or a maintenance of cellular function operations,

whereas a down regulation is more likely to be a shutdown of cellular functions and a changeover into a passive, energy and cell resources saving resting state. This different direction of gene expression regulation in our cell types already shows that different cell types react differently to the same ND.
Comparison of the differentially expressed genes of the specific cell types with little overlap also demonstrates that individual cell types respond to the same ND differently (Section 4.6.2, Section 4.7.2). Canonical pathway analyses also support our conclusion of cell-type specific responses caused by the same RML induced neurodegeneration. In summary, these results support our hypothesis that the phenomenon of selective vulnerability is caused by specific brain cells having unique strategies and capacities to cope with an emerging neurological disorder, RML prion disease in our study.

Interestingly, we found astrocytes to be highly altered and the most affected cell type in our study at the early 10 wpi disease time point. Therefore, astrocytes are probably the earliest affected cell type in RML prion disease. Studies of NDs are normally confined to neurons and neuronal death, showing the most targeted neuron type. In Alzheimer's disease cortical cholinergic neurons and hippocampal neurons are targeted, in Parkinson's disease dopaminergic neurons in the substantia nigra are targeted and in Huntington's disease neostriatal spiny neurons are affected (Graveland et al. 1985, Francis et al. 1999, Saxena and Caroni 2011, Sulzer and Surmeier 2013). In several studies GABA neurons were reported to be most vulnerable in different genetic NDs (Ferrer et al. 1993, Guentchev et al. 1997, Guentchev et al. 1998, Guentchev et al. 1999). In addition to neurons, other cells, namely neuroglia or vascular cells, are involved in the disease process influencing the selective vulnerability in neurodegeneration (Jackson 2014). If astrocytes are the first cell type to be affected and considering the various tasks in the brain to support neurons and neuronal network functioning (Araque and Navarrete 2010, Kimelberg and Nedergaard 2010), it is not surprising that later also neurons would be affected.

Surprisingly, investigating TSE as a model of a protein misfolding disease, we detect only little or no unfolded protein response (UPR) at our 10 wpi disease time point. A lot of members of the UPR pathways need to be phosphorylated for their activation, IRE1α, PERK or eIF2α for example (Ron and Walter 2007, Oslowski and Urano 2011). However, we are not able to detect this kind of activation with our analysis method. The RiboTag method combined with RNA-sequencing is in this

case limited to detect only pathways in which members are up or down regulated on their actively translated mRNA level. However, heat shock proteins and chaperones are part of the unfolded protein response and are known to be differently regulated (typically increased expression) in neurodegeneration caused by misfolded proteins (van Noort et al. 2016, Sweeney et al. 2017). At the 10 wpi time point there were few gene expression changes for heat shock proteins and chaperones. However, we know from other projects that gene expression changes within heat shock proteins and chaperones are detectable with the RiboTag method. Using 6h of sleep deprivation as a stress condition in different Rtag/Cre mice showed that a strong up regulation of heat shock proteins and chaperones in the sleep deprived group compared to an undisturbed control group is detectable in different mouse brain cell types (data not shown). Apparently, the UPR is not one of the earliest changes in our RML induced neurodegeneration in the analyzed cell types.

Up regulation of immediate early genes (IEGs) can be used to detect a cellular stress response (Gallitano-Mendel et al. 2007, Ronkina et al. 2011). A significant up regulation of known IEGs is only detectable in glutamatergic neurons and astrocytes at 10 wpi. For example Arc, Dusp1 and Nr4a1 in glutamatergic neurons or Arc, Jund and Nr4a1 in astrocytes are up regulated IEGs in these cell types. With a cutoff of pval<0.05 also Egr1, Egr2, Fos, Homer1 and Junb in glutamatergic neurons or Fos, Jun, and Junb in astrocytes are also up regulated. These results reflect a high number of significant up regulated IEGs in glutamatergic neurons and astrocytes, but not in GABAergic neurons or GABAergic subtypes. However, IEGs are up regulated in GABAergic cell types by another stress condition, namely the above mentioned RiboTag sleep deprivation experiment (data not shown). When cell types show no gene expression regulation due to the emerging prion disease like an up regulation of stress response pathways, the question arises whether they cannot detect the ongoing disease or are just not affected. Though, these data show that specific cell types not only respond to the same ND differently, but also the same cell type reacts to different stressors (RML infection or sleep deprivation) differently.

5.6.1 Gene expression regulation in glutamatergic neurons

Both next generation sequencing analyses show that glutamatergic neurons are altered at the preclinical disease time point (Section 4.6.3, Section 4.7.3). Most prominent pathways and gene ontology terms altered in glutamatergic neurons are

associated with actin, actin binding and cytoskeleton components including spectrins. Furthermore, molecular transport, cellular assembly and organization, cell morphology, signaling and cell death and survival are changed. Cellular compartment analysis detects genes in organelles and synapses to be enriched within the DEGs.

These results suggest, along with the up regulation of most mRNAs, that glutamatergic neurons try to maintain the signal transduction. Furthermore, necessary functions for signal transduction are also maintained including functional actin and cytoskeleton for cellular transport to the synapse. Signal transduction and the cytoskeleton are closely linked (Forgacs et al. 2004). The enriched organelle cellular compartment also includes vesicles, necessary for cellular transport and signal transduction at the synapses.

Enrichment of actin and cytoskeleton gene ontology terms also indicates an active stabilization of the glutamatergic cells. Stabilization of cells is an important function of the cytoskeleton (Huber et al. 2013). All these results indicate that the glutamatergic neurons recognize the emerging disease and react with maintenance of their most important cell functions. Because glutamate is the most abundant excitatory neurotransmitter in the brain (Meldrum 2000), functional glutamatergic neurons and glutamatergic signaling is essential in the central nervous system.

The detected effects on glutamatergic neurons could also be indirectly caused by the highly altered astrocytes, normally having functions to support neurons (Araque and Navarrete 2010, Kimelberg and Nedergaard 2010). Neuroglia, especially astrocytes, control and modulate extracellular glutamate levels. Under healthy conditions an adequate level of glutamate is provided by the glutamate-glutamine cycle. Extracellular glutamate near synapses is taken up by astrocytes and metabolized to glutamine. Glutamine is internalized by neurons and then converted back to glutamate (Rothman et al. 2003). Non healthy astrocytes could have problems performing this function. This would lead to an accumulation of glutamate outside cells near synapses, eventually causing excitotoxicity which is known to occur in several NDs (Hynd et al. 2004, Salinska et al. 2005). Another possibility is that the astrocytes still take up the glutamate but no glutamine is sent back to the neurons.

However, with analysis based on total gene reads no transport gene ontology terms are detectable. Instead, gene ontology terms associated with transcription, transcription factors and nervous system development were revealed, showing that glutamatergic neurons might also try to react on the transcriptional level to the emerging disease.

5.6.2 Gene expression regulation in GABAergic neurons and subtypes

With both gene expression analyses SST and PV neurons are unaltered at the 10 wpi disease time point. The analysis based on total gene reads shows changes in genes involved in the IPA canonical pathway “Circadian Rhythm Signaling” in overall GABAergic neurons at 10 wpi. With a less stringent cutoff the canonical pathway can also be found in the DEG analysis based on unique exon reads (Section 4.6.4, Section 4.7.4). Furthermore, if neither SST neurons nor PV neurons are altered, the question is which GABAergic neuron subtype is responsible for the gene expression change. GABAergic neurons have a high diversity and every subtype has its own unique features (Taniguchi 2014).

However, all these circadian rhythm genes are also known to be involved in oxidative stress response (Musiek et al. 2013, Mendez et al. 2016, Musiek and Holtzman 2016). Therefore, there are two possibilities: the gene regulation is changed either due to the circadian rhythm signaling itself or as an oxidative stress response. If the emerging disease affects the circadian clock signaling the responsible neuron subtype could be GABAergic neurons within the suprachiasmatic nucleus (SCN) not expressing Pvalb or SST. The SCN is a small brain region within the hypothalamus working as the master circadian clock pacemaker and therefore controlling the circadian rhythm (Welsh et al. 2010). The SCN consists of many different cell types, however, GABAergic neurons and GABAergic signaling play an especially important role within the SCN (Liu and Reppert 2000, DeWoskin et al. 2015, Myung et al. 2015). The GABAergic subtype is probably VIP expressing neurons because it was reported that the GABAergic neurotransmitter gamma-aminobutyric acid colocalizes with VIP within the SCN (Moore and Speh 1993). It is also reported that there is a connection between NDs, circadian rhythm and sleep (Hood and Amir 2017).

If the detected gene expression change is due to oxidative stress response, another yet unknown GABAergic neuron subtype has to be responsible for the detected DEGs. Finding SST neurons and PV neurons to be unaltered already narrows down the potential candidate subtypes. Surprisingly, with activation of the detected BMAL1 associated transcription factor complexes, the target genes responsible for oxidative stress response are not up regulated. Known analyzed redox genes are unchanged or, like DBP, significantly down regulated. However, DBP is also in the RiboTag sleep deprivation experiment significantly down regulated (data not

shown), but also known as one of the down regulated sleep deprivation marker genes (Wisor et al. 2008, Thompson et al. 2010). If an oxidative stress response is being attempted by GABAergic neurons, the question is whether this is not successful with a significant change of redox genes or is hindered by further gene expression regulation on a different level than mRNA.
The fact that GABAergic neurons show no or little reaction at the early disease time point could also be responsible for the fact that they are reported to be most vulnerable in several NDs (Ferrer et al. 1993, Guentchev et al. 1997, Guentchev et al. 1998, Guentchev et al. 1999). This strong vulnerability could be caused by the fact that these cell types fail to induce a strong enough protective reaction to the emerging disease to stay healthy and survive.

5.6.3 Gene expression regulation in astrocytes

Astrocytes show a highly altered, cell-type-specific disease response with both next generation sequencing analyses at the 10 wpi time point (Section 4.6.5, Section 4.7.5). Therefore, astrocytes are probably the most and earliest affected cell type in our study. DEGs changed are mainly down regulated ribosomal proteins (21 of 145 genes associated with KEGG pathway “Ribosome”) and down regulated members of the electron transport chain (cytochrome c and four of five complexes are affected). The upstream regulators responsible for this massive down regulation in astrocytes were also detected. The top regulator is RICTOR, it is associated with most of the down regulated ribosomal proteins and most of the proteins altered in the electron transport chain. Therefore, an activation of RICTOR is predicted. Altered molecular and cellular functions are cell death and survival, lipid metabolism, small molecule biochemistry, gene expression and protein synthesis. Nearly all DEGs in astrocytes are down regulated, indicating that astrocytes going into a resting state stopping to maintain their normal function.
Down regulated members of the electron transport chain in mitochondria lead to a mitochondrial dysfunction in astrocytes. Several TSEs and other NDs are known to show altered mitochondria function and mitochondrial dysfunction in different brain regions caused by the disease (Ferrer 2009, Ansoleaga et al. 2016, Frau-Mendez et al. 2017). In addition, some of these studies show altered protein synthesis during TSEs (Ansoleaga et al. 2016, Frau-Mendez et al. 2017). In our cell-type specific study we can detect that these changes of protein synthesis and energy metabolism are caused by astrocytes at an early time point, even before clinical disease.

Expression changes, namely a down regulation, of ribosomal proteins do not necessarily lead to a shutdown or decrease of protein synthesis. With expression changes of ribosomal proteins also the assembly of the ribosome can be altered to react to specific conditions to control protein synthesis of specific mRNAs (Xue and Barna 2012, Preiss 2016, Shi et al. 2017). Either the astrocytes reduce protein synthesis for energy saving reasons or actively react with a change in the availability of certain ribosomal proteins to the RML induced stress situation. For energy saving reasons it would make sense to reduce production of ribosomes. Biogenesis of ribosomes is the most energy consuming process in a cell (MacInnes 2016).

Using the RiboTag method for isolation of ribosome associated mRNA, the regulation of ribosomal proteins does not affect our results. Initially, the HA bearing ribosomal protein (Rpl22) is not regulated by RML prion infection. This is true for all cell types. Therefore, in all cell types the level of Rpl22 is the same in control and RML groups, suggesting that the different groups also have the same amount of HA bearing ribosomes. Furthermore, RiboTag is a sampling technique and often not all captured mRNA is analyzed. The amount of captured mRNA or differences of mRNA amounts between groups do not affect the DEG analysis. There are several normalization steps within the analysis of gene expression changes; for example, the DEG analysis included a sample normalization step (correction for library size and RNA composition bias) and the same absolute amounts of mRNA were used for RNA-sequencing.

Astrocytes perceive the ongoing disease at this preclinical time point and respond to the emerging disease with a massive down regulation of genes required for protein synthesis and respiration. Detected effects on other cell types could be indirectly caused by the highly altered astrocytes. Astrocytes have lots of functions supporting neurons (Araque and Navarrete 2010, Kimelberg and Nedergaard 2010). Non healthy astrocytes could have problems performing these functions, leading to adverse effects on neurons and other brain cell types.

5.7 Summary findings of RML infection

The summary findings of gene expression changes in specific mouse brain cells at 10 wpi and neuropathological changes at 18 wpi caused by RML prion infection are shown in figure 5.7.

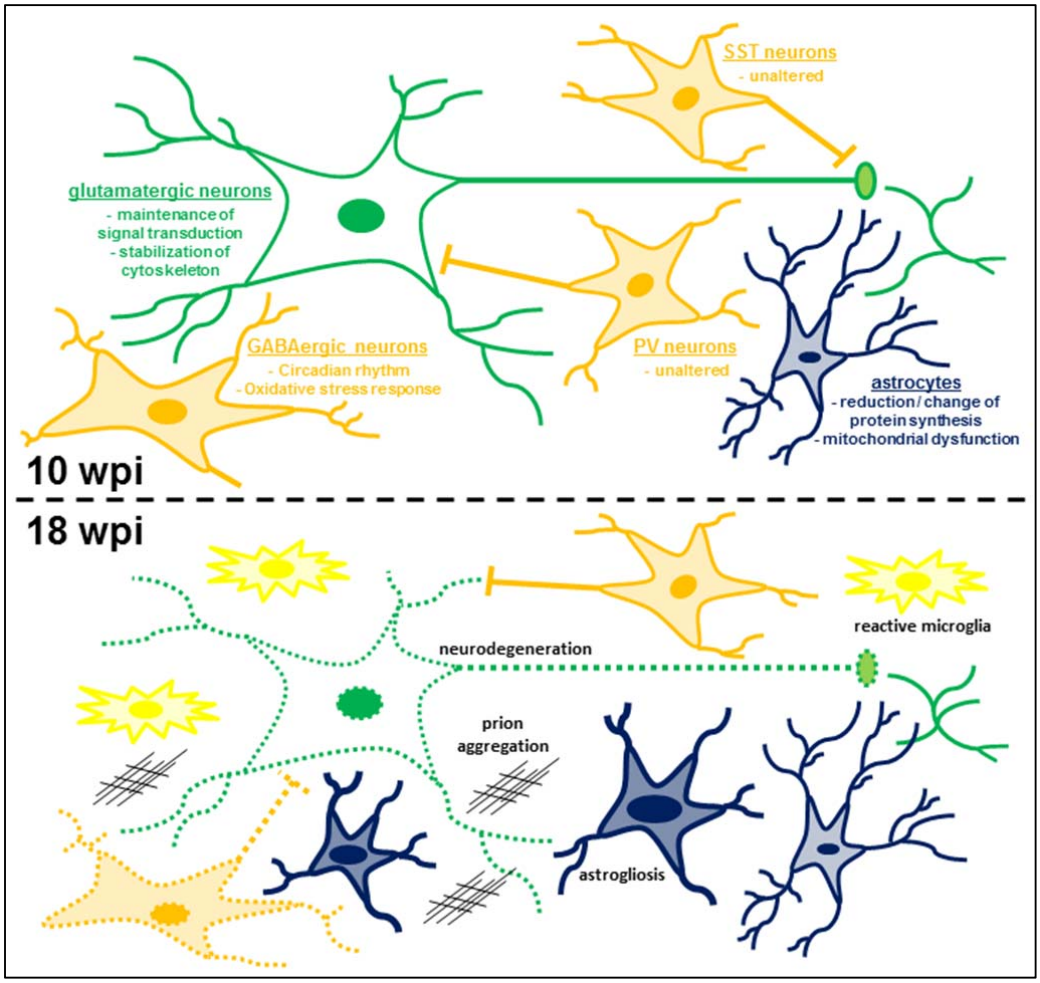

Figure 5.7: 10 wpi: Gene expression analyses demonstrate that glutamatergic neurons (green) react to RML prion infection with a maintenance of signal transduction and stabilization of the cell / cytoskeleton. GABAergic neurons (orange) show changes in circadian rhythm or oxidative stress response. GABAergic neuron subtypes (orange), namely SST neurons and PV neurons are unaltered. In astrocytes (blue) a reduction / change of protein synthesis and a mitochondrial dysfunction is detectable. 18 wpi: Neurophalological analyses demonstrate astrogliosis (dark blue, large astrocytes), reactive microglia (yellow), prion aggregation (black grids) and neurodegeneration (dashed lines).

5.8 Outlook

This work gives clues into which brain cells are affected earliest and most severely and how they respond to the emerging disease. Of course, we were limited in our study to a certain number of cell types to investigate. In our study astrocytes are the most and probably earliest affected cell type by RML induced neurodegeneration. In retrospect, it would be interesting to study if other subtypes of neuroglia are also highly affected by RML and how they respond to the emerging disease. If other neuroglia subtypes are affected earlier than neurons it would also be worth

investigating if their impairment has adverse effects on neurons or other neuroglia cell types. It is not surprising that when astrocytes, with their diverse supporting functions for neurons, are affected, neurons quickly show changes caused by this astrocyte functional impairment. This study provides evidence that for therapeutic approaches and a better understanding of mechanism in NDs a further investigation of the role of neuroglia, especially astrocytes, is essential. Other studies also show the important role of neuroglia for a functional central nervous system (Kimelberg and Nedergaard 2010) or a neuroprotective role during prion disease (Zhu et al. 2016).

We were also limited in the number of disease time points in our study. With hindsight, it would have been interesting to have more disease time points in addition to the chosen ones, especially with regard to the drastic gene expression regulation at the 18 wpi time point. This would lead to a better understanding of the course of the RML induced neurodegeneration at the level of gene expression regulation.

Furthermore, in addition to the RML induced neurodegeneration other scrapie strains, prion diseases or models of NDs could be used to investigate if the results are robust for different TSEs or even other NDs. In addition to actively translated mRNAs, other levels of gene expression including protein levels, protein activation, micro RNAs or even epigenetic changes and features could be analyzed. Using different disease models and different levels of gene expression in a cell-type-specific manner is needed for a better understanding of disease mechanisms, a better understanding of the selective vulnerability in NDs and for developing therapies.

6. Summary

Why neurodegenerative diseases target specific brain regions is poorly understood. We hypothesize that this selective vulnerability is caused by specific brain cells in these regions having unique strategies and capacities to cope with various disease related protein conformers that ultimately fail.

To study how specific cell types in the mouse brain respond to a neurodegenerative disease we used prion infection (RML scrapie strain) as a model of neurodegenerative disease. RML infection was combined with the RiboTag method to isolate ribosome associated mRNA from specific brain cell types. Mice expressing the epitope-tagged ribosomes specifically in astrocytes or subsets of neurons, including glutamatergic, GABAergic, parvalbumin or somatostatin neurons, were injected with brain homogenate from either normal or prion infected mice. Changes to gene expression were analyzed by next generation sequencing at a stage when clinical signs first become apparent (18 wpi) and at a much earlier stage (10 wpi) in the disease process. Neuropathological changes like microglia activation, astrogliosis, aggregated prions and spongiosis were analyzed by different IHC stainings. This work gives clues into which cells are affected earliest and how they respond to the emerging disease. Investigating cell-type-specific mechanisms of selective vulnerability are needed for a better understanding of mechanism in NDs and developing therapies.

At disease onset (18 wpi) an extensive regulation of gene expression is detectable, although mice show obviously no changes in their phenotype. Gene expression changes at 18 wpi were drastic with too many changes for an in-depth gene expression analysis of which cells were most affected and what were the most changed molecular pathways. To detect which cells are affected earliest and how they respond to the emerging disease the early disease time point (10 wpi) was chosen for analysis. First, we found glutamatergic neurons were changing. However, PV neurons and SST neurons were unaltered. Moreover, we found that astrocytes are highly altered and probably the most and earliest affected cell type. GABAergic neurons were found to be changed depending on the statistical output of two different next generation sequencing data analyses.

Glutamatergic neurons have more up regulation within differentially expressed genes, whereas GABAergic neurons and astrocytes show more down regulation within the differentially expressed genes. Comparison of the differentially expressed

genes of the different cell types with little overlap demonstrates that individual cell types respond to the same RML induced neurodegeneration differently.

Canonical pathway analysis show actively translated mRNAs changed in the astrocytes are mainly ribosomal proteins and members of the electron transport chain leading to an impairment or change of gene expression and a mitochondrial dysfunction. Glutametergic gene ontology analysis possess genes associated to actin, actin binding, cytoskeleton, cellular transport and signaling, probably leading to a stabilization of the cell and maintenance of essential glutamatergic neuron functions like signal transduction. GABAergic neurons show changes based on gene read analysis in genes involved in circadian rhythm signaling. All these circadian rhythm genes are also known to be involved in oxidative stress response.

7. References

Aguzzi, A. and Calella, A. M. (2009). "Prions: protein aggregation and infectious diseases." Physiol Rev 89(4): 1105-1152.

Aguzzi, A., Heikenwalder, M. and Polymenidou, M. (2007). "Insights into prion strains and neurotoxicity." Nat Rev Mol Cell Biol 8(7): 552-561.

Aguzzi, A. and Polymenidou, M. (2004). "Mammalian prion biology: one century of evolving concepts." Cell 116(2): 313-327.

Aguzzi, A. and Sigurdson, C. J. (2004). "Antiprion immunotherapy: to suppress or to stimulate?" Nat Rev Immunol 4(9): 725-736.

Andlin-Sobocki, P., Jonsson, B., Wittchen, H. U. and Olesen, J. (2005). "Cost of disorders of the brain in Europe." Eur J Neurol 12 Suppl 1: 1-27.

Ansoleaga, B., Garcia-Esparcia, P., Llorens, F., Hernandez-Ortega, K., Carmona Tech, M., Antonio Del Rio, J., Zerr, I. and Ferrer, I. (2016). "Altered Mitochondria, Protein Synthesis Machinery, and Purine Metabolism Are Molecular Contributors to the Pathogenesis of Creutzfeldt-Jakob Disease." J Neuropathol Exp Neurol.

Araque, A. and Navarrete, M. (2010). "Glial cells in neuronal network function." Philos Trans R Soc Lond B Biol Sci 365(1551): 2375-2381.

Bastian, F. O. and Foster, J. W. (2001). "Spiroplasma sp. 16S rDNA in Creutzfeldt-Jakob disease and scrapie as shown by PCR and DNA sequence analysis." J Neuropathol Exp Neurol 60(6): 613-620.

Battle, A., Khan, Z., Wang, S. H., Mitrano, A., Ford, M. J., Pritchard, J. K. and Gilad, Y. (2015). "Genomic variation. Impact of regulatory variation from RNA to protein." Science 347(6222): 664-667.

Beranger, F., Mange, A., Solassol, J. and Lehmann, S. (2001). "Cell culture models of transmissible spongiform encephalopathies." Biochem Biophys Res Commun 289(2): 311-316.

Biasini, E., Turnbaugh, J. A., Unterberger, U. and Harris, D. A. (2012). "Prion protein at the crossroads of physiology and disease." Trends Neurosci 35(2): 92-103.

Bishop, M. T., Pennington, C., Heath, C. A., Will, R. G. and Knight, R. S. (2009). "PRNP variation in UK sporadic and variant Creutzfeldt Jakob disease highlights genetic risk factors and a novel non-synonymous polymorphism." BMC Med Genet 10: 146.

Bosque, P. J., Ryou, C., Telling, G., Peretz, D., Legname, G., DeArmond, S. J. and Prusiner, S. B. (2002). "Prions in skeletal muscle." Proc Natl Acad Sci U S A 99(6): 3812-3817.

Bothe, G. W., Bolivar, V. J., Vedder, M. J. and Geistfeld, J. G. (2005). "Behavioral differences among fourteen inbred mouse strains commonly used as disease models." Comp Med 55(4): 326-334.

Bouzamondo-Bernstein, E., Hopkins, S. D., Spilman, P., Uyehara-Lock, J., Deering, C., Safar, J., Prusiner, S. B., Ralston, H. J., 3rd and DeArmond, S. J. (2004). "The neurodegeneration sequence in prion diseases: evidence from functional, morphological and ultrastructural studies of the GABAergic system." J Neuropathol Exp Neurol 63(8): 882-899.

Brookmeyer, R., Johnson, E., Ziegler-Graham, K. and Arrighi, H. M. (2007). "Forecasting the global burden of Alzheimer's disease." Alzheimers Dement 3(3): 186-191.

Bueler, H., Aguzzi, A., Sailer, A., Greiner, R. A., Autenried, P., Aguet, M. and Weissmann, C. (1993). "Mice devoid of PrP are resistant to scrapie." Cell 73(7): 1339-1347.

Bueler, H., Fischer, M., Lang, Y., Bluethmann, H., Lipp, H. P., DeArmond, S. J., Prusiner, S. B., Aguet, M. and Weissmann, C. (1992). "Normal development and behaviour of mice lacking the neuronal cell-surface PrP protein." Nature 356(6370): 577-582.

Casellas, J. (2011). "Inbred mouse strains and genetic stability: a review." Animal 5(1): 1-7.

Chapman, J., Ben-Israel, J., Goldhammer, Y. and Korczyn, A. D. (1994). "The risk of developing Creutzfeldt-Jakob disease in subjects with the PRNP gene codon 200 point mutation." Neurology 44(9): 1683-1686.

Chen, S., Mange, A., Dong, L., Lehmann, S. and Schachner, M. (2003). "Prion protein as trans-interacting partner for neurons is involved in neurite outgrowth and neuronal survival." Mol Cell Neurosci 22(2): 227-233.

Colby, D. W. and Prusiner, S. B. (2011). "Prions." Cold Spring Harb Perspect Biol 3(1): a006833.

Collinge, J. (1999). "Variant Creutzfeldt-Jakob disease." Lancet 354(9175): 317-323.

Collinge, J. (2005). "Molecular neurology of prion disease." J Neurol Neurosurg Psychiatry 76(7): 906-919.

Conesa, A., Madrigal, P., Tarazona, S., Gomez-Cabrero, D., Cervera, A., McPherson, A., Szczesniak, M. W., Gaffney, D. J., Elo, L. L., Zhang, X. and Mortazavi, A. (2016). "A survey of best practices for RNA-seq data analysis." Genome Biol 17: 13.

Crawley, J. N., Belknap, J. K., Collins, A., Crabbe, J. C., Frankel, W., Henderson, N., Hitzemann, R. J., Maxson, S. C., Miner, L. L., Silva, A. J., Wehner, J. M., Wynshaw-Boris, A. and Paylor, R. (1997). "Behavioral phenotypes of inbred mouse strains: implications and recommendations for molecular studies." Psychopharmacology (Berl) 132(2): 107-124.

Criado, J. R., Sanchez-Alavez, M., Conti, B., Giacchino, J. L., Wills, D. N., Henriksen, S. J., Race, R., Manson, J. C., Chesebro, B. and Oldstone, M. B. (2005). "Mice devoid of prion protein have cognitive deficits that are rescued by reconstitution of PrP in neurons." Neurobiol Dis 19(1-2): 255-265.

Damberger, F. F., Christen, B., Perez, D. R., Hornemann, S. and Wuthrich, K. (2011). "Cellular prion protein conformation and function." Proc Natl Acad Sci U S A 108(42): 17308-17313.

Dessau, R. B. and Pipper, C. B. (2008). ""R"-project for statistical computing." Ugeskr Laeger 170(5): 328-330.

Detwiler, L. A. (1992). "Scrapie." Rev Sci Tech 11(2): 491-537.

Detwiler, L. A. and Baylis, M. (2003). "The epidemiology of scrapie." Rev Sci Tech 22(1): 121-143.

DeWoskin, D., Myung, J., Belle, M. D., Piggins, H. D., Takumi, T. and Forger, D. B. (2015). "Distinct roles for GABA across multiple timescales in mammalian circadian timekeeping." Proc Natl Acad Sci U S A 112(29): E3911-3919.

Di Bari, M. A., Nonno, R. and Agrimi, U. (2012). "The mouse model for scrapie: inoculation, clinical scoring, and histopathological techniques." Methods Mol Biol 849: 453-471.

Diaz-Espinoza, R. and Soto, C. (2012). "High-resolution structure of infectious prion protein: the final frontier." Nat Struct Mol Biol 19(4): 370-377.

Dickinson, A. G. and Outram, G. W. (1988). "Genetic aspects of unconventional virus infections: the basis of the virino hypothesis." Ciba Found Symp 135: 63-83.

Dittrich, L., Morairty, S. R., Warrier, D. R. and Kilduff, T. S. (2015). "Homeostatic sleep pressure is the primary factor for activation of cortical nNOS/NK1 neurons." Neuropsychopharmacology 40(3): 632-639.

Dobson, C. M. (2003). "Protein folding and misfolding." Nature 426(6968): 884-890.

Eckardt, D., Theis, M., Doring, B., Speidel, D., Willecke, K. and Ott, T. (2004). "Spontaneous ectopic recombination in cell-type-specific Cre mice removes loxP-flanked marker cassettes in vivo." Genesis 38(4): 159-165.

Emard, J. F., Thouez, J. P. and Gauvreau, D. (1995). "Neurodegenerative diseases and risk factors: a literature review." Soc Sci Med 40(6): 847-858.

Enari, M., Flechsig, E. and Weissmann, C. (2001). "Scrapie prion protein accumulation by scrapie-infected neuroblastoma cells abrogated by exposure to a prion protein antibody." Proc Natl Acad Sci U S A 98(16): 9295-9299.

Endo, T., Groth, D., Prusiner, S. B. and Kobata, A. (1989). "Diversity of oligosaccharide structures linked to asparagines of the scrapie prion protein." Biochemistry 28(21): 8380-8388.

Ferrer, I. (2009). "Altered mitochondria, energy metabolism, voltage-dependent anion channel, and lipid rafts converge to exhaust neurons in Alzheimer's disease." J Bioenerg Biomembr 41(5): 425-431.

Ferrer, I., Casas, R. and Rivera, R. (1993). "Parvalbumin-immunoreactive cortical neurons in Creutzfeldt-Jakob disease." Ann Neurol 34(6): 864-866.

Fields, Bernard N., Knipe, David M., Howley, Peter M. and Griffin, Diane E. (2001). Fields virology. Philadelphia, Lippincott Williams & Wilkins.

Ford, M. J., Burton, L. J., Morris, R. J. and Hall, S. M. (2002). "Selective expression of prion protein in peripheral tissues of the adult mouse." Neuroscience 113(1): 177-192.

Forgacs, G., Yook, S. H., Janmey, P. A., Jeong, H. and Burd, C. G. (2004). "Role of the cytoskeleton in signaling networks." J Cell Sci 117(Pt 13): 2769-2775.

Foster, J. D., Parnham, D., Chong, A., Goldmann, W. and Hunter, N. (2001). "Clinical signs, histopathology and genetics of experimental transmission of BSE and natural scrapie to sheep and goats." Vet Rec 148(6): 165-171.

Francis, P. T., Palmer, A. M., Snape, M. and Wilcock, G. K. (1999). "The cholinergic hypothesis of Alzheimer's disease: a review of progress." J Neurol Neurosurg Psychiatry 66(2): 137-147.

Frau-Mendez, M. A., Fernandez-Vega, I., Ansoleaga, B., Blanco Tech, R., Carmona Tech, M., Antonio Del Rio, J., Zerr, I., Llorens, F., Jose Zarranz, J. and Ferrer, I. (2017). "Fatal familial insomnia: mitochondrial and protein synthesis machinery decline in the mediodorsal thalamus." Brain Pathol 27(1): 95-106.

Gallitano-Mendel, A., Izumi, Y., Tokuda, K., Zorumski, C. F., Howell, M. P., Muglia, L. J., Wozniak, D. F. and Milbrandt, J. (2007). "The immediate early gene early growth response gene 3 mediates adaptation to stress and novelty." Neuroscience 148(3): 633-643.

Giri, R. K., Young, R., Pitstick, R., DeArmond, S. J., Prusiner, S. B. and Carlson, G. A. (2006). "Prion infection of mouse neurospheres." Proc Natl Acad Sci U S A 103(10): 3875-3880.

Grassmann, A., Wolf, H., Hofmann, J., Graham, J. and Vorberg, I. (2013). "Cellular aspects of prion replication in vitro." Viruses 5(1): 374-405.

Graveland, G. A., Williams, R. S. and DiFiglia, M. (1985). "Evidence for degenerative and regenerative changes in neostriatal spiny neurons in Huntington's disease." Science 227(4688): 770-773.

Guentchev, M., Groschup, M. H., Kordek, R., Liberski, P. P. and Budka, H. (1998). "Severe, early and selective loss of a subpopulation of GABAergic inhibitory neurons in experimental transmissible spongiform encephalopathies." Brain Pathol 8(4): 615-623.

Guentchev, M., Hainfellner, J. A., Trabattoni, G. R. and Budka, H. (1997). "Distribution of parvalbumin-immunoreactive neurons in brain correlates with hippocampal and temporal cortical pathology in Creutzfeldt-Jakob disease." J Neuropathol Exp Neurol 56(10): 1119-1124.

Guentchev, M., Wanschitz, J., Voigtlander, T., Flicker, H. and Budka, H. (1999). "Selective neuronal vulnerability in human prion diseases. Fatal familial insomnia differs from other types of prion diseases." Am J Pathol 155(5): 1453-1457.

Halfmann, R., Jarosz, D. F., Jones, S. K., Chang, A., Lancaster, A. K. and Lindquist, S. (2012). "Prions are a common mechanism for phenotypic inheritance in wild yeasts." Nature 482(7385): 363-368.

Heath, C. A., Cooper, S. A., Murray, K., Lowman, A., Henry, C., MacLeod, M. A., Stewart, G. E., Zeidler, M., MacKenzie, J. M., Ironside, J. W., Summers, D. M., Knight, R. S. and Will, R. G. (2010). "Validation of diagnostic criteria for variant Creutzfeldt-Jakob disease." Ann Neurol 67(6): 761-770.

Heikenwalder, M., Zeller, N., Seeger, H., Prinz, M., Klohn, P. C., Schwarz, P., Ruddle, N. H., Weissmann, C. and Aguzzi, A. (2005). "Chronic lymphocytic inflammation specifies the organ tropism of prions." Science 307(5712): 1107-1110.

Hill, A. F., Desbruslais, M., Joiner, S., Sidle, K. C., Gowland, I., Collinge, J., Doey, L. J. and Lantos, P. (1997). "The same prion strain causes vCJD and BSE." Nature 389(6650): 448-450, 526.

Hippenmeyer, S., Vrieseling, E., Sigrist, M., Portmann, T., Laengle, C., Ladle, D. R. and Arber, S. (2005). "A developmental switch in the response of DRG neurons to ETS transcription factor signaling." PLoS Biol 3(5): e159.

Hofmann, J. and Vorberg, I. (2013). "Life cycle of cytosolic prions." Prion 7(5): 369-377.

Hol, E. M., Roelofs, R. F., Moraal, E., Sonnemans, M. A., Sluijs, J. A., Proper, E. A., de Graan, P. N., Fischer, D. F. and van Leeuwen, F. W. (2003). "Neuronal expression of GFAP in patients with Alzheimer pathology and identification of novel GFAP splice forms." Mol Psychiatry 8(9): 786-796.

Hood, S. and Amir, S. (2017). "Neurodegeneration and the Circadian Clock." Front Aging Neurosci 9: 170.

Hornshaw, M. P., McDermott, J. R., Candy, J. M. and Lakey, J. H. (1995). "Copper binding to the N-terminal tandem repeat region of mammalian and avian prion protein: structural studies using synthetic peptides." Biochem Biophys Res Commun 214(3): 993-999.

Huang, D. W., Sherman, B. T., Tan, Q., Collins, J. R., Alvord, W. G., Roayaei, J., Stephens, R., Baseler, M. W., Lane, H. C. and Lempicki, R. A. (2007). "The DAVID Gene Functional Classification Tool: a novel biological module-centric algorithm to functionally analyze large gene lists." Genome Biol 8(9): R183.

Huang da, W., Sherman, B. T. and Lempicki, R. A. (2009a). "Bioinformatics enrichment tools: paths toward the comprehensive functional analysis of large gene lists." Nucleic Acids Res 37(1): 1-13.

Huang da, W., Sherman, B. T. and Lempicki, R. A. (2009b). "Systematic and integrative analysis of large gene lists using DAVID bioinformatics resources." Nat Protoc 4(1): 44-57.

Huber, F., Schnauss, J., Ronicke, S., Rauch, P., Muller, K., Futterer, C. and Kas, J. (2013). "Emergent complexity of the cytoskeleton: from single filaments to tissue." Adv Phys 62(1): 1-112.

Hynd, M. R., Scott, H. L. and Dodd, P. R. (2004). "Glutamate-mediated excitotoxicity and neurodegeneration in Alzheimer's disease." Neurochem Int 45(5): 583-595.

Jackson, W. S. (2014). "Selective vulnerability to neurodegenerative disease: the curious case of Prion Protein." Dis Model Mech 7(1): 21-29.

Jackson, W. S., Borkowski, A. W., Faas, H., Steele, A. D., King, O. D., Watson, N., Jasanoff, A. and Lindquist, S. (2009). "Spontaneous generation of prion infectivity in fatal familial insomnia knockin mice." Neuron 63(4): 438-450.

Jackson, W. S., Krost, C., Borkowski, A. W. and Kaczmarczyk, L. (2014). "Translation of the prion protein mRNA is robust in astrocytes but does not amplify during reactive astrocytosis in the mouse brain." PLoS One 9(4): e95958.

Jendroska, K., Heinzel, F. P., Torchia, M., Stowring, L., Kretzschmar, H. A., Kon, A., Stern, A., Prusiner, S. B. and DeArmond, S. J. (1991). "Proteinase-resistant prion protein accumulation in Syrian hamster brain correlates with regional pathology and scrapie infectivity." Neurology 41(9): 1482-1490.

Kanaani, J., Prusiner, S. B., Diacovo, J., Baekkeskov, S. and Legname, G. (2005). "Recombinant prion protein induces rapid polarization and development of synapses in embryonic rat hippocampal neurons in vitro." J Neurochem 95(5): 1373-1386.

Katsuno, M., Tanaka, F. and Sobue, G. (2012). "Perspectives on molecular targeted therapies and clinical trials for neurodegenerative diseases." J Neurol Neurosurg Psychiatry 83(3): 329-335.

Kawasaki, Y., Kawagoe, K., Chen, C. J., Teruya, K., Sakasegawa, Y. and Doh-ura, K. (2007). "Orally administered amyloidophilic compound is effective in prolonging the incubation periods of animals cerebrally infected with prion diseases in a prion strain-dependent manner." J Virol 81(23): 12889-12898.

Kimelberg, H. K. and Nedergaard, M. (2010). "Functions of astrocytes and their potential as therapeutic targets." Neurotherapeutics 7(4): 338-353.

Kitamoto, T., Muramoto, T., Mohri, S., Doh-Ura, K. and Tateishi, J. (1991). "Abnormal isoform of prion protein accumulates in follicular dendritic cells in mice with Creutzfeldt-Jakob disease." J Virol 65(11): 6292-6295.

Kong, Q. (2006). "RNAi: a novel strategy for the treatment of prion diseases." J Clin Invest 116(12): 3101-3103.

Korth, C., May, B. C., Cohen, F. E. and Prusiner, S. B. (2001). "Acridine and phenothiazine derivatives as pharmacotherapeutics for prion disease." Proc Natl Acad Sci U S A 98(17): 9836-9841.

Krakauer, D. C., Pagel, M., Southwood, T. R. and Zanotto, P. M. (1996). "Phylogenesis of prion protein." Nature 380(6576): 675.

Krauss, S. and Vorberg, I. (2013). "Prions Ex Vivo: What Cell Culture Models Tell Us about Infectious Proteins." Int J Cell Biol 2013: 704546.

Kukurba, K. R. and Montgomery, S. B. (2015). "RNA Sequencing and Analysis." Cold Spring Harb Protoc 2015(11): 951-969.

Laird, P. W., Zijderveld, A., Linders, K., Rudnicki, M. A., Jaenisch, R. and Berns, A. (1991). "Simplified mammalian DNA isolation procedure." Nucleic Acids Res 19(15): 4293.

Langmead, B. and Salzberg, S. L. (2012). "Fast gapped-read alignment with Bowtie 2." Nat Methods 9(4): 357-359.

Lasmezas, C. and Zhou, M. (2012). "Newly defined toxic alpha-helical prion protein monomer: implications for other neurodegenerative diseases?" Expert Rev Proteomics 9(3): 233-235.

Li, B. and Dewey, C. N. (2011). "RSEM: accurate transcript quantification from RNA-Seq data with or without a reference genome." BMC Bioinformatics 12: 323.

Li, B., Ruotti, V., Stewart, R. M., Thomson, J. A. and Dewey, C. N. (2010). "RNA-Seq gene expression estimation with read mapping uncertainty." Bioinformatics 26(4): 493-500.

Liberski, P. P. (2012). "Historical overview of prion diseases: a view from afar." Folia Neuropathol 50(1): 1-12.

Linden, R., Martins, V. R., Prado, M. A., Cammarota, M., Izquierdo, I. and Brentani, R. R. (2008). "Physiology of the prion protein." Physiol Rev 88(2): 673-728.

Liu, C. and Reppert, S. M. (2000). "GABA synchronizes clock cells within the suprachiasmatic circadian clock." Neuron 25(1): 123-128.

Liu, L., Li, Y., Li, S., Hu, N., He, Y., Pong, R., Lin, D., Lu, L. and Law, M. (2012). "Comparison of next-generation sequencing systems." J Biomed Biotechnol 2012: 251364.

Livak, K. J. and Schmittgen, T. D. (2001). "Analysis of relative gene expression data using real-time quantitative PCR and the 2(-Delta Delta C(T)) Method." Methods 25(4): 402-408.

Love, M. I., Huber, W. and Anders, S. (2014). "Moderated estimation of fold change and dispersion for RNA-seq data with DESeq2." Genome Biol 15(12): 550.

Ma, J. (2012). "The role of cofactors in prion propagation and infectivity." PLoS Pathog 8(4): e1002589.

Ma, J. and Wang, F. (2014). "Prion disease and the 'protein-only hypothesis'." Essays Biochem 56: 181-191.

MacInnes, A. W. (2016). "The role of the ribosome in the regulation of longevity and lifespan extension." Wiley Interdiscip Rev RNA 7(2): 198-212.

Manson, J. C., Clarke, A. R., Hooper, M. L., Aitchison, L., McConnell, I. and Hope, J. (1994a). "129/Ola mice carrying a null mutation in PrP that abolishes mRNA production are developmentally normal." Mol Neurobiol 8(2-3): 121-127.

Manson, J. C., Clarke, A. R., McBride, P. A., McConnell, I. and Hope, J. (1994b). "PrP gene dosage determines the timing but not the final intensity or distribution of lesions in scrapie pathology." Neurodegeneration 3(4): 331-340.

Manson, J. C. and Tuzi, N. L. (2001). "Transgenic models of the transmissible spongiform encephalopathies." Expert Rev Mol Med 2001: 1-15.

Manuelidis, L. (2007). "A 25 nm virion is the likely cause of transmissible spongiform encephalopathies." J Cell Biochem 100(4): 897-915.

Manuelidis, L., Yu, Z. X., Barquero, N. and Mullins, B. (2007). "Cells infected with scrapie and Creutzfeldt-Jakob disease agents produce intracellular 25-nm virus-like particles." Proc Natl Acad Sci U S A 104(6): 1965-1970.

Mardis, E. R. (2008). "The impact of next-generation sequencing technology on genetics." Trends Genet 24(3): 133-141.

Masel, J., Jansen, V. A. and Nowak, M. A. (1999). "Quantifying the kinetic parameters of prion replication." Biophys Chem 77(2-3): 139-152.

Mattsson, N., Schott, J. M., Hardy, J., Turner, M. R. and Zetterberg, H. (2016). "Selective vulnerability in neurodegeneration: insights from clinical variants of Alzheimer's disease." J Neurol Neurosurg Psychiatry 87(9): 1000-1004.

Maxam, A. M. and Gilbert, W. (1977). "A new method for sequencing DNA." Proc Natl Acad Sci U S A 74(2): 560-564.

Meldrum, B. S. (2000). "Glutamate as a neurotransmitter in the brain: review of physiology and pathology." J Nutr 130(4S Suppl): 1007S-1015S.

Mendez, I., Vazquez-Martinez, O., Hernandez-Munoz, R., Valente-Godinez, H. and Diaz-Munoz, M. (2016). "Redox regulation and pro-oxidant reactions in the physiology of circadian systems." Biochimie 124: 178-186.

Montagna, P., Gambetti, P., Cortelli, P. and Lugaresi, E. (2003). "Familial and sporadic fatal insomnia." Lancet Neurol 2(3): 167-176.

Moore, R. Y. and Speh, J. C. (1993). "GABA is the principal neurotransmitter of the circadian system." Neurosci Lett 150(1): 112-116.

Morairty, S. R., Dittrich, L., Pasumarthi, R. K., Valladao, D., Heiss, J. E., Gerashchenko, D. and Kilduff, T. S. (2013). "A role for cortical nNOS/NK1 neurons in coupling homeostatic sleep drive to EEG slow wave activity." Proc Natl Acad Sci U S A 110(50): 20272-20277.

Musiek, E. S. and Holtzman, D. M. (2016). "Mechanisms linking circadian clocks, sleep, and neurodegeneration." Science 354(6315): 1004-1008.

Musiek, E. S., Lim, M. M., Yang, G., Bauer, A. Q., Qi, L., Lee, Y., Roh, J. H., Ortiz-Gonzalez, X., Dearborn, J. T., Culver, J. P., Herzog, E. D., Hogenesch, J. B., Wozniak, D. F., Dikranian, K., Giasson, B. I., Weaver, D. R., Holtzman, D. M. and Fitzgerald, G. A. (2013). "Circadian clock proteins regulate neuronal redox homeostasis and neurodegeneration." J Clin Invest 123(12): 5389-5400.

Myung, J., Hong, S., DeWoskin, D., De Schutter, E., Forger, D. B. and Takumi, T. (2015). "GABA-mediated repulsive coupling between circadian clock neurons in the SCN encodes seasonal time." Proc Natl Acad Sci U S A 112(29): E3920-3929.

Nieoullon, André (2011). "Neurodegenerative disease and neuroprotection: current views and prospects." Journal of APPLIED BIOMEDICINE 9: 173-183.

Oesch, B., Westaway, D., Walchli, M., McKinley, M. P., Kent, S. B., Aebersold, R., Barry, R. A., Tempst, P., Teplow, D. B., Hood, L. E. and et al. (1985). "A cellular gene encodes scrapie PrP 27-30 protein." Cell 40(4): 735-746.

Oslowski, C. M. and Urano, F. (2011). "Measuring ER stress and the unfolded protein response using mammalian tissue culture system." Methods Enzymol 490: 71-92.

Pan, K. M., Baldwin, M., Nguyen, J., Gasset, M., Serban, A., Groth, D., Mehlhorn, I., Huang, Z., Fletterick, R. J., Cohen, F. E. and et al. (1993). "Conversion of alpha-helices into beta-sheets features in the formation of the scrapie prion proteins." Proc Natl Acad Sci U S A 90(23): 10962-10966.

Panegyres, P. K. and Armari, E. (2013). "Therapies for human prion diseases." Am J Neurodegener Dis 2(3): 176-186.

Parks, G. S., Warrier, D. R., Dittrich, L., Schwartz, M. D., Palmerston, J. B., Neylan, T. C., Morairty, S. R. and Kilduff, T. S. (2016). "The Dual Hypocretin Receptor Antagonist Almorexant is Permissive for Activation of Wake-Promoting Systems." Neuropsychopharmacology 41(4): 1144-1155.

Pattison, I. H. and Millson, G. C. (1961). "Scrapie produced experimentally in goats with special reference to the clinical syndrome." J Comp Pathol 71: 101-109.

Peralta, O. A. and Eyestone, W. H. (2009). "Quantitative and qualitative analysis of cellular prion protein (PrP(C)) expression in bovine somatic tissues." Prion 3(3): 161-170.

Peretz, D., Williamson, R. A., Kaneko, K., Vergara, J., Leclerc, E., Schmitt-Ulms, G., Mehlhorn, I. R., Legname, G., Wormald, M. R., Rudd, P. M., Dwek, R. A., Burton, D. R. and Prusiner, S. B. (2001). "Antibodies inhibit prion propagation and clear cell cultures of prion infectivity." Nature 412(6848): 739-743.

Pettersson, E., Lundeberg, J. and Ahmadian, A. (2009). "Generations of sequencing technologies." Genomics 93(2): 105-111.

Preiss, T. (2016). "All Ribosomes Are Created Equal. Really?" Trends Biochem Sci 41(2): 121-123.

Prusiner, S. B. (1982). "Novel proteinaceous infectious particles cause scrapie." Science 216(4542): 136-144.

Prusiner, S. B. (1991). "Molecular biology of prion diseases." Science 252(5012): 1515-1522.

Prusiner, S. B. (1998). "Prions." Proc Natl Acad Sci U S A 95(23): 13363-13383.

Prusiner, S. B. (2012). "Cell biology. A unifying role for prions in neurodegenerative diseases." Science 336(6088): 1511-1513.

Prusiner, S. B. (2013). "Biology and genetics of prions causing neurodegeneration." Annu Rev Genet 47: 601-623.

Prusiner, S. B., Groth, D., Serban, A., Koehler, R., Foster, D., Torchia, M., Burton, D., Yang, S. L. and DeArmond, S. J. (1993). "Ablation of the prion protein (PrP) gene in mice prevents scrapie and facilitates production of anti-PrP antibodies." Proc Natl Acad Sci U S A 90(22): 10608-10612.

Raeber, A. J., Sailer, A., Hegyi, I., Klein, M. A., Rulicke, T., Fischer, M., Brandner, S., Aguzzi, A. and Weissmann, C. (1999). "Ectopic expression of prion protein (PrP) in T lymphocytes or hepatocytes of PrP knockout mice is insufficient to sustain prion replication." Proc Natl Acad Sci U S A 96(7): 3987-3992.

Ramanan, V. K. and Saykin, A. J. (2013). "Pathways to neurodegeneration: mechanistic insights from GWAS in Alzheimer's disease, Parkinson's disease, and related disorders." Am J Neurodegener Dis 2(3): 145-175.

Requena, J. R., Groth, D., Legname, G., Stadtman, E. R., Prusiner, S. B. and Levine, R. L. (2001). "Copper-catalyzed oxidation of the recombinant SHa(29-231) prion protein." Proc Natl Acad Sci U S A 98(13): 7170-7175.

Ron, D. and Walter, P. (2007). "Signal integration in the endoplasmic reticulum unfolded protein response." Nat Rev Mol Cell Biol 8(7): 519-529.

Ronkina, N., Menon, M. B., Schwermann, J., Arthur, J. S., Legault, H., Telliez, J. B., Kayyali, U. S., Nebreda, A. R., Kotlyarov, A. and Gaestel, M. (2011). "Stress induced gene expression: a direct role for MAPKAP kinases in transcriptional activation of immediate early genes." Nucleic Acids Res 39(7): 2503-2518.

Rothman, D. L., Behar, K. L., Hyder, F. and Shulman, R. G. (2003). "In vivo NMR studies of the glutamate neurotransmitter flux and neuroenergetics: implications for brain function." Annu Rev Physiol 65: 401-427.

Roucou, X., Gains, M. and LeBlanc, A. C. (2004). "Neuroprotective functions of prion protein." J Neurosci Res 75(2): 153-161.

Rubinsztein, D. C. (2006). "The roles of intracellular protein-degradation pathways in neurodegeneration." Nature 443(7113): 780-786.

Saa, P., Castilla, J. and Soto, C. (2006). "Ultra-efficient replication of infectious prions by automated protein misfolding cyclic amplification." J Biol Chem 281(46): 35245-35252.

Saborio, G. P., Permanne, B. and Soto, C. (2001). "Sensitive detection of pathological prion protein by cyclic amplification of protein misfolding." Nature 411(6839): 810-813.

Safar, J. G., DeArmond, S. J., Kociuba, K., Deering, C., Didorenko, S., Bouzamondo-Bernstein, E., Prusiner, S. B. and Tremblay, P. (2005a). "Prion clearance in bigenic mice." J Gen Virol 86(Pt 10): 2913-2923.

Safar, J. G., Kellings, K., Serban, A., Groth, D., Cleaver, J. E., Prusiner, S. B. and Riesner, D. (2005b). "Search for a prion-specific nucleic acid." J Virol 79(16): 10796-10806.

Safar, J., Wille, H., Itri, V., Groth, D., Serban, H., Torchia, M., Cohen, F. E. and Prusiner, S. B. (1998). "Eight prion strains have PrP(Sc) molecules with different conformations." Nat Med 4(10): 1157-1165.

Salinska, E., Danysz, W. and Lazarewicz, J. W. (2005). "The role of excitotoxicity in neurodegeneration." Folia Neuropathol 43(4): 322-339.

Sanger, F., Nicklen, S. and Coulson, A. R. (1977). "DNA sequencing with chain-terminating inhibitors." Proc Natl Acad Sci U S A 74(12): 5463-5467.

Sanz, E., Yang, L., Su, T., Morris, D. R., McKnight, G. S. and Amieux, P. S. (2009). "Cell-type-specific isolation of ribosome-associated mRNA from complex tissues." Proc Natl Acad Sci U S A 106(33): 13939-13944.

Saxena, S. and Caroni, P. (2011). "Selective neuronal vulnerability in neurodegenerative diseases: from stressor thresholds to degeneration." Neuron 71(1): 35-48.

Scott, M., Foster, D., Mirenda, C., Serban, D., Coufal, F., Walchli, M., Torchia, M., Groth, D., Carlson, G., DeArmond, S. J., Westaway, D. and Prusiner, S. B. (1989). "Transgenic mice expressing hamster prion protein produce species-specific scrapie infectivity and amyloid plaques." Cell 59(5): 847-857.

Sheikh, S., Safia, Haque, E. and Mir, S. S. (2013). "Neurodegenerative Diseases: Multifactorial Conformational Diseases and Their Therapeutic Interventions." J Neurodegener Dis 2013: 563481.

Shi, Z., Fujii, K., Kovary, K. M., Genuth, N. R., Rost, H. L., Teruel, M. N. and Barna, M. (2017). "Heterogeneous Ribosomes Preferentially Translate Distinct Subpools of mRNAs Genome-wide." Mol Cell 67(1): 71-83 e77.

Sigurdson, C. J., Manco, G., Schwarz, P., Liberski, P., Hoover, E. A., Hornemann, S., Polymenidou, M., Miller, M. W., Glatzel, M. and Aguzzi, A. (2006). "Strain fidelity of chronic wasting disease upon murine adaptation." J Virol 80(24): 12303-12311.

Silveira, J. R., Raymond, G. J., Hughson, A. G., Race, R. E., Sim, V. L., Hayes, S. F. and Caughey, B. (2005). "The most infectious prion protein particles." Nature 437(7056): 257-261.

Sim, V. L. and Caughey, B. (2009). "Recent advances in prion chemotherapeutics." Infect Disord Drug Targets 9(1): 81-91.

Soto, C. (2011). "Prion hypothesis: the end of the controversy?" Trends Biochem Sci 36(3): 151-158.

Sparkes, R. S., Simon, M., Cohn, V. H., Fournier, R. E., Lem, J., Klisak, I., Heinzmann, C., Blatt, C., Lucero, M., Mohandas, T. and et al. (1986). "Assignment of the human and mouse prion protein genes to homologous chromosomes." Proc Natl Acad Sci U S A 83(19): 7358-7362.

Spudich, S., Mastrianni, J. A., Wrensch, M., Gabizon, R., Meiner, Z., Kahana, I., Rosenmann, H., Kahana, E. and Prusiner, S. B. (1995). "Complete penetrance of Creutzfeldt-Jakob disease in Libyan Jews carrying the E200K mutation in the prion protein gene." Mol Med 1(6): 607-613.

Stahl, N., Baldwin, M. A., Burlingame, A. L. and Prusiner, S. B. (1990). "Identification of glycoinositol phospholipid linked and truncated forms of the scrapie prion protein." Biochemistry 29(38): 8879-8884.

Steele, A. D., Emsley, J. G., Ozdinler, P. H., Lindquist, S. and Macklis, J. D. (2006). "Prion protein (PrPc) positively regulates neural precursor proliferation during developmental and adult mammalian neurogenesis." Proc Natl Acad Sci U S A 103(9): 3416-3421.

Steele, A. D., Jackson, W. S., King, O. D. and Lindquist, S. (2007a). "The power of automated high-resolution behavior analysis revealed by its application to mouse models of Huntington's and prion diseases." Proc Natl Acad Sci U S A 104(6): 1983-1988.

Steele, A. D., Lindquist, S. and Aguzzi, A. (2007b). "The prion protein knockout mouse: a phenotype under challenge." Prion 1(2): 83-93.

Stuermer, C. A., Langhorst, M. F., Wiechers, M. F., Legler, D. F., Von Hanwehr, S. H., Guse, A. H. and Plattner, H. (2004). "PrPc capping in T cells promotes its association with the lipid raft proteins reggie-1 and reggie-2 and leads to signal transduction." FASEB J 18(14): 1731-1733.

Sulzer, D. and Surmeier, D. J. (2013). "Neuronal vulnerability, pathogenesis, and Parkinson's disease." Mov Disord 28(1): 41-50.

Sun, S., Sun, Y., Ling, S. C., Ferraiuolo, L., McAlonis-Downes, M., Zou, Y., Drenner, K., Wang, Y., Ditsworth, D., Tokunaga, S., Kopelevich, A., Kaspar, B. K., Lagier-Tourenne, C. and Cleveland, D. W. (2015). "Translational profiling identifies a cascade of damage initiated in motor neurons and spreading to glia in mutant SOD1-mediated ALS." Proc Natl Acad Sci U S A 112(50): E6993-7002.

Supattapone, S., Nguyen, H. O., Cohen, F. E., Prusiner, S. B. and Scott, M. R. (1999). "Elimination of prions by branched polyamines and implications for therapeutics." Proc Natl Acad Sci U S A 96(25): 14529-14534.

Supattapone, S., Wille, H., Uyechi, L., Safar, J., Tremblay, P., Szoka, F. C., Cohen, F. E., Prusiner, S. B. and Scott, M. R. (2001). "Branched polyamines cure prion-infected neuroblastoma cells." J Virol 75(7): 3453-3461.

Sweeney, P., Park, H., Baumann, M., Dunlop, J., Frydman, J., Kopito, R., McCampbell, A., Leblanc, G., Venkateswaran, A., Nurmi, A. and Hodgson, R. (2017). "Protein misfolding in neurodegenerative diseases: implications and strategies." Transl Neurodegener 6: 6.

Takeuchi, A., Kobayashi, A., Ironside, J. W., Mohri, S. and Kitamoto, T. (2013). "Characterization of variant Creutzfeldt-Jakob disease prions in prion protein-humanized mice carrying distinct codon 129 genotypes." J Biol Chem 288(30): 21659-21666.

Taniguchi, H. (2014). "Genetic dissection of GABAergic neural circuits in mouse neocortex." Front Cell Neurosci 8: 8.

Taniguchi, H., He, M., Wu, P., Kim, S., Paik, R., Sugino, K., Kvitsiani, D., Fu, Y., Lu, J., Lin, Y., Miyoshi, G., Shima, Y., Fishell, G., Nelson, S. B. and Huang, Z. J. (2011).

"A resource of Cre driver lines for genetic targeting of GABAergic neurons in cerebral cortex." Neuron 71(6): 995-1013.

Taylor, J. P., Hardy, J. and Fischbeck, K. H. (2002). "Toxic proteins in neurodegenerative disease." Science 296(5575): 1991-1995.

Telling, G. C., Parchi, P., DeArmond, S. J., Cortelli, P., Montagna, P., Gabizon, R., Mastrianni, J., Lugaresi, E., Gambetti, P. and Prusiner, S. B. (1996). "Evidence for the conformation of the pathologic isoform of the prion protein enciphering and propagating prion diversity." Science 274(5295): 2079-2082.

Thompson, C. L., Wisor, J. P., Lee, C. K., Pathak, S. D., Gerashchenko, D., Smith, K. A., Fischer, S. R., Kuan, C. L., Sunkin, S. M., Ng, L. L., Lau, C., Hawrylycz, M., Jones, A. R., Kilduff, T. S. and Lein, E. S. (2010). "Molecular and anatomical signatures of sleep deprivation in the mouse brain." Front Neurosci 4: 165.

Tiwana, H., Wilson, C., Pirt, J., Cartmell, W. and Ebringer, A. (1999). "Autoantibodies to brain components and antibodies to Acinetobacter calcoaceticus are present in bovine spongiform encephalopathy." Infect Immun 67(12): 6591-6595.

Tobler, I., Deboer, T. and Fischer, M. (1997). "Sleep and sleep regulation in normal and prion protein-deficient mice." J Neurosci 17(5): 1869-1879.

Tobler, I., Gaus, S. E., Deboer, T., Achermann, P., Fischer, M., Rulicke, T., Moser, M., Oesch, B., McBride, P. A. and Manson, J. C. (1996). "Altered circadian activity rhythms and sleep in mice devoid of prion protein." Nature 380(6575): 639-642.

Trevitt, C. R. and Collinge, J. (2006). "A systematic review of prion therapeutics in experimental models." Brain 129(Pt 9): 2241-2265.

True, H. L., Berlin, I. and Lindquist, S. L. (2004). "Epigenetic regulation of translation reveals hidden genetic variation to produce complex traits." Nature 431(7005): 184-187.

True, H. L. and Lindquist, S. L. (2000). "A yeast prion provides a mechanism for genetic variation and phenotypic diversity." Nature 407(6803): 477-483.

Tuzi, N. L., Cancellotti, E., Baybutt, H., Blackford, L., Bradford, B., Plinston, C., Coghill, A., Hart, P., Piccardo, P., Barron, R. M. and Manson, J. C. (2008). "Host PrP glycosylation: a major factor determining the outcome of prion infection." PLoS Biol 6(4): e100.

Tyedmers, J., Madariaga, M. L. and Lindquist, S. (2008). "Prion switching in response to environmental stress." PLoS Biol 6(11): e294.

van Noort, J. M., Bugiani, M. and Amor, S. (2016). "Heat Shock Proteins: Old and Novel Roles in Neurodegenerative Diseases in the Central Nervous System." CNS Neurol Disord Drug Targets.

van Rheede, T., Smolenaars, M. M., Madsen, O. and de Jong, W. W. (2003). "Molecular evolution of the mammalian prion protein." Mol Biol Evol 20(1): 111-121.

Voelkerding, K. V., Dames, S. A. and Durtschi, J. D. (2009). "Next-generation sequencing: from basic research to diagnostics." Clin Chem 55(4): 641-658.

Vong, L., Ye, C., Yang, Z., Choi, B., Chua, S., Jr. and Lowell, B. B. (2011). "Leptin action on GABAergic neurons prevents obesity and reduces inhibitory tone to POMC neurons." Neuron 71(1): 142-154.

Wang, F. and Ma, J. (2013). "Role of lipid in forming an infectious prion?" Acta Biochim Biophys Sin (Shanghai) 45(6): 485-493.

Ward, H. J. (2000). "Surveillance of Creutzfeldt Jakob disease in the United Kingdom." Euro Surveill 5(9): 90-94.

Weissmann, C. (2004). "The state of the prion." Nat Rev Microbiol 2(11): 861-871.

Weissmann, C., Enari, M., Klohn, P. C., Rossi, D. and Flechsig, E. (2002). "Transmission of prions." Proc Natl Acad Sci U S A 99 Suppl 4: 16378-16383.

Welsh, D. K., Takahashi, J. S. and Kay, S. A. (2010). "Suprachiasmatic nucleus: cell autonomy and network properties." Annu Rev Physiol 72: 551-577.

White, M. D. and Mallucci, G. R. (2009). "RNAi for the treatment of prion disease: a window for intervention in neurodegeneration?" CNS Neurol Disord Drug Targets 8(5): 342-352.

Whitechurch, B. C., Welton, J. M., Collins, S. J. and Lawson, V. A. (2017). "Prion Diseases." Adv Neurobiol 15: 335-364.

Wiseman, F., Cancellotti, E. and Manson, J. (2005). "Glycosylation and misfolding of PrP." Biochem Soc Trans 33(Pt 5): 1094-1095.

Wiseman, F. K., Cancellotti, E., Piccardo, P., Iremonger, K., Boyle, A., Brown, D., Ironside, J. W., Manson, J. C. and Diack, A. B. (2015). "The glycosylation status of PrPC is a key factor in determining transmissible spongiform encephalopathy transmission between species." J Virol 89(9): 4738-4747.

Wisor, J. P., Pasumarthi, R. K., Gerashchenko, D., Thompson, C. L., Pathak, S., Sancar, A., Franken, P., Lein, E. S. and Kilduff, T. S. (2008). "Sleep deprivation effects on circadian clock gene expression in the cerebral cortex parallel electroencephalographic differences among mouse strains." J Neurosci 28(28): 7193-7201.

Xue, S. and Barna, M. (2012). "Specialized ribosomes: a new frontier in gene regulation and organismal biology." Nat Rev Mol Cell Biol 13(6): 355-369.

Zhang, C. C., Steele, A. D., Lindquist, S. and Lodish, H. F. (2006). "Prion protein is expressed on long-term repopulating hematopoietic stem cells and is important for their self-renewal." Proc Natl Acad Sci U S A 103(7): 2184-2189.

Zhang, Y., Chen, K., Sloan, S. A., Bennett, M. L., Scholze, A. R., O'Keeffe, S., Phatnani, H. P., Guarnieri, P., Caneda, C., Ruderisch, N., Deng, S., Liddelow, S. A., Zhang, C., Daneman, R., Maniatis, T., Barres, B. A. and Wu, J. Q. (2014). "An RNA-sequencing transcriptome and splicing database of glia, neurons, and vascular cells of the cerebral cortex." J Neurosci 34(36): 11929-11947.

Zhu, C., Herrmann, U. S., Falsig, J., Abakumova, I., Nuvolone, M., Schwarz, P., Frauenknecht, K., Rushing, E. J. and Aguzzi, A. (2016). "A neuroprotective role for microglia in prion diseases." J Exp Med 213(6): 1047-1059.

III. Acknowledgment / Danksagung

Mein ganz besonderer Dank gebührt Dr. Walker Jackson für die Bereitstellung des interessanten Themas meiner Dissertation, die Möglichkeit diese in seiner Arbeitsgruppe am Deutschen Zentrum für Neurodegenerative Erkrankungen anzufertigen, die umfangreiche Unterstützung und den unermüdlichen Einsatz zur Fertigstellung dieser Arbeit.

Frau Prof. Dr. Ina Vorberg und Herrn Prof. Dr. Walter Witke danke ich für die freundliche Bereitschaft, als Gutachter dieser Dissertation zur Verfügung zu stehen. Ebenso danke ich den weiteren Mitgliedern des Prüfungskomitees, Herrn Prof. Dr. Michael Hofmann und Herrn Prof. Dr. Thomas Kistemann, für die Begutachtung dieser Dissertation.

Den Kollegen meiner Arbeitsgruppe und den Kollaborationspartnern danke ich für die Unterstützung meiner Labortätigkeiten und für das Teilen ihres Wissens und ihrer Erfahrung. Allen voran sind durch ihren Beitrag zu dieser Arbeit Dr. Clemens Krost (ehemaliges Mitglied AG Jackson, DZNE Bonn), Dr. Lars Dittrich (AG Jackson, DZNE Bonn), Dr. Stefan Bonn (AG Bonn, DZNE Göttingen) und Dr. Vikas Bansai (AG Bonn, DZNE Göttingen) zu nennen.

Zudem danke ich allen Mitarbeitern des Deutschen Zentrums für Neurodegenerative Erkrankungen für ihre Hilfsbereitschaft und Unterstützung während der gemeinsamen Zeit.

Mein Dank gilt ebenso meiner Familie, die mit ihrer Unterstützung und ihrem Glauben an mich einen großen Beitrag zur Fertigstellung dieser Arbeit geleistet haben.